2013

Identifying Ditch Geometry and Top of the Bank Location Using Airborne LiDAR Point Cloud

Naime Celik
Purdue University

Graduate School ETD Form 9
(Revised 12/07)

PURDUE UNIVERSITY
GRADUATE SCHOOL
Thesis/Dissertation Acceptance

This is to certify that the thesis/dissertation prepared

By Naime Celik

Entitled
Identifying Ditch Geometry and Top of the Bank Location Using Airborne LiDAR Point Cloud

For the degree of Master of Science in Engineering

Is approved by the final examining committee:

Melba M. Crawford
Chair

Jane R. Frankenberger

James S. Bethel

Boudewijn H. W. Van Gelder

To the best of my knowledge and as understood by the student in the *Research Integrity and Copyright Disclaimer (Graduate School Form 20)*, this thesis/dissertation adheres to the provisions of Purdue University's "Policy on Integrity in Research" and the use of copyrighted material.

Approved by Major Professor(s): Melba M. Crawford

Approved by: Michael E. Kreger 12/04/2013
Head of the Graduate Program Date

IDENTIFYING DITCH GEOMETRY AND TOP OF THE BANK LOCATION USING AIRBORNE LIDAR POINT CLOUD

A Thesis

Submitted to the Faculty

of

Purdue University

by

Naime Celik

In Partial Fulfillment of the

Requirements for the Degree

of

Master of Science in Engineering

December 2013

Purdue University

West Lafayette, Indiana

To those who serves for universal human rights and equality

Evrensel insan hakları ve eşitlik için hizmet edenlere

ACKNOWLEDGEMENTS

Firstly, I would like to express my gratitude to the Ministry of National Education of the Republic of Turkey and Turkish Petroleum Corporation (TPAO) for their financial support that enabled me to pursue this research.

I am heartily thankful to my co-advisors Prof. Jane Frankenberger and Prof. Melba Crawford for their guidance, encouragement and understanding during this research. I also would like to thank Dr. Jinha Jung for sharing his ideas and his contribution. Their support of my master's thesis research enhanced my programming ability, inspired me to learn practical application of my field and help me to gain self-learning skills. Our nearly twice-monthly meetings taught me the importance and benefit of working in collaboratively. I would like to seek out and establish similar group works in my future career. In terms of learning how to conduct a research, I had an invaluable experience thanks to my advisers. I would not have been to carry out this research without their supervision, assistance and support.

I would like to also thank to my committee members Prof. Jim Bethel and especially Prof. Boudewijn H. W. van Gelder who assisted me during thesis writing process with his profound knowledge of Geodesy.

I would like to thank the Agricultural and Biological Department at Purdue University for providing me transportation vehicles and surveying equipment with which to conduct the site surveys.

I also thank a graduate student, Julie Speelman from Department of Entomology, who drove us many times to distance locations and obtained permissions for survey sites. Additionally, an undergraduate student, Kirsten E. Paff, from Agricultural and Biological Department, deserves much thanks for being a survey crew together.

I am deeply grateful to the students in our department and friends in the US and as well as in Turkey for their help on my questions and discussions that facilitated me to learn more.

Lastly, I would like to thank those closest to me. To my mother, Gülizar, my father Şahin and my other family members who have endless love and encouragement. In a world in which women are still living with many disadvantages, having parents and family members that did not hesitate one minute to support me in my academic and extracurricular activities was precious to me. I hope that someday, there will no longer be discrimination among people due to sex, race, age, religion, wealth or nationality; and many more women will gain their fundamental human right of education. Finally, I would like to thank my boyfriend, Jeff, who has provided never-ending support and has shown me how to find humor even in the gloomiest of times and to look at life from a broader perspective.

Thank you all.

TABLE OF CONTENTS

Page

Page

Page

LIST OF TABLES

Table Page

LIST OF FIGURES

Figure Page

Figure Page

Figure Page

Figure Page

Figure Page

Figure Page

Figure Page

LIST OF ABBREVIATIONS

CA	Cumulative Area
LiDAR	Light Detection and Ranging
DEM	Digital Elevation Model
DSM	Digital Surface Model
DTM	Digital Terrain Model
EGM	Earth Gravitational Model
FGDC	Federal Geographic Data Committee
GPS	Global Positioning System
G-LiHT	Goddard's LiDAR, Hyperspectral and Thermal
NPS	Nominal Point Spacing
NAD	North American Datum
NASSDA	National Standard for Spatial Data Accuracy
RTK	Real Time Kinematic
WGS	World Geodetic System

ABSTRACT

Celik, Naime. M.S.E., Purdue University, December 2013. Identifying Ditch Geometry and Top of the Bank Location Using Airborne LiDAR Point Cloud. Major Professors: Jane R. Frankenberger and Melba M.Crawford.

The geometry of agricultural drainage ditches is very important in crop production as it impacts drainage of cropland and affects vegetation and soil erosion along the banks of the ditches. Thus, implementation of water conservation and management practices in engineered and natural ditches necessitates determination of ditch geometry along the reach of the ditch. This study explores the use of airborne commercial Light Detection and Ranging (LiDAR) technology to identify the top of the ditch banks. The method was developed to obtain the normalized cross sectional shape of the ditch using one-dimensional spline fits to ground classified points from the extracted LiDAR points in the cross sectional area and to determine the tops of corresponding banks. The method was applied iteratively along the length of the ditch. RTK GPS point validation data were collected from cross sections of seven ditches in Howard, Clinton and Boone County, Indiana. The Indiana Statewide LiDAR data products and NASA Goddard`s LiDAR, Hyperspectral and Thermal (G-LiHT) airborne imager data were used in the study. The impacts of vegetation along the ditch and LiDAR point density on the top of the bank results, as well as improvement from using the LiDAR point cloud data instead of the Digital Elevation Model (DEM) were explored.

CHAPTER 1. INTRODUCTION

1.1 Benefits of Knowing Ditch Geometry

Ditches, which are open drainage ways constructed by humans to convey excess surface water or groundwater (CBBEL, 1999), are an important feature of landscapes wherever natural drainage is not adequate. In Indiana, a vast network of ditches was dug in the late 19th and early 20th centuries to allow farming and settlement of the poorly-drained areas that existed in much of the northern part of the state. These ditches now are an important component of rural infrastructure, managed by county drainage boards and elected county surveyors (CSAbrochure, 2010).

Despite the important role played by ditches and their management by county officials, records providing information on their depth or the width of the tops of the ditch banks are not generally available, except for relatively short lengths of ditches that have been recently reconstructed. Such information could be very useful information both for officials responsible for their management, and for researchers seeking to better understand hydrology of the rural areas and develop new techniques to improve water quality from these areas. From a legal or management point of view, delineation of the ditch top of bank would be useful for determining the area of the easement in which the county surveyor or authorized representative has a right of entry. The Indiana Drainage Code(2003) states that this right extends 75 feet "measured at right angles to [] the top edge of each bank of an open drain" (IC-9-27-33). Besides the right of entry, there are a number of restrictions on landowners' use of this "right-of-way" land. Permanent structures are prohibited without written permission of the drainage board, and temporary structure, crops, and trees and shrubs are at risk if access is needed by the county surveyor or authorized representative, or if they feel that they might impede drainage.

Most counties have no map of this easement, making such restrictions difficult for landowners to understand and for county officials to enforce. Top of the bank locations for calculation of easement area is also required in other states. (Greenville County , 2013)

In addition to mapping the right-of-way, there would be conservation benefits in knowing the width of the top of the ditch. A new conservation practice called a "two-stage ditch" is being promoted as a more stable ditch shape that provides water quality benefits. According to Roley et al. (2012), a two stage ditch improves water quality by reducing nitrogen input from fields, due to the additional surface area of the benches. The wider and shallower discharge area of a two-stage ditch reduces sediment and nutrient transport (Ward & Mecklenburg, 2005).

The Ohio State Department of Natural Resources, Division of Soil and Water Conservation Report (ODNR DSWC, 2008) indicates that replacement of trees and shrubs with grass is primary water quality impairment. Hydromodification leads to a negative outcome in health of watershed. The report also points out benefits of alternative drainage design corporates with natural stream characteristics with trees. LiDAR (Light Detection and Ranging) data products could potentially be useful for monitor the desired streams vegetation in areas that discharge in to the stream existence of vegetation also would be possible using LIDAR point data.

Water volume and flow calculation involves determination of cross sectional area (Martin, 2011). Terrio (1997) used the cross-section area to calculate stream cross sectional segment volume multiplying by segment length. Williams (1986), described cross-section dimensions with the bankfull area, width, and mean depth. Estimating water capacity of a ditch also could be achieved using calculation from LiDAR derived top of the banks and normalized cross sectional shape of the ditch.

1.2 LiDAR

Airborne LiDAR (Light Detection and Ranging) systems are being used for a wide range of applications including corridor mapping (road, railways, pipelines etc.), developing Digital Terrain Models (DTM) and Digital Surface Models (DSM) for forestry and urban applications (Wehr & Lohr, 1999). As an optical remote sensing technology, LiDAR measures the time between the outgoing pulse and the scattered and reflected light to determine range by using laser pulses. (Karp & Stotts, 2012). A LiDAR system has three main components. The Laser scanner emits a laser pulse and records the returns from emitted laser pulse. Data from the Global Positioning System (GPS) determines the trajectory of the plane and the Inertial Measurement System (IMU) determines dynamic orientation of the plane via accelerometers (Schmid, 2008).

LiDAR point cloud data is typically stored in LASer (LAS) files according to specifications developed by the American Society for Photogrammetry & Remote Sensing (ASPRS). A LAS file contains point records, including 3D point coordinate, point class code and number of returns (ASPRS, 2010).

1.3 Previous Investigations of LiDAR for Determining Ditch Geometry

Due to difficulties on handling large LiDAR point data files, most studies related to stream and ditch cross sectional geometry have utilized Digital Elevation Models (DEM) derived from LiDAR. Dietterick et al., (2012) compared channel dimensions calculated from the DEM obtained from three LiDAR datasets to ground survey results. Data were acquired in 2002, 2008 and 2010 (3m, 1m and 0.49m point spacing respectively). The ground survey was implemented with a total station using 53 cross sectional transect and was performed annually from 2002 to 2011 to monitor channel change for a long-term watershed-monitoring project. Bankfull elevation, thalweg elevation and the edge of water were identified for calculation of bankfull depth, bankfull width and bankfull area for each cross section. They showed that smaller point spacing in the of LiDAR data leads higher linear correlation between LiDAR and ground survey

results on depth, width and area of the bankfull. The study showed the capability of LiDAR data by comparing the geometries from field survey data and the DEM derived from LiDAR, but did not suggest any technique for practical use of LiDAR for detection of channel geometry. G. Sofia et al. (2013) proposed a statistical method for obtaining cross sections and bankfull elevation from DTM (1m cell size) derived from LiDAR. They used a topographic index (Elevation Percentile - EP) to obtain a proxy for cross sections. The pre-selected radius of a circle was used to define a window. The center grid cell was evaluated among the cells in this window. Comparing the elevation of the central point to others in the window, the lowest value was assigned 0 and the highest value was assigned 1, if all the points had same elevation, then the center point was assigned 0.5 (Wilson & Gallant, 2000). The QQ-plot threshold approach, which assumes deviation from normality as threshold, was used to determine the bankfull elevation. The study concluded there was a high linear correlation between extracted bankfull from the DTM and measured bankfull width. The RMSE from their results ranged between ±022m to±0.53m. The study indicated that the error was dependable to resolution of the grid cells in DTM and claimed that the proposed approach actually could have smaller error than the pixel resolution. This study showed bankfull width calculation was possible with DTMs derived from LiDAR.

Faux et al. (2009) focused on three type of stream (pool riffle, plane bed, and step pool) and comparison of a DEM derived from LiDAR and ground survey results. After processing raw data, LiDAR data with 1.2/m^2 ground point density was used to create a DEM (2m grid cell). In the survey, Faux et al. (2009) measured 80 cross sections with a total station and selected five as permanent cross sections constantly monitored by PNAMP as control. The point density was 0.4-3.7 /m^2 along the bankfull channel profile. The point elevation in the DEM (0.5 m cell size) was extracted at same location as the ground survey points along the corresponding transect. To identify the bankfull locations, they utilized the hydraulic depth function, a function of flow area divided by width. The maximum value of this function was assumed as bankfull elevation. In 69% of their results, DEM overestimated the bank width. They also compared bed slope, bankfull width, and terrace elevations from field survey to those calculated from the DEMs.

Bater &Coops (2009) implemented a study to evaluate effects of the seven interpolation methods and three grid resolutions on DEMs derived from LiDAR. Results of their study indicated spline and IDW could create outliers up to 6m (Table 1 - minimum and maximum errors) in 0.5m resolution DEMs especially in areas with high slope change.

Table 1.1 DEM Statistics depending on interpolation method (Bater &Coops,2009)

Interpolation method	**Resolution**	**Mean error**	**Min error**	**Max error**	**Range**	**RMSE**	**Mean absolute**
(weight or power)	(m)	(m)	(m)	(m)	(m)	(m)	error (m)
Linear	0.5	0.00140	-3.26	4.86	8.12	0.18	0.11
Quintic	0.5	0.00150	-4.49	4.99	9.48	0.17	0.10
Natural neighbour	0.5	0.00059	-3.27	4.70	7.96	0.17	0.11
Spline with tension (2)	0.5	-0.00030	-4.80	4.76	9.55	0.17	0.10
Regularized spline (0)	0.5	-0.00022	-5.67	5.04	10.72	0.18	0.10
IDW (3)	0.5	-0.00450	-4.50	6.34	10.85	0.20	0.11
ANUDEM	0.5	-0.00350	-4.23	3.91	8.14	0.18	0.11
Linear	1.0	-0.00088	-3.53	4.82	8.34	0.19	0.12
Quintic	1.0	-0.00022	-4.69	4.95	9.64	0.19	0.11
Natural neighbour	1.0	-0.00150	-3.55	4.74	8.29	0.19	0.11
Spline with tension (2)	1.0	0.00061	-4.80	4.70	9.50	0.19	0.11
Regularized spline (0)	1.0	0.00075	-5.75	4.94	10.69	0.19	0.11
IDW (3)	1.0	-0.00410	-4.68	6.28	10.97	0.20	0.12
ANUDEM	1.0	-0.00350	-5.79	4.38	10.17	0.20	0.12
Linear	1.5	0.00160	-3.53	5.12	8.64	0.19	0.12
Quintic	1.5	0.00260	-4.69	5.21	9.90	0.19	0.12
Natural neighbour	1.5	0.00100	-3.55	4.90	8.45	0.19	0.12
Spline with tension (2)	1.5	0.00210	-4.87	4.23	9.10	0.21	0.13
Regularized spline (0.1)	1.5	0.00510	-6.76	5.09	11.84	0.25	0.15
IDW (3)	1.5	-0.00375	-4.61	7.46	12.07	0.21	0.13
ANUDEM	1.5	-0.00370	-5.01	4.35	9.36	0.22	0.13

In addition to the interpolation method, Faux et al. (2009) noted that quality of the ground point classification from non-ground LiDAR points, ground return density, and

existence of the vegetation affect the resultant DEM product quality. Interpolation errors are higher where the banks heavily vegetated. Guo et al. (2010) also indicated that topographic variability (elevation coefficient of variations) and data density have influence on accuracy of the DEM as well as interpolation method.

1.4 Research Objective

The specific goals of this research are

- to evaluate potential use of LIDAR point data and data products on determination of ditch top of the banks
- to develop and evaluate operational method for extracting ditch geometry from LiDAR point data
- to compare results obtained from the Indiana Statewide LiDAR data products and the NASA G-LiHT LiDAR data with surveyed Real Time Kinematic (RTK) GPS points
- to assess the effect of nominal point spacing and the effect of misclassified points on determination of the ditch geometry

1.5 Organization of Thesis

This thesis consists of five chapters. Chapter 1 includes introductory information about the benefits of knowing ditch geometry and top of the banks, LiDAR technology and the objectives of the research. Chapter 2 provides information about the data sets used for this study and focuses on the importance of classification of point data and methods to reclassify to misclassified LiDAR data. Chapter 3 elaborates on the methods used for identifying top of the ditch and intermediate results; smoothed ditch cross sectional shape , separated ground and non-ground points visualization. Chapter 4 examines width and height difference on top of the banks between RTK GPS and statewide LiDAR data and NASA G-LiHT LiDAR data and ditch area. Chapter 5 summarizes and draws conclusions with future suggestions.

CHAPTER 2. DATA

2.1 Remote Sensing Data Sets

Two LiDAR data sets were used in this study. The State of Indiana data was the primary data set used in the study. The National Aeronautics and Space Administration (NASA) also acquired LiDAR data over a small area containing a small part of Indiana with lower Nominal Point Spacing (NPS). This data set was included for the purpose of comparison with results obtained using the Indiana State LiDAR data set.

2.1.1 Indiana State LiDAR

The state of Indiana acquired Orthophotography (RGBI), LiDAR and gridded elevation data over a 3-year period from 2011 to 2013. The data are public domain and without warranties of the State of Indiana and its contractor Woolpert, Inc. (IN LiDAR Metadata, 2011). Figure 2.1 shows LiDAR source dates in color and their Nominal Point Spacing (NPS). Area 1 data acquired from March 13, 2011, to April 30, 2011, for ditches in Howard County, Clinton County and Boone County were used in this study. The LiDAR data were delivered in the NAD 1983 State Plane Indiana East (Feet) and the NAD 1983 State Plane Indiana West Coordinate Systems. Geoid 09 was used to reduce GPS heights to orthometric heights.

Figure 2.1 2011-2013 LiDAR source dates in color and Nominal Point Spacing (NPS) in cross hatch, (Indiana University Spatial Data Portal, 2011)

In the metadata (IN LiDAR Metadata, 2011) , horizontal positional accuracy was indicated at 95% confidence level using RMSE (r) x1.96 although no value was provided for RMSE. It was also indicated that horizontal positional accuracy report is available upon request from the Contractor Company. Vertical positional accuracy (Table 2.1) was presented for subset of data which are designated in the flight plan. The main project was separated to three tiers (Central Tier 2011, Eastern Tier 2012 and Western Tier 2013). The central tier contains three blocks. All data used in this study were from Boone, Clinton and Howard counties, which are in Block 2.

Table 2.1 Indiana State LiDAR data acquisition information

System Info	Blocks 1&3	Block 2
Type of LIDAR Scanner	Optech Gemini	LH Systems ALS50
Swath Width(feet)	4223	5678
Data Acquisition Height (feet)	7380	6500 and 7800
Scan Frequency (Hertz)	32	35.8
Ground Control Points	119	35
Pulse Repetition Rate (Kilohertz)	100	99
Missions	35	13
Field of View (Degree)	40	40
Aircraft Speed(Knots)	150	140
Distance Between Flight Lines (ft)	3,973	3,973
Number of Returns Per Pulse	Maximum of 4	Maximum of 4
RMSE for 95% confidence level	11.2 cm (0.366 ft) 12.8 cm (0.421 ft)	14.4 cm (0.472 ft)

The Indiana Statewide LIDAR point data are also available in the NSF Open Topography Facility ((http://www.opentopography.org/, OpenTopography, 2013) to download in NAD83 State Plane West and East Coordinate System and NAD83 UTM Zone 16, in LAS file or in ASCII format with a choice of unclassified points, ground classified or all class points(Figure 2.2) . The appendix contains the LiDAR Class Code table for Indiana State LiDAR (Appendix-Table A.2).

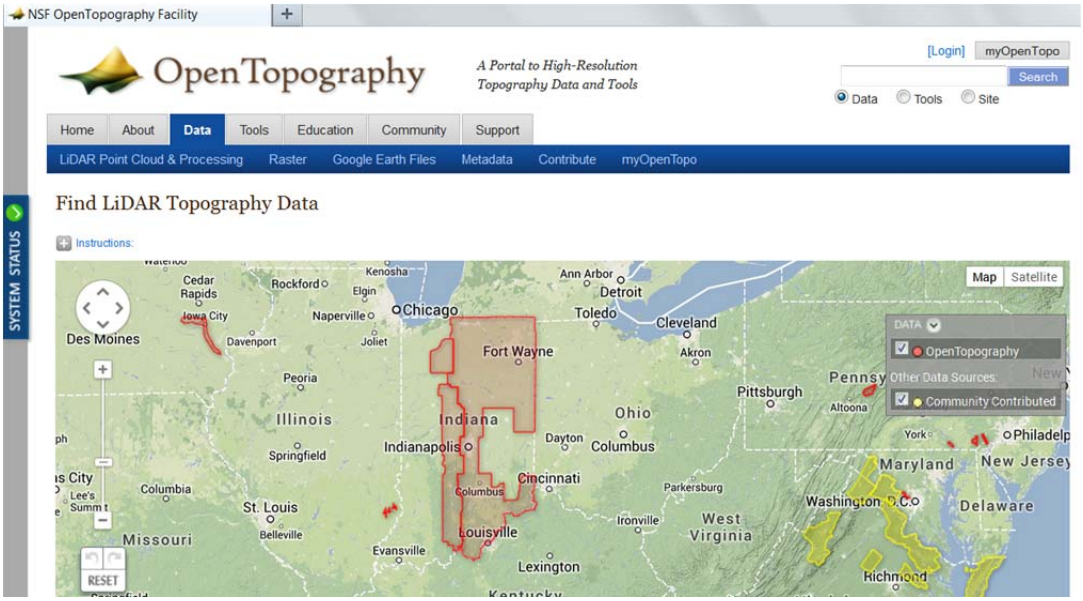

Figure 2.2 Available LiDAR data in Indiana via OpenTopography (2013)

The Indiana Department of Natural Resource conducted an independent vertical accuracy assessment of the DEM created from Indiana Statewide LiDAR data using 203 static GPS points and leveled total station points, acquired for various projects between 2007 and 2010. Those 203 points selected from 3422 points by manually checking and confirming that they had not changed. The points located in areas including repaved road, grading and excavation area were excluded. Their results indicated that vertical positional accuracy in 95% confidence level is 9.8 cm (0.32ft) RMSE for Boone County, 10.1 cm (0.33ft) for Clinton County and 9.1 cm (0.30ft) for Howard County (Wilkinson& Wilkinson, 2013).

2.1.2 NASA G-LiHT LiDAR

The recent NASA data set was acquired by multi-sensor instrument system called Goddard's LiDAR, Hyperspectral and Thermal (G-LiHT) airborne imager (Cook et al.,2013) The data tile used for this research obtained from webpage, ftp://fusionftp.gsfc.nasa.gov/G-LiHT/ with an acquisition date of June 2012. The

horizontal coordinates are WGS84 UTM Zone 16 and vertical coordinates (orthometric heights) were referenced to Earth Gravitational Model 1996 (EGM96). During point data acquisition, single-solution GPS-INS was used and real time differential correction was performed using OmniStar HP. Due to lack of a base station, vertical offset bias occurs (<1m) for absolute accuracy of the LiDAR data. Relative accuracy of the points is less than 10cm. (Cook et al., 2013) G-LiHT LiDAR points were spaced 0.23 m apart within a line perpendicular to the flight direction and 0.57 m between lines with a nominal aircraft speed of 110 knots. Riegl VQ-480 Airborne LiDAR Scanning Instrument was used to acquire points (Cook et al., 2013). Data products are freely available for public use under NASA's Data and Information policy (http://gliht.gsfc.nasa.gov). Figure 2.3 shows measurement characteristic of the G-LiHT airborne imager.

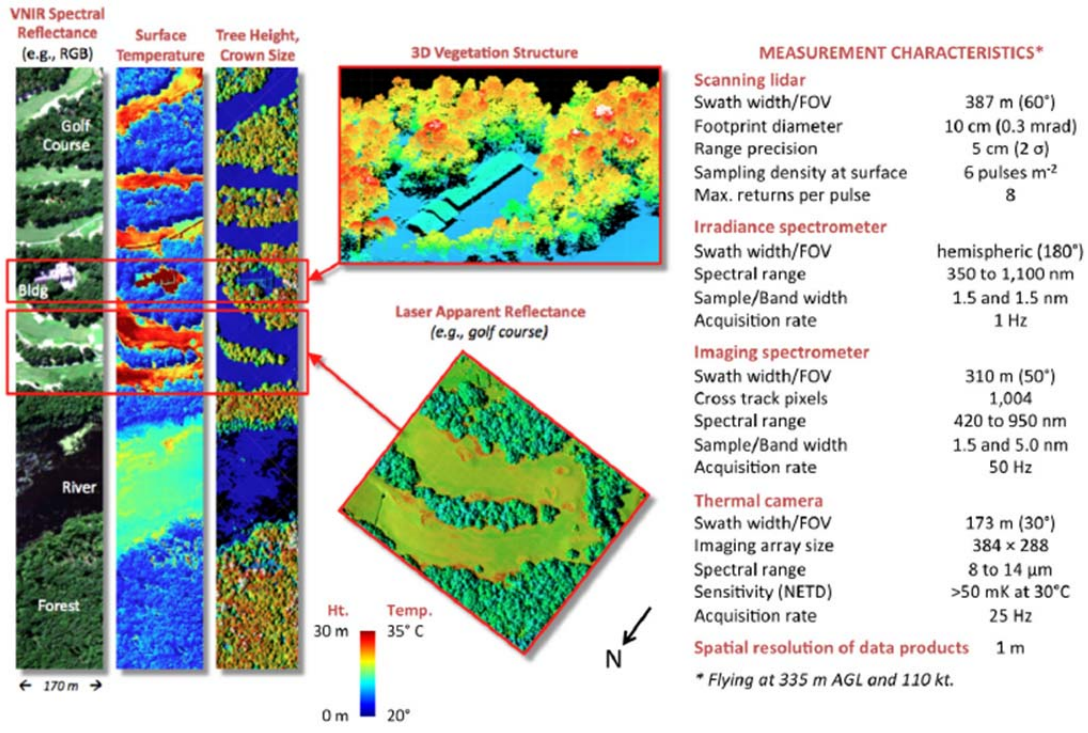

Figure 2.3 Measurement Characteristics of Goddard's LiDAR, Hyperspectral and Thermal (G-LiHT) airborne imager (Cook et al., 2013)

Horizontal coordinates of the data were projected to NAD83 UTM Zone 16 using ArcGIS software. After conversion of the EGM96 orthometric heights to Geoid09 orthometric height, still about 1.1m vertical offset was observed between RTK GPS and G-LiHT LiDAR points. To make visual comparison possible in our method, 1.3m offset was added to heights of G-LiHT LiDAR points.

2.1.3 Pre-Processing of LiDAR Data

2.1.3.1 Using ASCII Format LiDAR Data

LiDAR data format prescribed by ASPRS for LAS files which is a binary data format that contains point data records. ASPRS (2013) indicated two problems with ASCII (American Standard Code for Information Interchange) relative to LiDAR point data; 1) large data size, which slows down the processing, and 2) all information is not retained in the ASCII format.

To process LiDAR data in MATLAB programming software, it is necessary to either use the ASCII format or read and convert the binary data via other programs. However, for large data sets, reading LAS data format may take minutes in MATLAB (with LASRead (2008) exchange file for 1.1 Format). To overcome slow processing performance of MATLAB with LAS format for this study, ASCII files in which LiDAR point data were clipped with polygon shape files over the study area. Public domain FUSION software (McGaughey, 2013) and some LASTOOLS software (Isenburg,2013) commands were used to extract these subsets. ASCII format LiDAR data can also be obtained from OpenTopography, which archives nationwide data and provides a portal for downloading LiDAR point data as raw file (LAS or ASCII format) or the DEM derived from LiDAR in specified locations. ASCII format LiDAR point files also contain the assigned point class, which was used in this study. Statewide LiDAR data was obtained as ASCII format from OpenTopograpy and G-LiHT LiDAR data were converted to ASCII format via FUSION and LASTOOLS software.

2.1.3.2 Digital Elevation Model (DEM) Derived from Indiana State LiDAR

The DEM also was derived from acquired LiDAR data, which has 1m or 1.5m Nominal Point Spacing (NPS) depending on the County based data purchase agreements. The contractor standardized the statewide DEM in 5-foot (1.52 m) NPS. Points classified as bare-earth were used for developing the DEM. Hydro-flattening was also applied for lakes, stream and rivers wider than 30.5 meters. The Interpolation method for DEM was not specified in the metadata.

2.1.4 Indiana State Orthoimagery

Indiana Statewide Imagery were acquired at the same time as the statewide LiDAR. Figure 2.4 shows map for Orthophotography source dates and their spatial resolution.

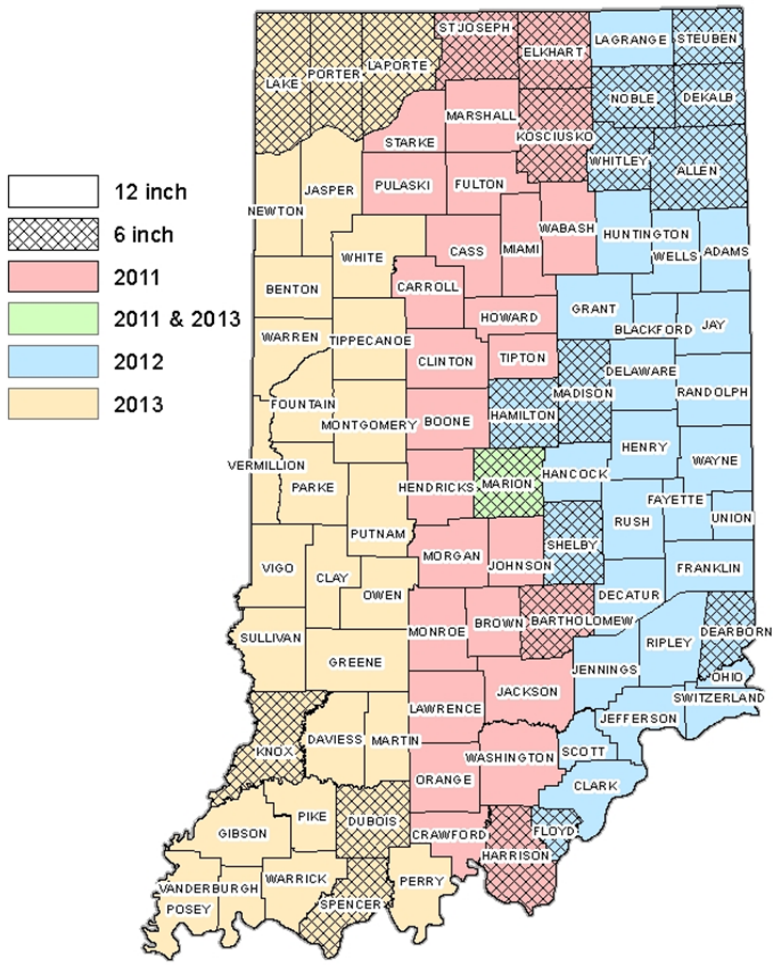

Figure 2.4 IndianaMap 2011-2013 Orthophotography Source Date and Spatial Resolution (Indiana University Spatial Data Portal ,2011)

The orthoimagery was utilized in this study as a base map for digitalizing the stream points. The data for the Howard, Clinton and Boone Counties have 12-inch (30.48m) resolution with four bands (RGBI).

2.2 Ground Reference Data Set

Ground reference data were also obtained to evaluate the LiDAR data and methods for extracting ditch geometry. Using a Real Time Kinematic (RTK) Global

Positioning System (GPS) ground data were collected at sites in central Indiana where the Indiana State LiDAR data acquisition was completed in 2011. Seven sites were surveyed. However, three were found to have undergone construction between the LiDAR data acquisition date and ground survey. Those three were not included in this study.

2.2.1 Survey Sites

Sites were identified in counties where LiDAR data were available for survey in May 2013 within 100km of Purdue University Campus. Contacts were made through the Soil and Water Conservation Distinct and the County Surveyor's office. The appendix contains maps of sites showing the location and collected points. Table 2.2 provides an overview of the sites.

Table 2.2 Survey Sites Permissions

Site No	Ditch Name	County	Land owner permission allowing access to the study sites	Longitude (Degree)	Latitude (Degree)
1	Browns Wonder Creek	Boone	Scheryl Vaughn, District Administrator with the Boone County Soil and Water Conservation District	-86.422631	40.090621
2	Man Ditch	Clinton	Ben Reinhart, Resource Conservation Specialist with Clinton County Soil and Water Conservation District	-86.446723	40.269772
3	Little Potato Creek	Clinton		-86.543606	40.246103
4	Honey Creek	Howard	Sarah Brichford, Water Quality Specialist and Greg Lake, Deputy Surveyor	-85.950090	40.550386
5	Cannon Goyer	Howard		-86.088953	40.470059
6	Rice Bell	Howard		-86.387471	40.514748
7	Goodland	Newton	Chris Knochel, Newton County Surveyor	-87.287722	40.764988

Obtaining permission to do surveying and transportation as well as availability of the LiDAR data influenced survey site determination. The selected sites had also not experienced major modification after the LiDAR data acquisition.

2.2.2 Collection of RTK GPS Data with the In-CORS Network

Ground reference points were collected via a Topcon HYPERLITE-Plus GPS receiver and Topcon FC-250 data collector provided by the Purdue Agricultural and Biological Engineering Department. The Indiana Department of Transportation (INDOT) provided the Continuously Operating Reference Station (CORS) Network, which provides Real Time Correction Message (RTCM) by using Network Transport of RTCM via Internet (NTRIP).The wireless capability of Topcon FC-250 was used in conjunction with the In-CORS network for the RTK GPS surveys. Depending on chosen mount point, the data can be processed at the rover or at the server. From the available mount points, RTCM 3.1 Max and RTCM 3.1 I-Max were used. The data collector configuration followed Topcon documentation (Cantu, 2011). Using the In-CORS Network with those mount points requires the use of Geoid12A and NAD83 (2011) Reference Frame for Ellipsoid. In accordance with Topcon (2012) documentation, the transformation parameters between NAD83 to WGS 84 were set to zero and a new geoid file were uploaded into data collectors.

The RTK GPS point accuracy tested with rapid static measurement of three points in the Agricultural Mall at Purdue University was compared to RTK GPS measurements. The output rapid static GPS measurement in RINEX file format was uploaded to Online Positioning User Service (OPUS) and corrected point information was received by email. Error between corrected rapid static GPS points and RTK GPS points were calculated as instructed in Geospatial Positioning Accuracy Standards by Federal Geographic Data Committee (FGDC, 2013). The resulting RMSE for horizontal position was ±0.014m and for vertical position ±0.027m. In 95% confidence interval for horizontal position is ±0.024m and for vertical position ±0.053m. The calculation details were included in the appendix A-Table A.3.

2.2.3 RTK GPS Point Data Collection

Data were collected between May 12, 2013 and August 15, 2013. At each site, cross section point data were collected as approximately straight lines and perpendicular to the stream direction. RTK GPS points were spaced at approximately 0.5m intervals and additional locations, which had visible changes in slope. Cross sections were at least 10 m apart. Table 2.3 shows the number of cross sections for survey sites and LiDAR data availability. Cross sections were extended at least 5m or more beyond the top of the bank, although, in some sites, existence of the corn and soybean crops prevented collection of extended point data. Figure 2.6 shows crops bordering survey site 3. Points were also collected along the stream at approximately the deepest points (thalweg).These stream points were collected approximately 0.5m apart and except for site 4 and continuous along cross sectional site area. Each cross section and center point was separated by using different codes during the survey. Figure 2.5 shows an image during RTK GPS field survey at Site 1 and Figure 2.7 shows RTK GPS surveys during stream center (thalweg) point collection at Site 4.

The lowest values of the RTK GPS points do not correspond to the lowest value of the LiDAR points in survey area if there is water in the ditch, LiDAR data acquisition via the LiDAR scanner of the LH Systems ALS50 cannot penetrate to the water to obtain depth (Abbitt et. al., 2011).

Table 2.3 Survey Site and Survey Dates

Site No	State LiDAR NPS (m)	Number of Cross Sections	Survey Date	County	Description
1	1	5	8/15/2013	Boone	Available State LiDAR
2	1.5	5	7/22/2013	Clinton	Available State LiDAR
3	1.5	5	7/22/2013	Clinton	Available State LiDAR
4	1.5	5	8/1/2013	Howard	Available State LiDAR and G-LiHT LiDAR
5	1.5	4	7/2/2013	Howard	Undergone Construction
6	1.5	5	6/12/2013	Howard	Undergone Construction
7	-	5	6/24/2013	Newton	No LiDAR Data

Figure 2.5 Cross Section RTK GPS field survey at Site 1

Figure 2.6 Example of crops bordering the RTK GPS field survey transect at Site 3

Figure 2.7 RTK GPS Stream center (thalweg) points collection at Site 4

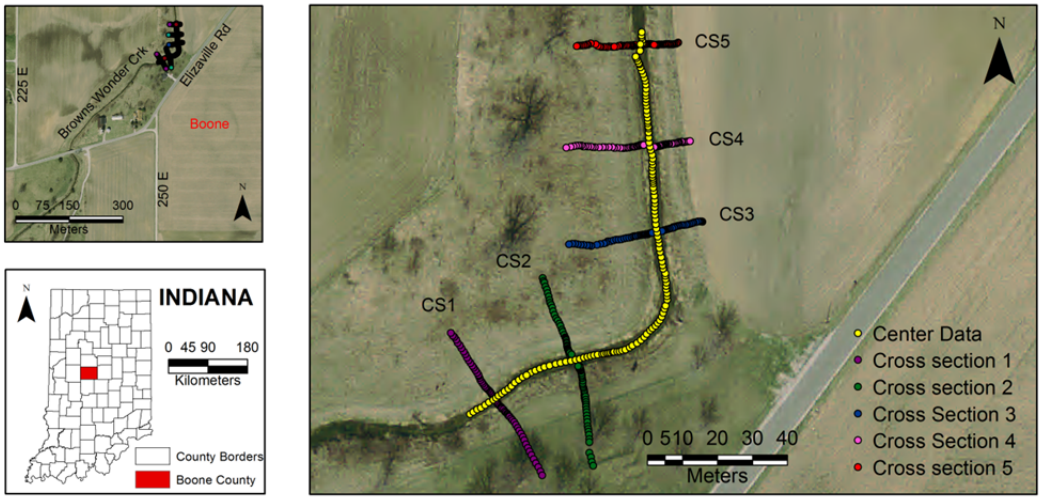

Figure 2.8 RTK GPS Points after data collection at Site 1

Figure 2.8 shows a map for collected RTK GPS points over Indiana State Orthoimagery. The maps for other survey sites were included in the appendix A. The known specific location of the stream points and cross section points were used as shown in Figure 2.9.

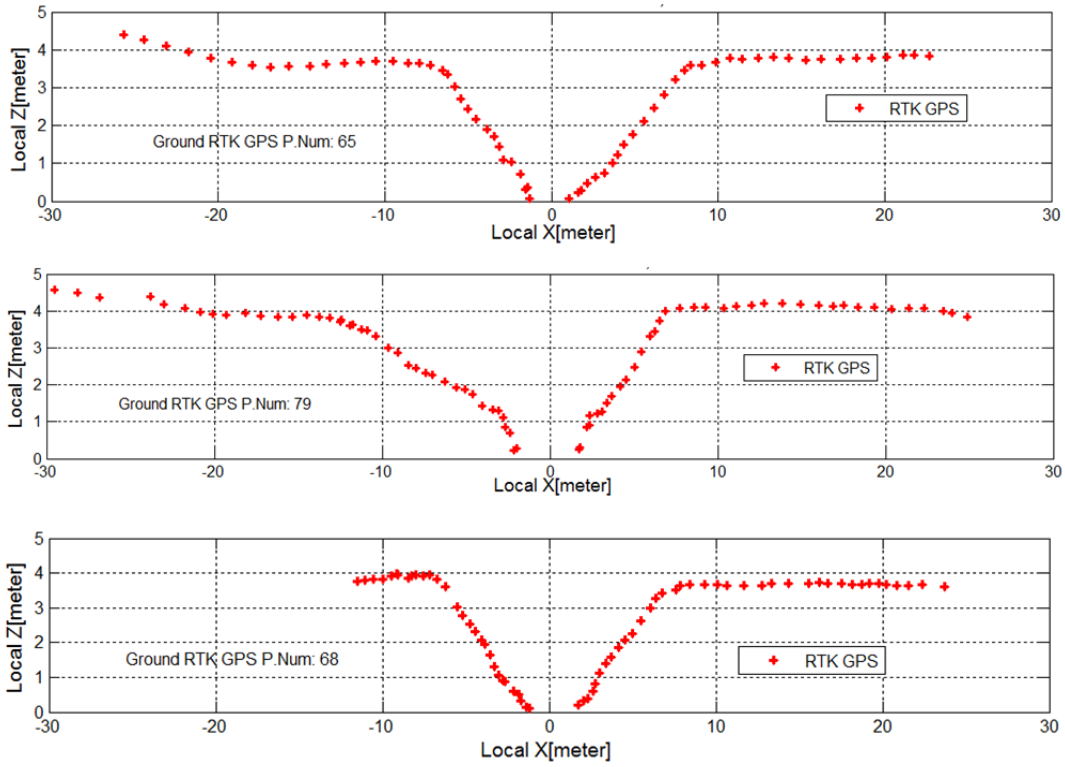

Figure 2.9 Cross-Sections 1, 2 and 4, RTK GPS Points at Site 1

2.3 Point Cloud Data Classification

2.3.1 Classification Methods Used by Data Providers

Classification of the LiDAR data was extremely important because the ground point data was being used to determine top of the banks. According to Indiana Statewide Imagery and LiDAR Program Airborne LiDAR Report obtained from Woolpert Inc. (2011), the classification and DEM processing was performed with TerraScan v.11.006 and TerraModeller commercial software. TerraScan works with MicroStation CAD software from Terrasolid Ltd. The classification process was comprised of two phases; 1) building a temporary Triangular Irregular Network (TIN) on initial ground points, which are ground points after the lowest points filtered out, and 2) including new points in the TIN according to the user-defined parameters, which elevates the model iteratively. The user-defined parameters include terrain angle, iteration angle (maximum angle between

point to projected plane on triangle) iteration distance (maximum distance from point to triangle), and maximum building size (for initial points), (Soininen, 2009). The maximum building size provides information to the software such that in the user-defined size of the terrain (ex. 60m by 60m area), there would be at least one ground point. The software builds initial ground points from the lowest points of those building size areas. Until reaching the user defined other parameters of iteration angle and iteration distance, the ground points is being added up and ground model is being lifted. Other iteration parameters determine the proximity of a point to triangle to be chosen as ground (Soininen, 2011). Finding the best parameters for TerraScan software requires much trial and error (Habib et al., 2009) although, selection of parameters determines the quality of the point classification. TerraModeler creates terrain surface models (DEM or DTM) from classified points. The lowest or height points within search radius or closest point to mouse click points can be reclassified from classed points to create surface (Soinine 2011).

NASA`s G-LiHT LiDAR was classified as ground and non-ground using Riegl's RiPROCESS software that employs a progressive morphological filter (Cook et al., 2013) which is based on opening (erosion with dilatation) and closing operations (dilatation with erosion) via the user defined window size (Zhang et al, 2003) to identify ground points.

During the experiments with G_LiHT LiDAR and Indiana State LiDAR data, it was observed that in some of locations, data contained points on the top of the banks that were misclassified as non-ground. That misclassification of points became one of the sources of error in this study. Figure 2.10 shows LiDAR points on same location as the RTK GPS points surveyed (Cross Section 2- Site 4) and were extracted with 60m by 2m cross sectional box. The LiDAR points were also colored according to their class code; green is non-ground, dark blue is ground points. The bank tops were shown as non-ground instead of ground. The figure 2.11 shows Indiana State LiDAR points (Cross Section 1 and Cross Section 5 at Site 4) and banks were also classified as non-ground.

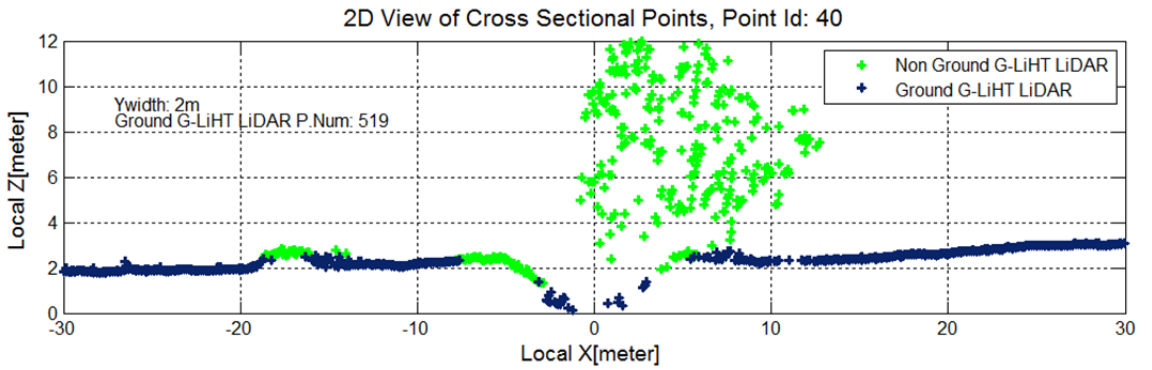

Figure 2.10 NASA G-LiHT LiDAR points, class information shows top of the bank as non-ground (green)

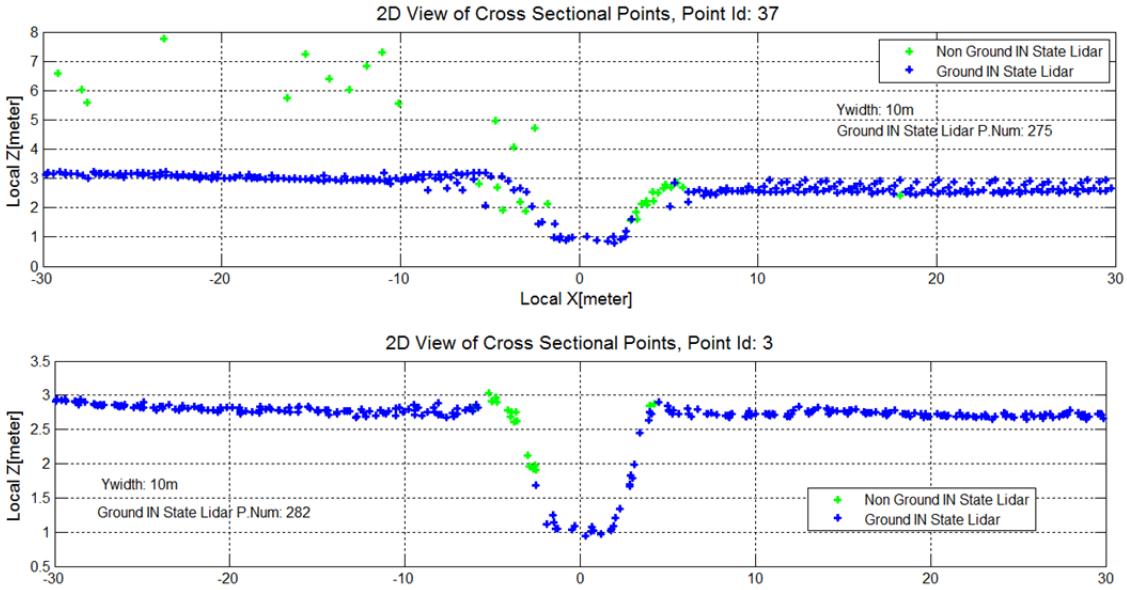

Figure 2.11 IN State LiDAR points, class information shows one side of the bench as non-ground.

The DEM and DSM are commonly used LiDAR derived products. To process the LiDAR data properly, correct classification of the LiDAR point data is necessary (Ma, 2005). After misclassification of the State LiDAR data on the top of the banks was observed, the DEM was also investigated. DEMs were obtained from Indiana University

Spatial Data portal, where they were archieved in State Plane coordinates. The data were re-projected to UTM NAD83 Zone 16 coordinate system and converted to ArcGIS Arcgrid format to facilitate use of the DEMs in MATLAB. In MATLAB, reference matrix in Ascii grid file contains the coordinates of the DEM Z matrix. The center location coordinates were obtained by using **pixcenter** command in MATLAB with Z matrix and reference matrix. The **map2pix** command was used to find the row and the column of the stream data. The study area was extracted from the DEM by using these row and column coordinates.

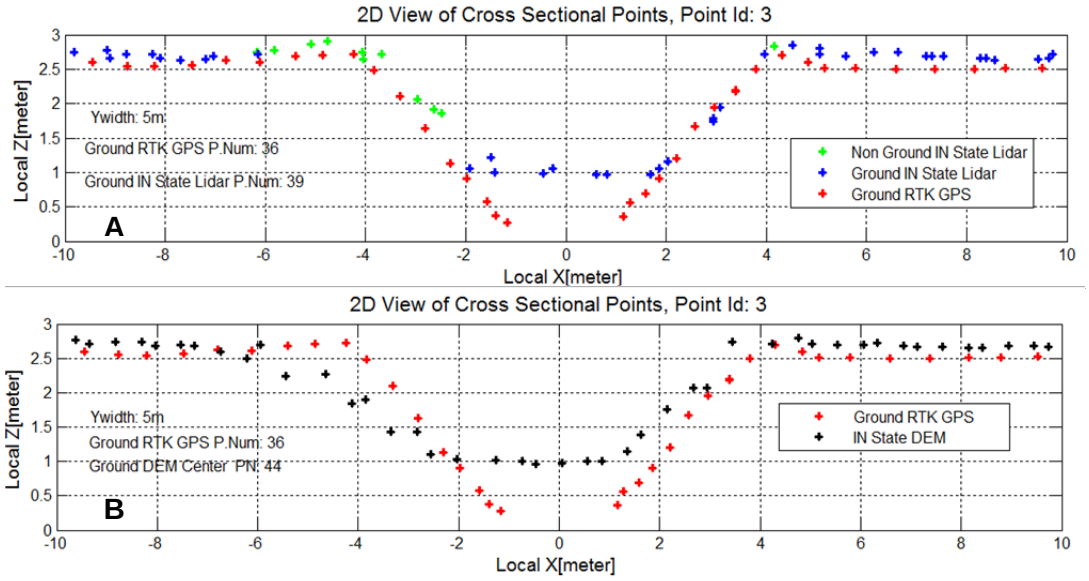

Figure 2.12 RTK GPS was compared to LiDAR points (A) and DEM center points (B) in Site 4 Cross Section 5

In comparison A of Figure 2.12, RTK GPS points were plotted with LiDAR points within the 20m by 5m cross section box. In left side of Figure 2.12-A, LiDAR points classified as non-ground in location (-4, 2.5) that RTK GPS showed as ground. In Figure 2.12-B, RTK GPS points were compared with the DEM grid center locations. Due to misclassification ground points, DEM grid center points are below than RTK GPS points and top of the bank was located further to left than the actual location. In Figure

2.13, misclassified points are shown on the right side. As seen on Figure 2.13-B, the top of the bank was stretched further.

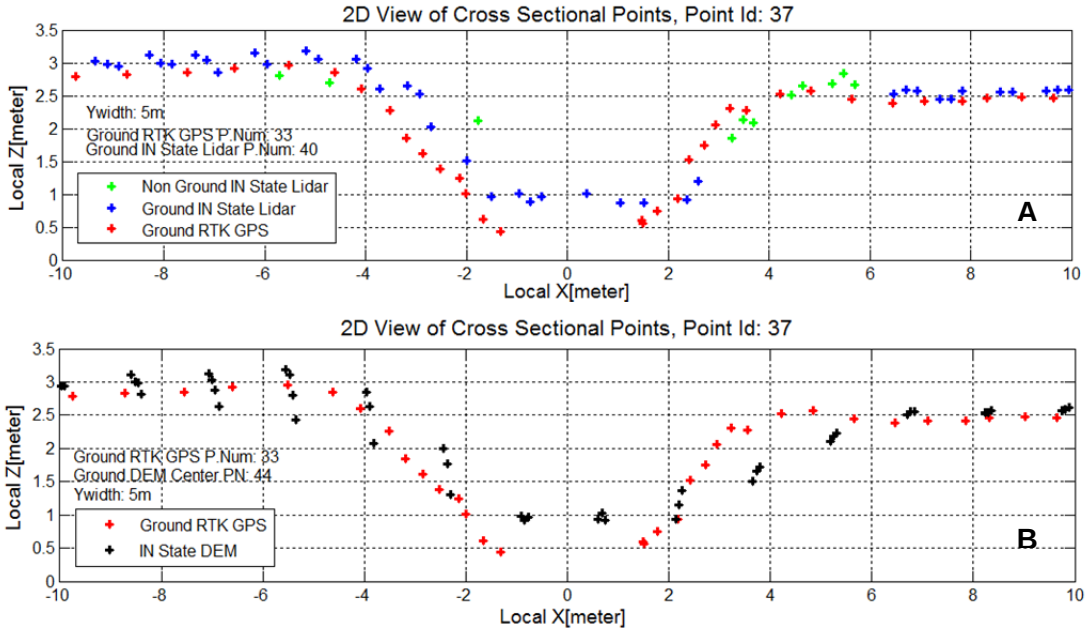

Figure 2.13 RTK GPS was compared to LiDAR points (A) and DEM center points (B) in Site 4 Cross Section 1

2.3.2 Reclassification of LiDAR Data

Due to misclassified points, the resultant spline could not pass through actual top of the banks. Reclassification of the data was investigated using LASTOOLS and MCC_LIDAR point classification software. The LASTOOL **lasground** command was used for classifying ground and non-ground points .The algorithm of LASTOOLS are based on progressive densification method which was developed by Axelsson (2002). Korzeniowska et al., (2013) also discussed the LASTOOL classification algorithm. The same algorithm was used by Pérez-García et al. (2012).The process starts with using small number of points to create an initial ground classification and initial surface. A TIN is used to generate this surface from the lowest points. New points are added iteratively to the initial ground points. All points are evaluated in those iterations based on the distance

from triangles to points and angles between points and triangle vertices. In LASTOOLS the **lasground** command has an extra fine and ultrafine option that use spike and step values to separate ground from non-grounds. The user also can determine step and spike parameters manually.

An alternative open source software was also investigated. MCC_LIDAR combines curvature filtering with scale factor and a variable for curvature tolerance (Evans &Hudak, 2007). Ground points are segregated from non-ground points if the positive curvature threshold is exceeded. The curvature filtering is based on the virtual deforestation (VDF) method (Haugerud, & Harding,2001) and implements a despike algorithm which creates a TIN, finds points with strong curvatures on surfaces, and segregates those point as non-ground until only a few or no points remains. MCC_LIDAR uses scale factor to avoid creation of large triangles, and curvature tolerance to compensate for slope effect (Evans &Hudak, 2007). The user needs to provide a scale ('s') and curvature threshold ('t'). In addition to suggesting post spacing of the LIDAR data as scale and a spatial sampling frequency (pulse/m^2) as curvature threshold, authors suggests a trial and error method to find the best parameters for the user`s data.

2.3.2.1 Selection of Parameters for LASTOOLS Data Classification

In this section, different parameters setting were investigated to determine ideal values to classify the data. The reclassification parameters applied to entire LiDAR data subset of the survey sites and effects of different parameter setting were inspected on LiDAR points extracted by cross sectional box. Figure 2.14 shows an image from Site 4 -Cross Section 2 and extracted G-LiHT LiDAR points via 60m by 2m cross section box. The class codes from the original data show both top of the banks were represented with non-ground points.

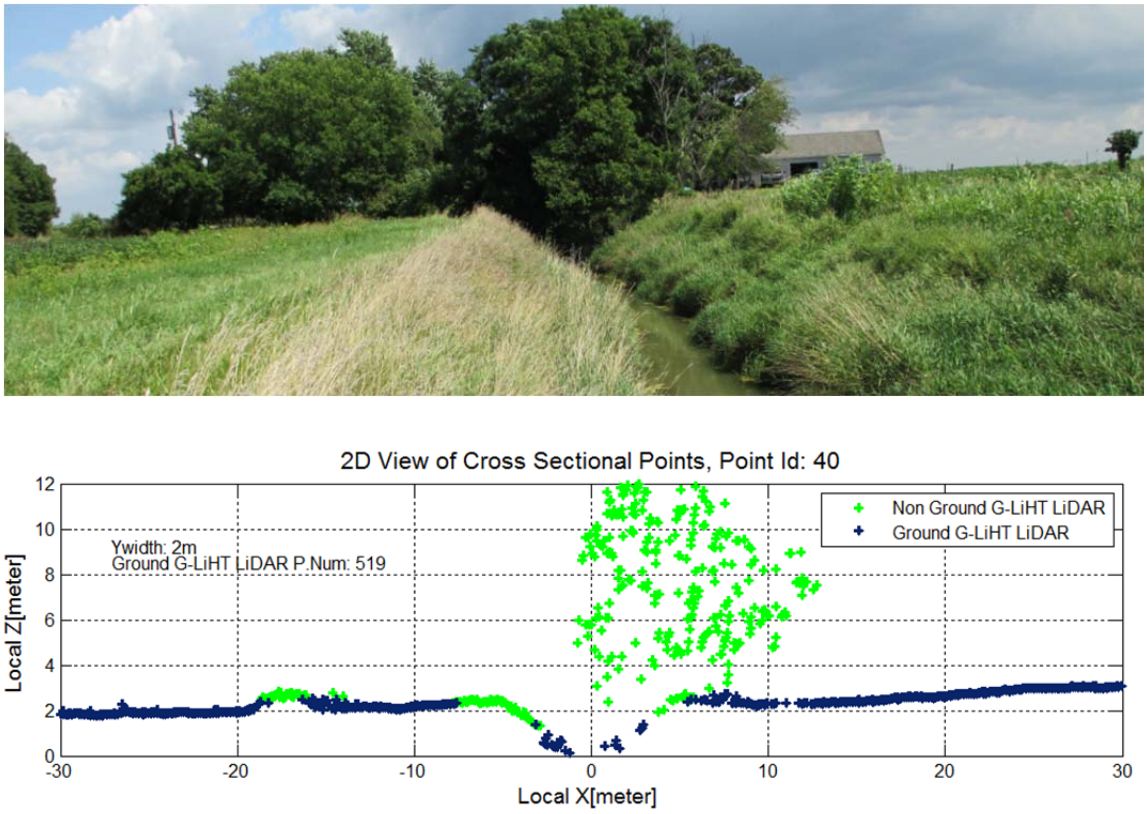

Figure 2.14 Site 4 Cross Section 2- Original G-LiHT Classification

In applying the LASTOOLS **lasground** command, ultrafine option (step value was defined as 5m and spike 1m) was investigated with other manual step and spike parameters. Figure 2.15-A shows the vendor`s classification (on left side, the top of the bank was shown with non-ground points in red circle). Figure 2.15-B demonstrates the ultrafine option results that the top of the banks have points classified as ground. Figure 2.15-C shows classification result with the same step value (5m) as ultrafine option and smaller spike parameter value (0.2m). With smaller spike value, the top of the banks were represented with fewer ground points and the total number of ground points dropped from 591 to 499. 2.15-D shows classification result with same spike value (1m) as ultrafine option and smaller step size (0.5m). The total number of ground points increased from 591 to 617 and some points on the tree (in red circle above the ditch) were represented as ground due to inadequate step size.

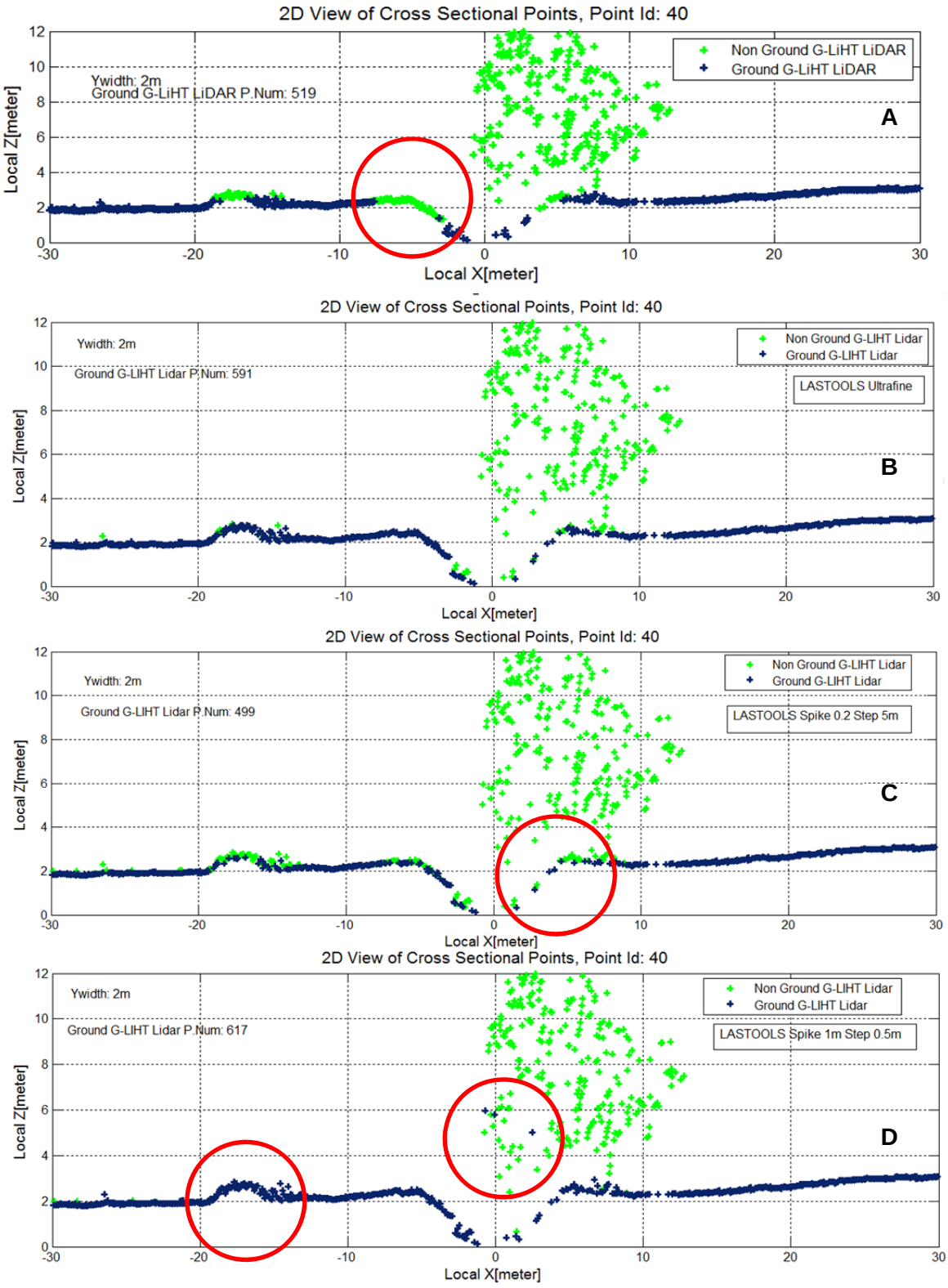

Figure 2.15 LASTOOLS Ultrafine (step 5m/spike 1m) ground classification versus the effect different spike and step parameters on data

When the step value was the same but different values were specified for the spike parameter, the smaller the magnitude of the spike, the smaller the resulting number of points classified as ground. With the same spike value, effects of step varied depending on terrain attributes. If different step values are used in flat areas, results do not change. If larger step value became effective in steeper areas, rougher terrain has more non-ground points.

The LASTOOLS commands works via Command Prompt. After browsing the folder of the command, the user provides a command as shown in the following examples.

lasground -i inputname.las –o outputname.las –ultra_fine

lasground -i inputname.las –o outputname.las –extra_fine

lasground -i inputname.las –o outputname.las –spike 1 –step 10

Then to convert results to ascii files contains X, Y, Z and Class Code

las2txt –i outputfromlasgroundname.las -o outputname.txt –parse xyzc

2.3.2.2 Selection of Parameters for MCC_LIDAR Data Classification

For MCC_LIDAR the suggested scale value was the NPS of LiDAR data or the object size. For the curvature threshold, it was suggested to start from 0.3 and use a grid search on smaller and larger values. MCC_LIDAR also works in command prompt as in following example

mcc_lidar –s 1 –t 0.3 inputname.las outputname.las

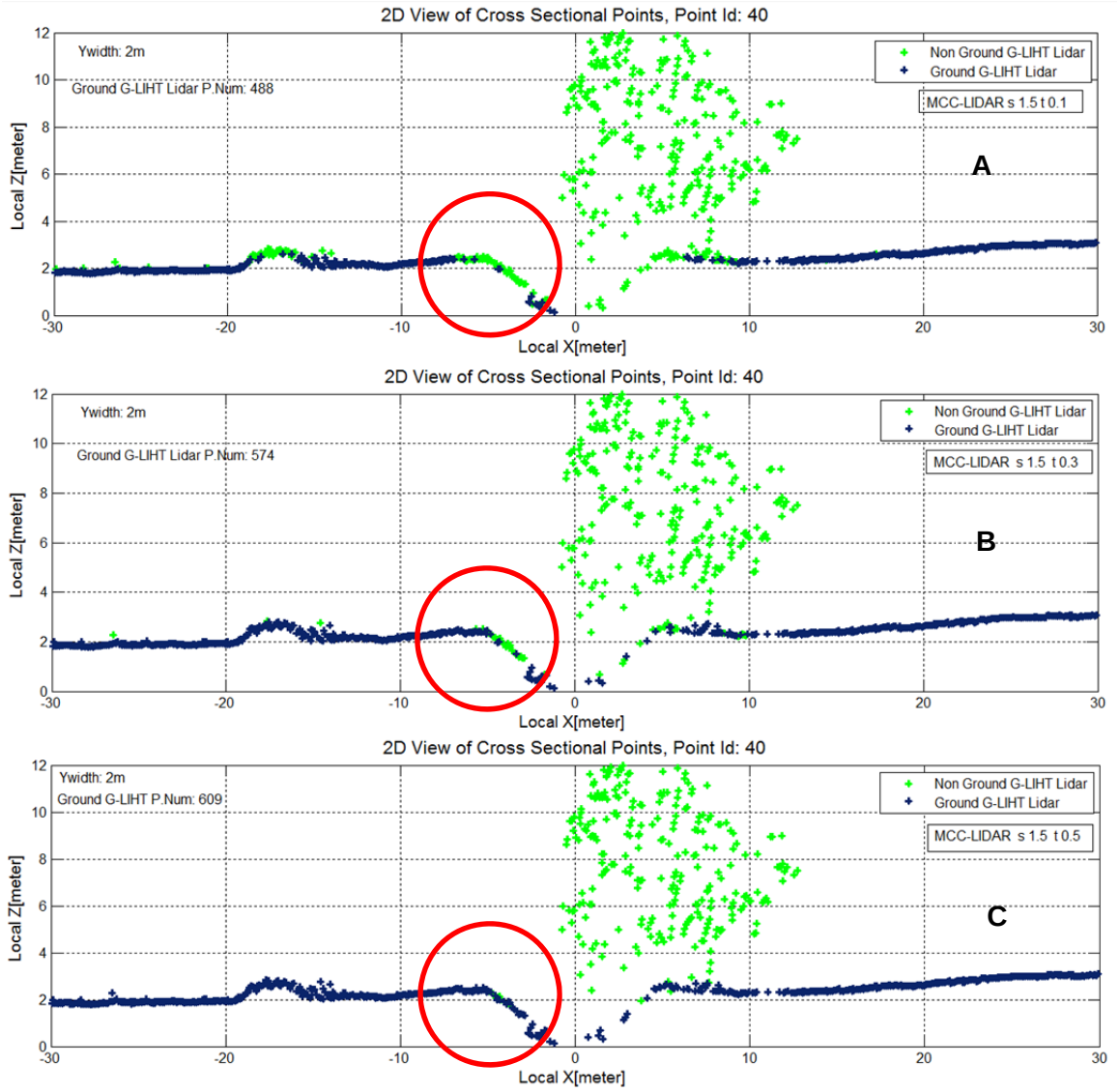

Figure 2.16 Effect of different values of the curvature (t) parameter in MCC_LIDAR

The impact of changing the curvature parameter is shown in Figure 2.16. The scale was held constant (1.5) and the curvature parameter was changed. Figure 2.16-A shows the top of the banks as non-ground and Figure 2.16-C shows same area as ground. The larger the curvature value, which indicates the threshold for considering a feature as non-ground, the more points were classified as ground.

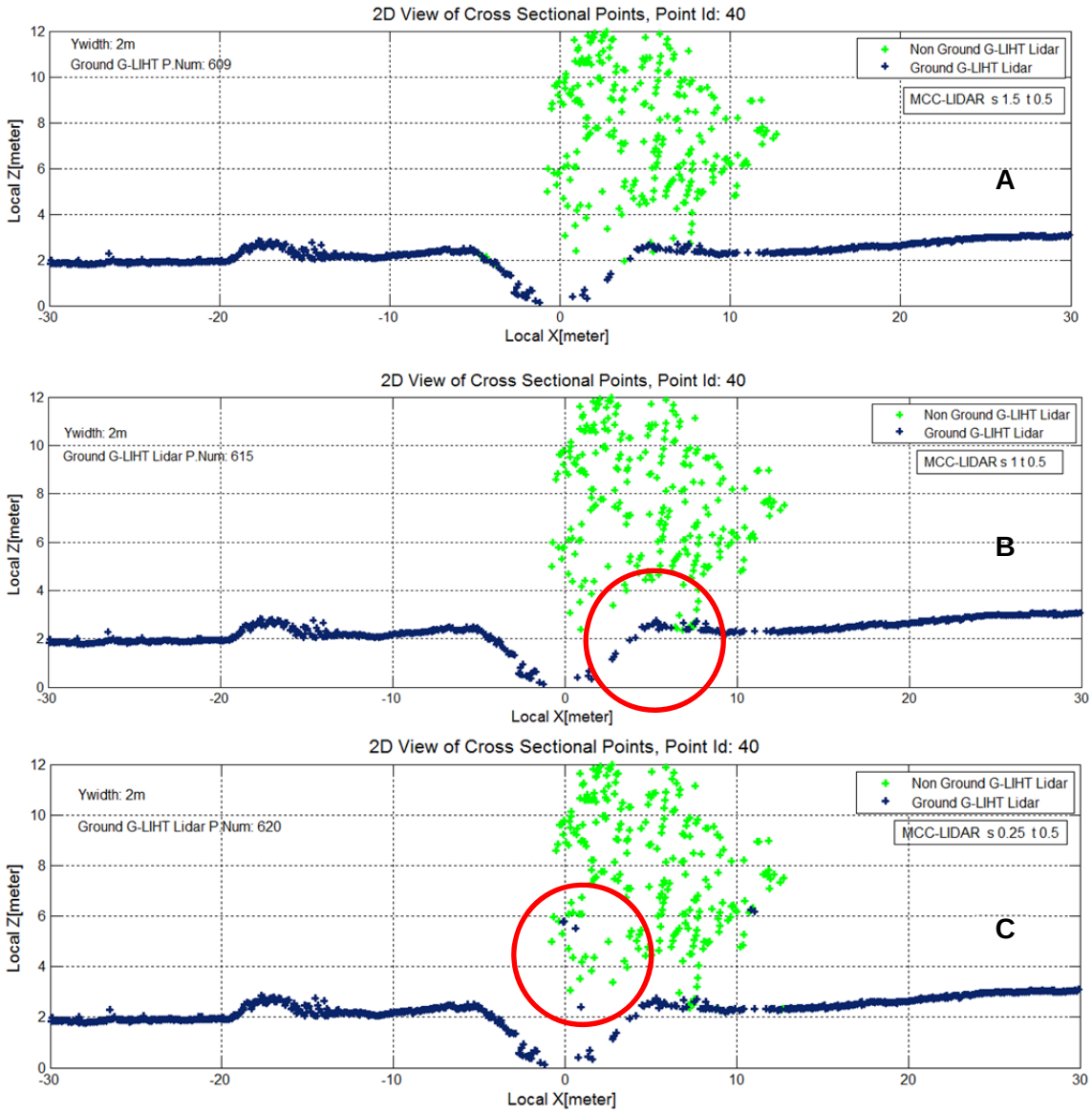

Figure 2.17 Effect of different values of the scale (s) parameter in MCC-LIDAR

The effect of the scale value also was investigated where the curvature was held constant (0.5) and the scale parameter was changed. Figure 2.17-A has the largest scale parameter value (1.5) resulted with total 609 ground points, and Figure 2.17-C has the smallest scale value (0.25) resulted with 620 ground points and some of the points were located on the tree with ground class code. Figure 2.16 and Figure 2.17 indicate for ditches in this study, ground classification obtained with value of 1.5 for the scale

parameter and value of 0.5 for the curvature parameter could be considered sufficient. After processing classification, LASTOOLS was also used to convert results to ASCII format.For Indiana State LiDAR, LASTOOLS ultrafine option and MCC-LIDAR 1.5 scale and 0.3 curvature value provided sufficient ground classification.

CHAPTER 3. METHODS FOR IDENTIFYING THE TOP OF THE DITCH BANK

Previous studies applied an interpolation method over all the LiDAR point data and used the resulting DEM to determine ditch geometry (Dietterick et al.,2012, Sofia G. et al., 2013 , Faux et al.,2009).The method proposed here used actual ground classified LiDAR point data. Cross section box was defined by the user with width X and Y and, all points within the box were selected (Figure 3.1).

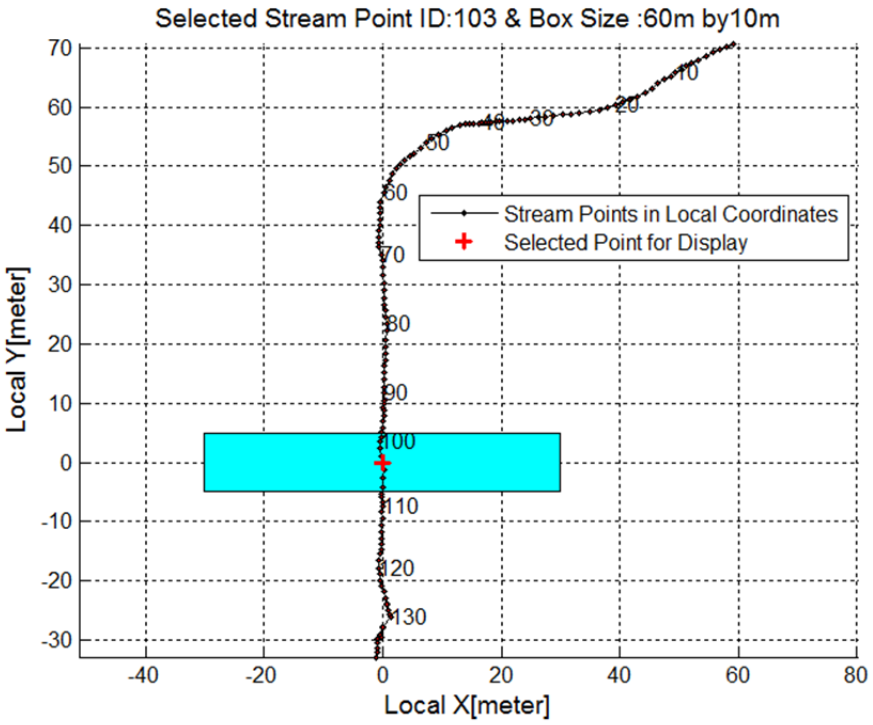

Figure 3.1 Cross section box overlaid on selected stream point

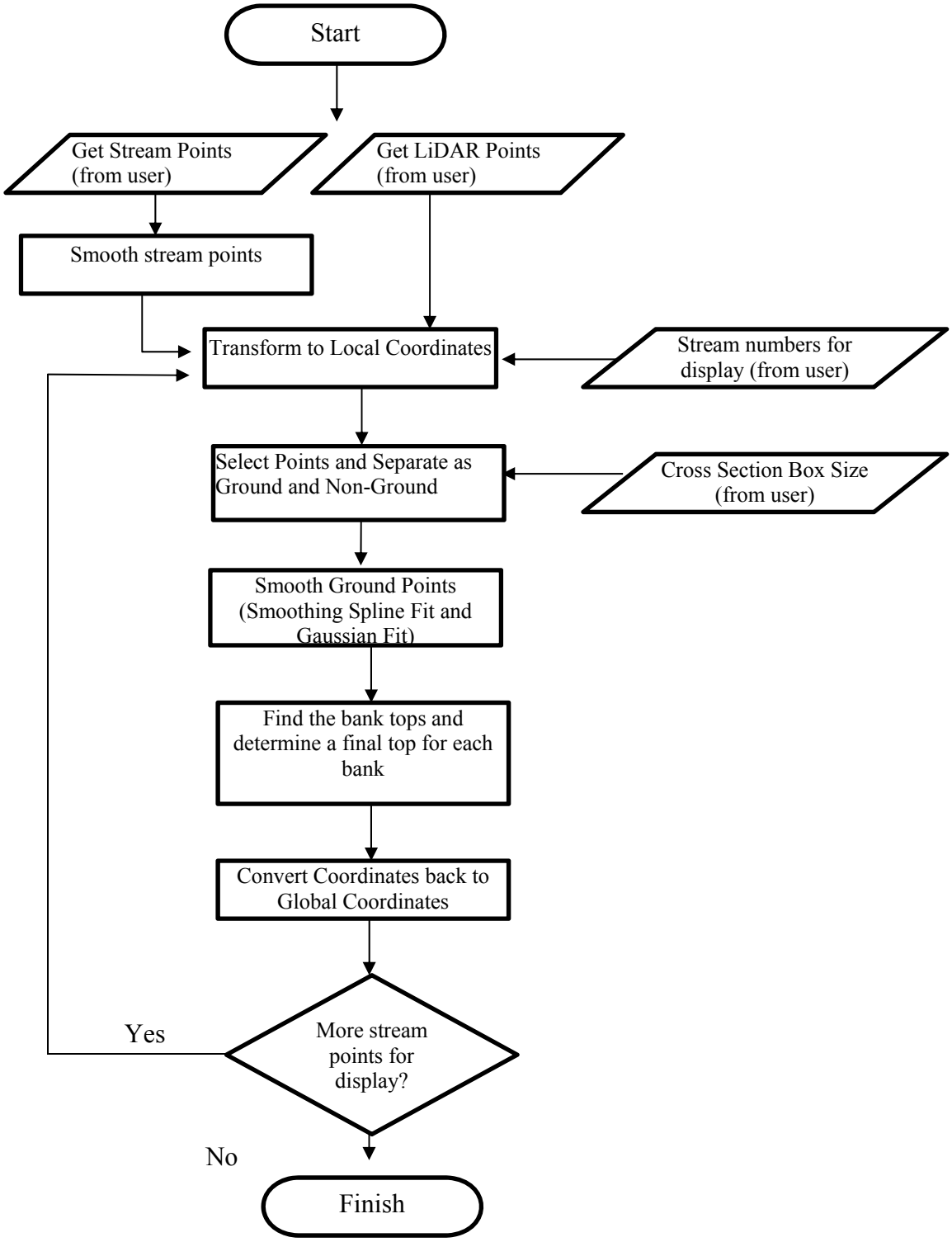

Figure 3.2 Process Flowchart of the Method

The cross section box was placed perpendicular to the stream direction in user specified stream point location or locations, and LiDAR points were extracted. The extracted points were converted to local coordinates and processed as described below to determine locations of the top of the banks. In addition to final calculation of the top of the banks, a smoothed shape of the ditch and separated ground and non-ground points were obtained in intermediate steps in local coordinates that depend upon stream point location and converted to global coordinates belonging to the initial input data set.

3.1 Obtaining and Smoothing Stream Points

3.1.1 Obtaining Stream Points

The stream points were obtained with multiple approaches; 1) RTK GPS Survey, 2) Digitizing from Indiana State Orthoimagery via MATLAB and ArcGIS software. Surveyed stream points were used to compare results of the top of the banks for the cross sections obtained from RTK GPS and LiDAR points. The digitized stream points were used as a part of proposed method to obtained top of the banks for entire sections of the ditches. Points were digitized in two steps for ArcGIS. The line feature class was created by connecting locations where the streams were curving in the orthoimagery. After digitizing the line, another feature class was created by constructing equal distanced points with the 'Construct Points' command in the Editing Tool in ArcGIS. The feature class was defined in a shp format. The points were also digitized in MATLAB using a script that reads the orthoimagery. In the script, the user zooms the stream location and clicks the location of the stream where it is curving. The script then interpolates the points between the user-initialized points. Figure 3.25 in section 3.6 shows digitizing steps in MATLAB. Since digitized points did not have elevation values, after reading shape file in MATLAB or digitizing in MATLAB, the lowest elevation of the LiDAR points in the range of stream data coordinates was assigned as stream elevation.

An alternative approach for obtaining stream points is, which was not implemented in this study, 3) GEONET Morphological Feature Extraction Tools. GeoNet

MATLAB Tools, which allow the user to extract channel network and channel heads by using non-linear filtering and geodesic cost functions from a DEM (Passalacqua et al. 2012). The user can obtain stream networks in very large areas in shape file format, however selection of the appropriate thresholds for the DEM requires grid search. Instruction on how to use the tools was given in their webpage (https://sites.google.com/site/geonethome/home).

3.1.2 Smoothing Stream Shape

The direction of the stream needs to be determined to place cross section box as perpendicular as possible. The user selected stream point and successive point were used in this study to determine rotation angle for local coordinate transformation. Digitized stream points had sharp turns where the angle between points did not reflect angle for general direction of the stream and curves, particularly after digitizing, so smoothing was required. The cross section box needs to be placed as perpendicular as possible to the stream line so that extracted and ground classified LiDAR points reflect corresponding "benches" in the ditch. As detailed in the next subsection, local coordinates were calculated depending on the user specified stream points, and the perpendicular placement of the cross section box depended on rotation of the points with the appropriate angle. This angle was calculated from two consecutive smoothed stream points.

3.1.2.1 Locally Weighted Scatter Plot Smoothing

Locally weighted scatter plot smoothing, referred to as "lowess", and was used to smooth stream point data. The method applies weighted linear least-squares regression with a low (1th and 2nd degree) degree polynomial (Cleveland (1979). The method requires the user to provide a span value that is a percentage of the total number of data points to determine the number of points in smoothing each value. The nearest number of

points given as a percentage value is selected for linear regression. The distance of the estimate from points also determines the weight of those nearest points according to

$$w_i = \left(1 - \left|\frac{x - x_i}{d(x)}\right|^3\right)^3 \quad 3.1$$

$x =$ the value of the point to be smoothed,

x_i = the nearest neighbors of x as defined by the span,

$d(x)$ =the distance a between x to the furthest nearest neighbor of x within the span

The closer the weighted distance of a nearest point from point of the estimate, the more influence it has on linear regression. This estimation process is being applied for all data points. If the user uses the rlowess command in MATLAB for robust local regression, the additional processes are performed to eliminate outliers from the data point. The resulting data smooth with robust weights calculated with weight function (3.2);

$$wi = \begin{cases} (1 - (r_i/6MAD)^2)^2, & |ri| < 6MAD, \\ 0, & |ri| \geq 6MAD, \end{cases} \quad 3.2$$

$$MAD = median(|r|) \quad 3.3$$

If the residual (r_i) of each point is smaller than *6MAD* (median of absolute residuals), the weight is calculated as above. If it is smaller, the robust weight is zero. The data are smoothed using the robust weight and the process is repeated with five times (Mathworks, 2013). In this study, the method was used to smooth the stream points. For very curving streams, a lower span value, for straight stream geometry, a higher span value was used.

3.1.2.2 Determining Independent and Dependent Variable

When smoothing was applied to stream points, the user needs to decide either X or Y value should be dependent. In horizontal coordinates of the ditch if range of X values was bigger than range of Y values, X needed to become independent and Y values became dependent. For data shown in the Figures 3.3, X should be independent and Y should be dependent values as in B. For this data if we use Y values as independent as in A, because data tries to fit very small range, it created artifacts as below.

The data still fit if the user does not take the range of the data into account. However, the fit occurs poorly in that case. Additional MATLAB algorithm was written to look the range of X and Y to determine which one needs to be independent and smoothing was performed according to that parameter.

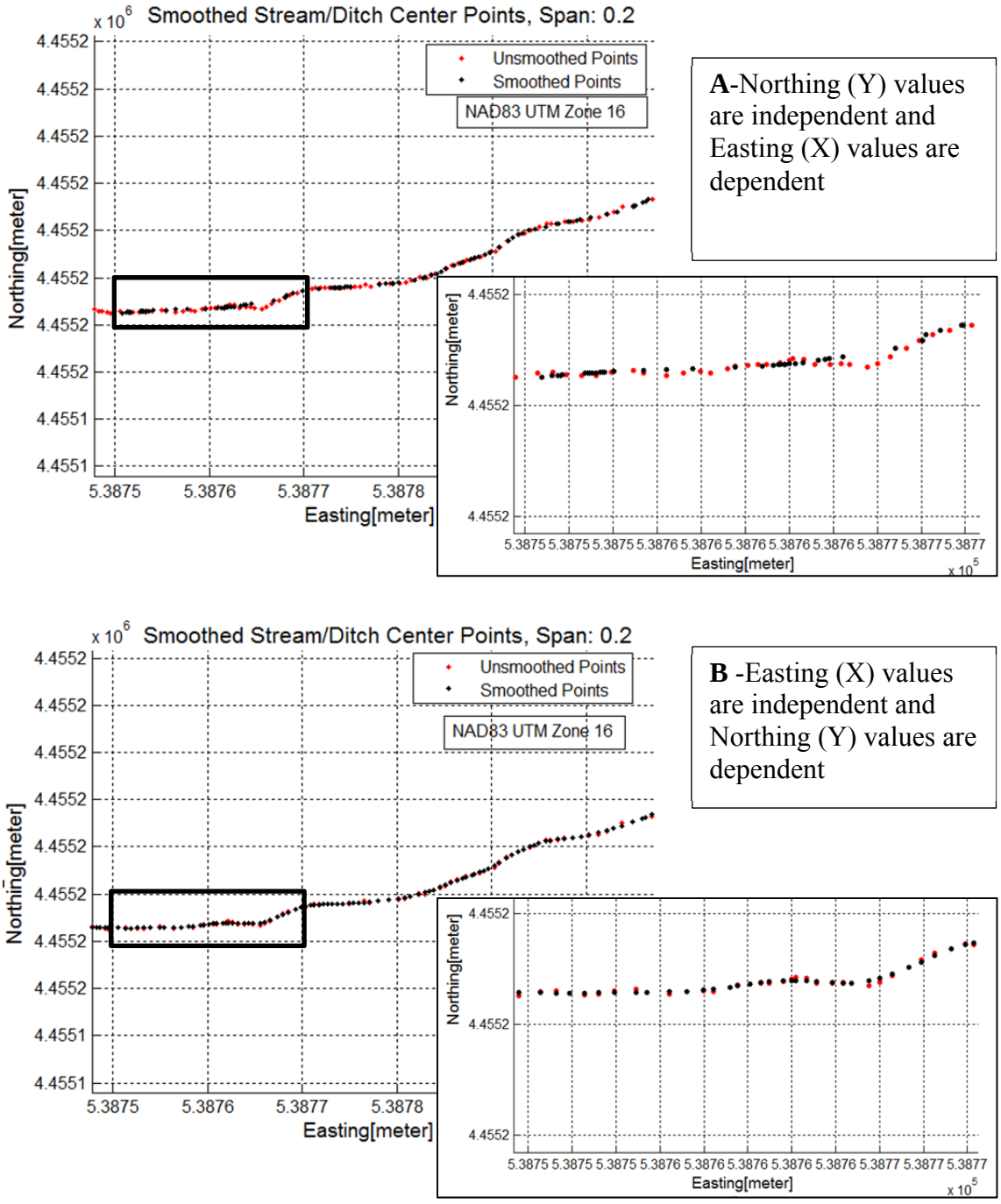

Figure 3.3 Importance of determining dependent and independent values in smoothing stream points. (A) Y values are independent (B) X values are independent

3.2 Extracting Ground Points and Conversion to Local Coordinate System

LiDAR data have point class codes. After extracting points with the cross section box, ground points were separated from other points by using code attributes. Before performing this separation, to place the cross section box perpendicular to the stream direction, stream points were smoothed and local coordinate transformation were applied.

3.2.1 Local Coordinate Transformation

LiDAR and stream points in the same coordinate system were transformed to the local coordinates in which origin was the user selected stream point coordinates. Three-dimensional linear transformations consist of a rotation and shift.

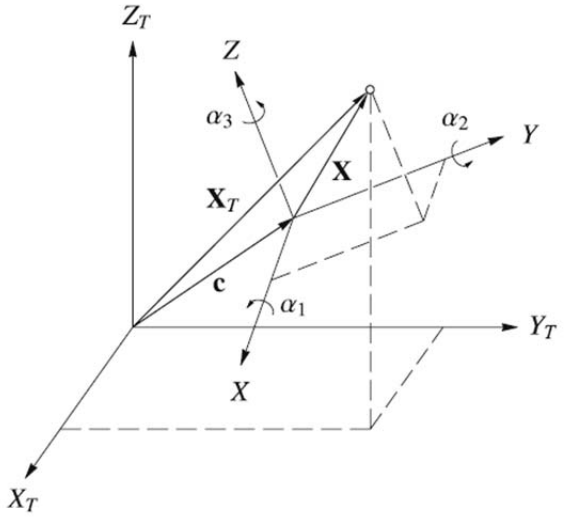

Figure 3.4 Three Dimensional Coordinate Transformation (Hofmann-Wellenhof et. al, 2008)

$$\mathrm{X}_t = \mu \mathrm{RX} + \mathrm{c} \qquad 3.4$$

In the Helmert (similarity) transformation formula (3.3), X is a vector of Cartesian coordinates which is to be transformed, and X_t is a vector of transformed Cartesian coordinates, μ is a scale factor, R is rotation matrix and c is the shift (translation), (Hofmann-Wellenhof et. al, 2008). In this study, the local coordinate transformation used shift and rotation (about the Z-axis) to obtain local coordinates at each stream point.

$$c = \begin{bmatrix} X_s \\ Y_s \\ Z_s \end{bmatrix}$$ The shift is the coordinate of the selected stream point.

$$R = \begin{bmatrix} \cos(k) & sin\,(k) & 0 \\ -\sin(k) & \cos(k) & 0 \\ 0 & 0 & 1 \end{bmatrix}$$ Rotation was applied only around the Z-axis.

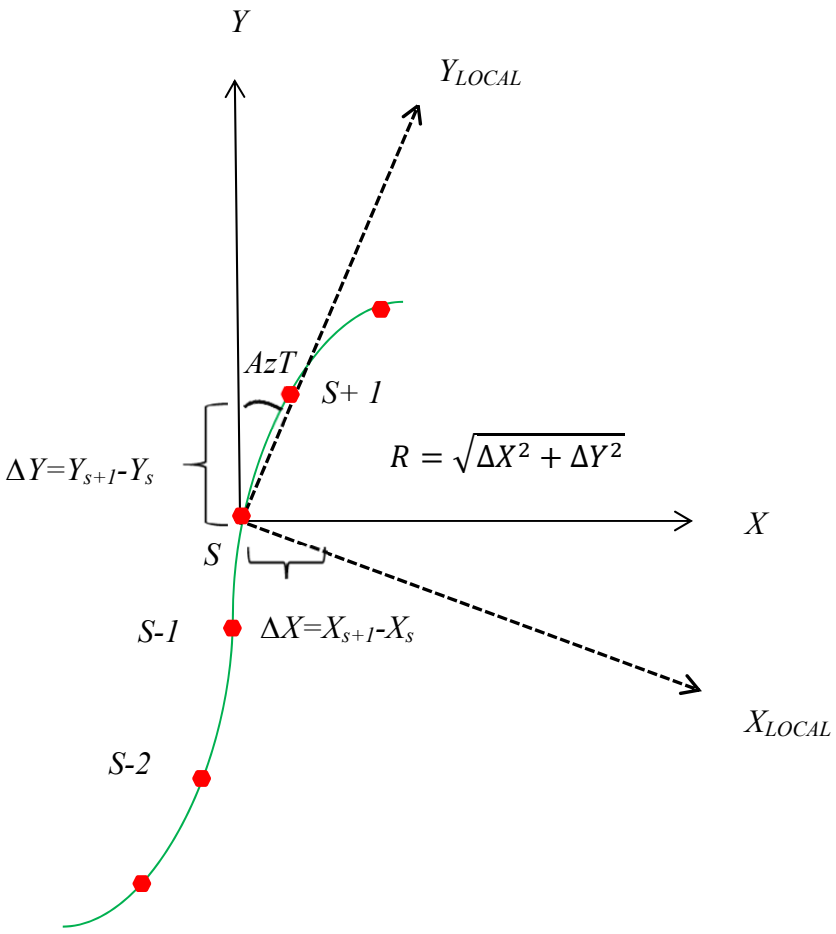

Figure 3.5 Azimuth angle (*AzT*) between grid north to tangent of the given point, used for determination of the rotation angle *k*

To determine the rotation angle *k*, the location of subsequent points was used in the matrix of the stream points. In Figure 3.5, the green line represents the stream line and red points represent stream points. For the point (*S*) where the coordinate frames were shown the next point(*S+1*) are used to calculate the rotation angle. To calculate rotation angle, the azimuth angle between grid north to tangent of our interest of stream point is calculated by following equations (3.4). The azimuth angle changes according to the quadrant as shown in Figure 3.6

$$AzT = \cos^{-1}\left(\frac{|(\Delta Y)|}{R}\right) \quad \text{or} \quad AzT = \sin^{-1}\left(\frac{|(\Delta X)|}{R}\right) \tag{3.5}$$

I. $Az = AzT$

II. $Az = 180° - AzT$

III. $Az = AzT + 180°$

IV. $Az = 360 - AzT$

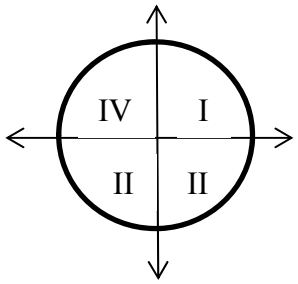

Figure 3.6 Azimuth angle in each quadrant

The angle *Az* calculation can be obtain **atan2** command which gives proper quadrant in MATLAB. The rotation would be negative rotation (clockwise), therefore the rotation angle:

$$k = -Az \tag{3.6}$$

The local coordinate is calculated according to,

$$\begin{bmatrix} X_t \\ Y_t \\ Z_t \end{bmatrix} = \begin{bmatrix} \cos(k) & \sin(k) & 0 \\ -\sin(k) & \cos(k) & 0 \\ 0 & 0 & 1 \end{bmatrix} \begin{bmatrix} X \\ Y \\ Z \end{bmatrix} + \begin{bmatrix} -X_s \\ -Y_s \\ -Z_s \end{bmatrix} \tag{3.7}$$

In Figure 3.7, cross section boxes of different size were placed in two different stream points. The selection boxes are perpendicular to the stream and after transformation; selected points are the origin of local coordinates system.

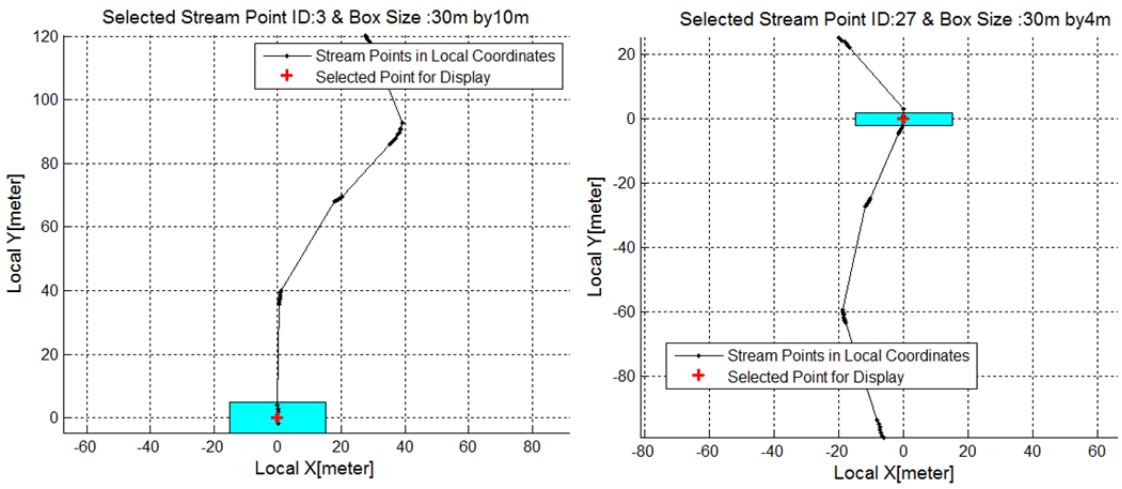

Figure 3.7 Cross section box perpendicular to stream points in a straight and curving portion of the stream. The selected point is center of the local coordinate system

Within the extent of the user defined cross section box, LiDAR points in local coordinates were extracted and segregated as ground and non-ground depending on their given classification code.

3.2.2 Stream Curving Effect and Determination Cross Section Box Size

The box size and the LiDAR NPS affect the number of points selected. If the stream points curve within the selected box size, there is more variability on points as illustrated in Figure 3.8 which shows collected stream points on RTK GPS survey from Site 4.

The cross section in Figure 3.9 shows LiDAR points within the user given box size in 3D. The origin of the coordinate system is the point selected from the stream points for display. The selected point occurs immediately behind the first tree shown in the image. 2D figure shows X-axis and Z-axis in local coordinates. The points shown in the 3D figure were projected to 2D on the X –Z plane on the local coordinate of the selected stream points. Each stream point location would have unique local coordinate system due to rotation angle and stream point height difference.

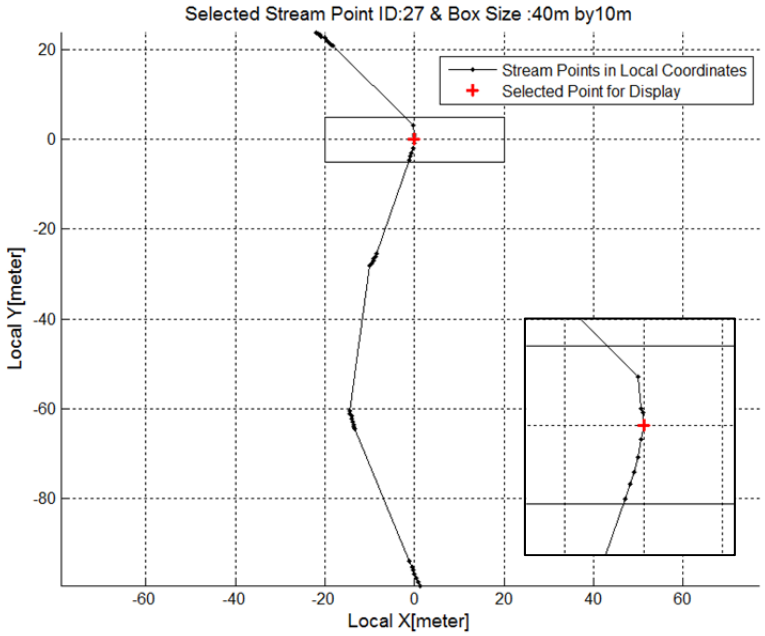

Figure 3.8 Site 4 Cross Section 2, the RTK GPS surveyed stream points and the cross section box.

As shown the Figure 3.10, when the selection box was placed on the curving part of the stream, the ground LiDAR points (in blue) do not correspond well with the RTK GPS points (in red) if Y width of selection box is large. The Figure 3.10 C1-2 shows points within the cross section box size of 30m by 14m. In the left side of Figure 3.10-C2, ground points were not matching with surveyed RTK GPS points. In the straight part of the stream, with same large Y width, the points showed the shape of the ditch without the curvature effect as shown in Figure 3.11 C2. Therefore, it is important to have a small Y width in curving areas of the stream; if the user intends for terrain features to relate that curving area.

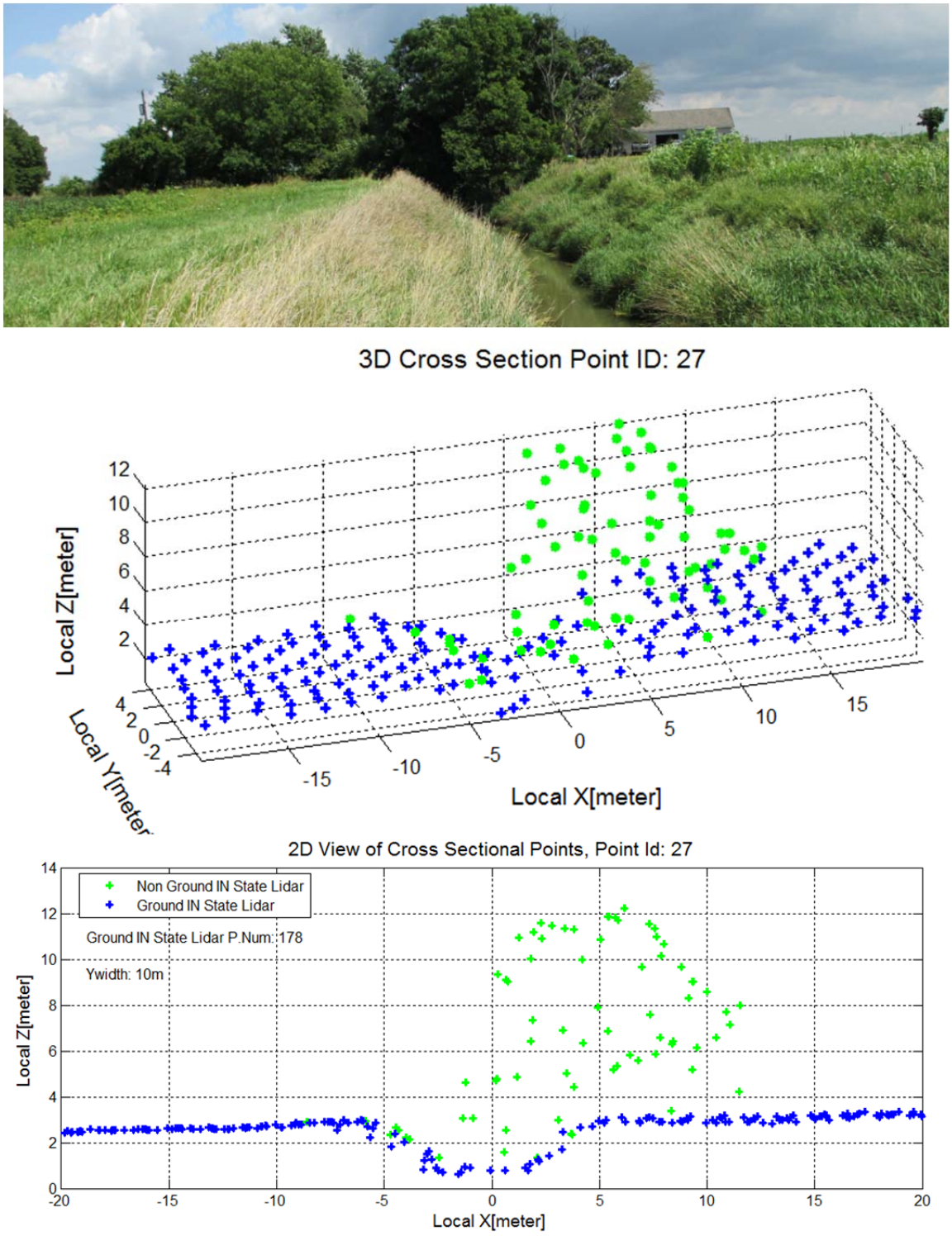

Figure 3.9 Site 4 Cross Section 2, 2D and 3D view of LiDAR points selected via the cross section box

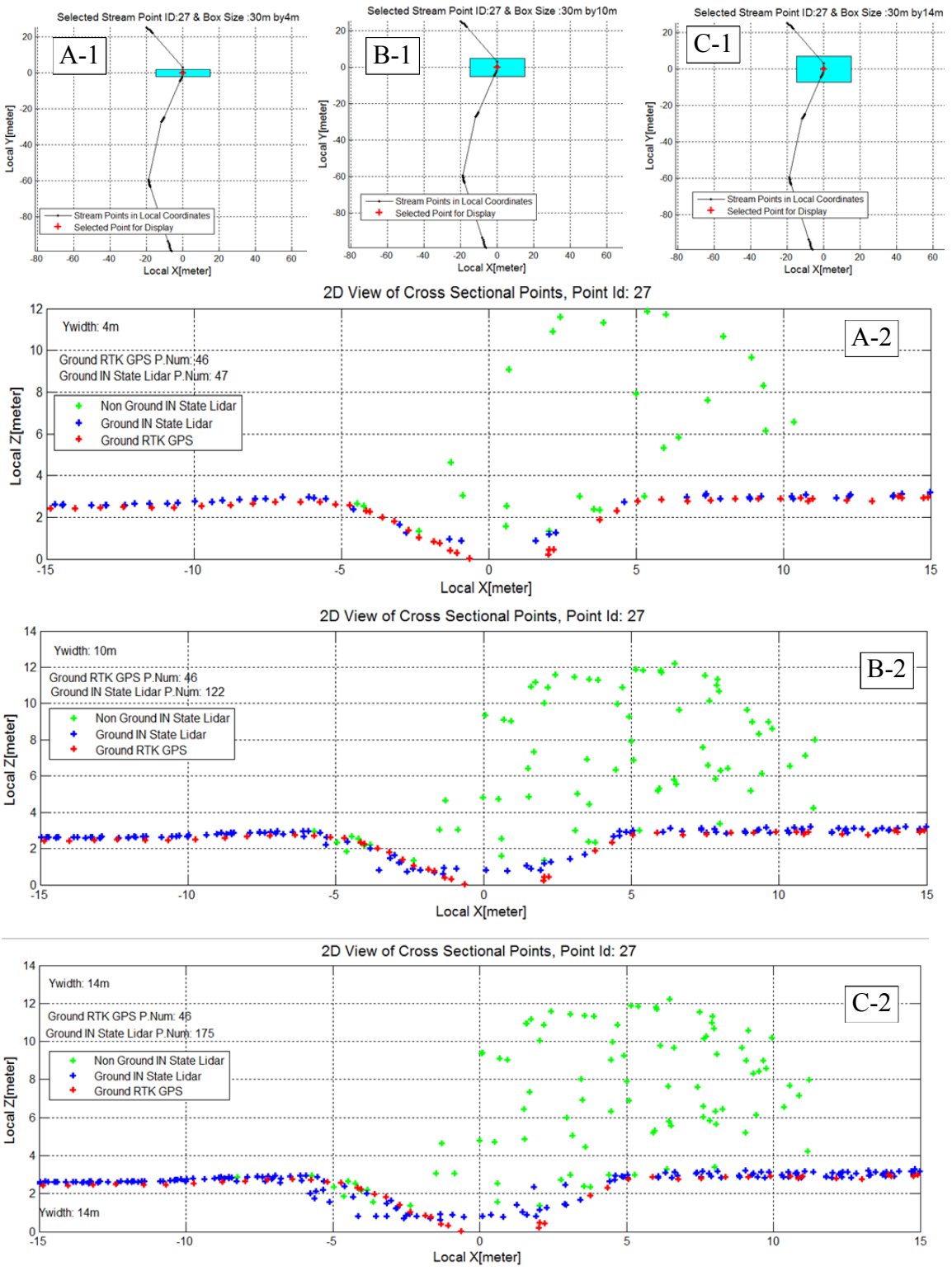

Figure 3.10 Cross Section box size and effect of stream curvature

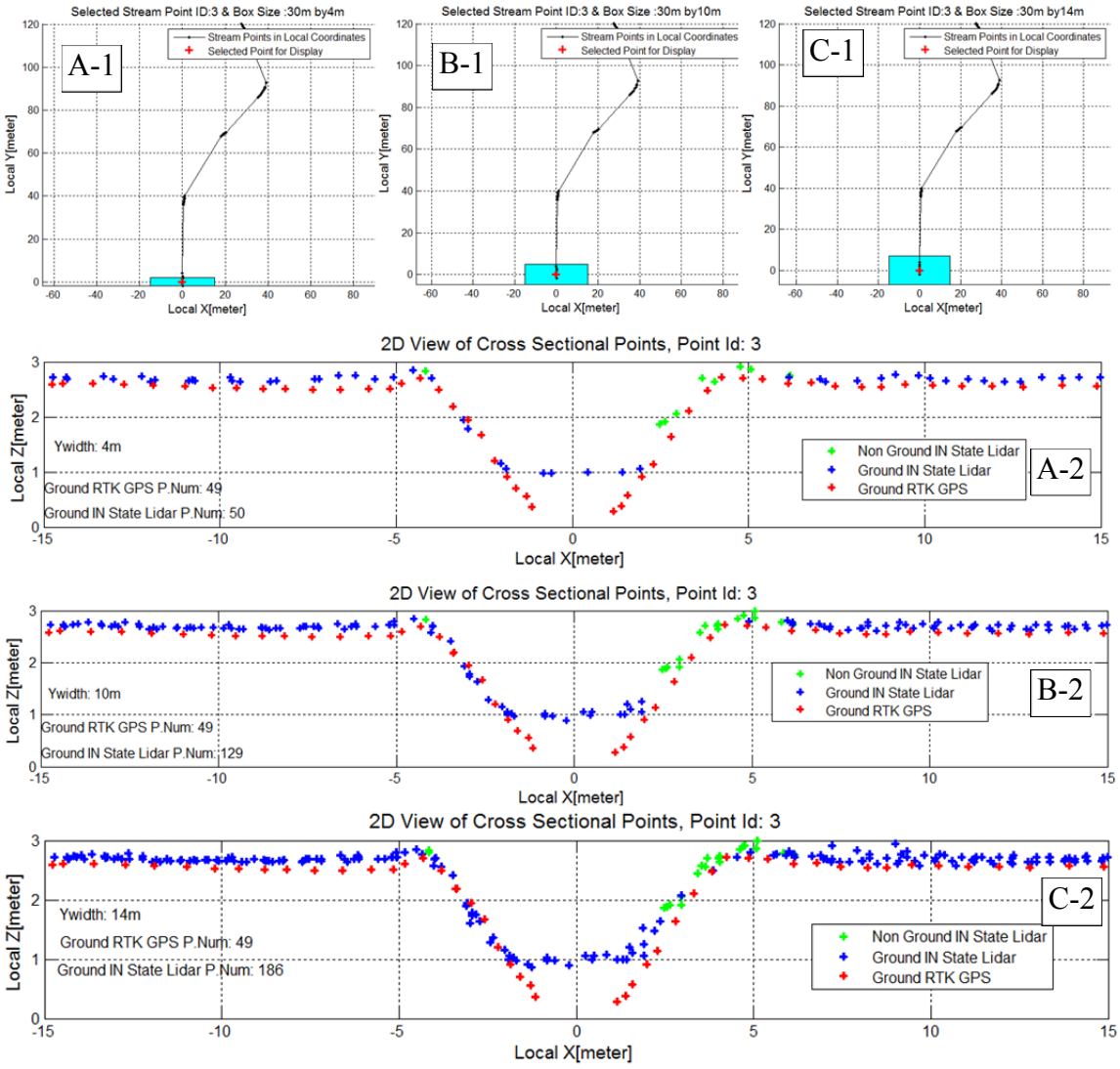

Figure 3.11 Straight section of the stream and points distribution in different cross section boxes

While selection of a small box may track curving streams, the box size may result in an inadequate number of points if NPS is low. In that case, it would be necessary to increase the Y width of the box. In this study, from 5m-10m were adequate for Indiana Statewide LiDAR (1.5m and 1m NPS) to obtain enough points to represent ditch banks and obtain the general shape of the ditch.

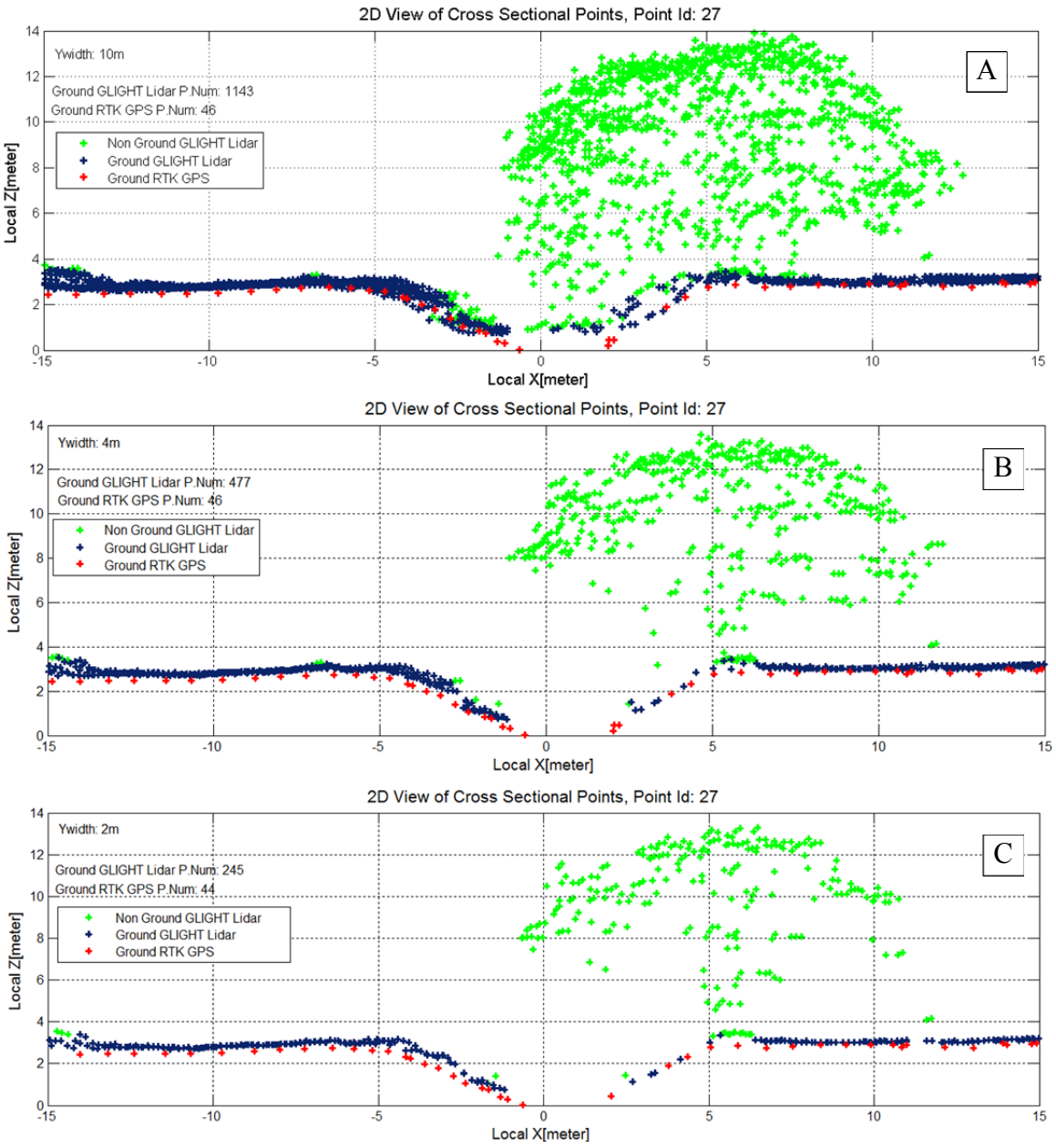

Figure 3.12 G-LiHT LiDAR, which has lower NPS, shows similar shape of the ditch with RTK GPS point with smaller cross section Y (along the stream) width (10m,4m and 2m)

LiDAR data with lower NPS allowed use of a smaller Y width. When compared with RTK GPS, the smallest cross section Y width (2m) enabled to obtain very similar terrain features compared to surveyed RTK GPS data (Figure 3.12-C).

3.3 Obtaining Smoothed Cross Sectional Points and Top of the Banks

In this section, cross sections of ground LiDAR points were used to obtain smoothed cross sections of ditch shape and determine the top of the banks.

3.3.1 Smoothing Cross Sectional Point Data

Spline fits were used initially to smooth stream points .Ground points were used to obtain a smoothed shape of the ditch cross section using two spline fit methods; 1) Cubic spline smoothing, 2) Gaussian smoothing. The MATLAB **fit** command was used by specifying the fit options as "smoothing spline" or "gauss". In 2 dimensional (Local X and Local Z) processing, irregular point spacing and the numbers of LiDAR points influenced weightings with in span in locally weighted scatter plot smoothing applied to the stream points. Selection of the respective parameters for cubic spline smoothing and Gaussian mixture model was determined by using RMSE from the resultant fit with grid search to obtain smoothed shape of the ditch.

3.3.1.1 Smoothing Spline Fit

In the MATLAB command **fit,** the user provides the (smoothing parameter) p, used to construct smoothing function (s (x_i)) by minimizing value (3.7)

$$p\sum_i w_i\left(y_i - s(x_i)\right)^2 + (1-p)\int\left(\frac{d^2s}{dx^2}\right)^2 dx \qquad 3.8$$

The user specifies a p value between 0 to 1. If this value is approximately to zero the result is approximately linear least square regression and if this value is approximately 1, the result is approximately cubic spline interpolation. (Mathworks, 2013) Generally, the data are fit using a cubic spline interpolation in the ditch area.

Wang (2011) described a cubic spline as a special case of polynomial spline where piecewise polynomials are joined smoothly at knots (joint locations). All data points can be possible knots, and the smoothing spline function estimate is penalized during least square estimation with a quadratic penalty function (Fan & Yao, 2005). If the user does not specified the weight matrix in the MATLAB built in command, it will assume equal weights for all values.

3.3.1.2 Gaussian Mixture Model

The Gaussian mixture model fit uses the Gauss Newton non-linear optimization method, to solve the least squares problem. The Gaussian Mixture Model is represented as,

$$y = \sum_{i=1}^{n} a_i e^{\left[-\left(\frac{x-b_i}{c_i}\right)^2\right]} \qquad 3.9$$

where a is the amplitude (height of the distribution) , b is the centroid (location), c is related to the peak width, n is the number of peaks to fit, and $1 \leq n \leq 8$. (Mathworks, 2013) and e, Euler`s number (2.71828).

The method solves nonlinear least square problem via a sequence of linear least squares problems using the Gauss-Newton method (Deuflhard, 2004),(Chapra, 2012).

3.3.1.3 Determining Smoothing Parameters

After ground points were selected with the selection box with specified X and Y widths, one dimensional data smoothing was implemented on the local coordinates of X – Z plane.

For the smoothing spline fit, the smoothing value p is specified, for the Gaussian fit, the number of terms, which control the number of coefficients must be determined. In

both methods, RMSE goodness of the fit is specified to determine the best parameter values (Fox, 2012).

The grid search approach was implemented to find the numbers of terms (values changes from 1 to 8) and smoothing value *p* (values changes from 0.01 to 0.99 with increment value of 0.01) result with minimum RMSE. Figure 3.13 and Figure 3.14 show points with Gaussian Mixture Model and Smoothing Spline Fit for two of the cross sections

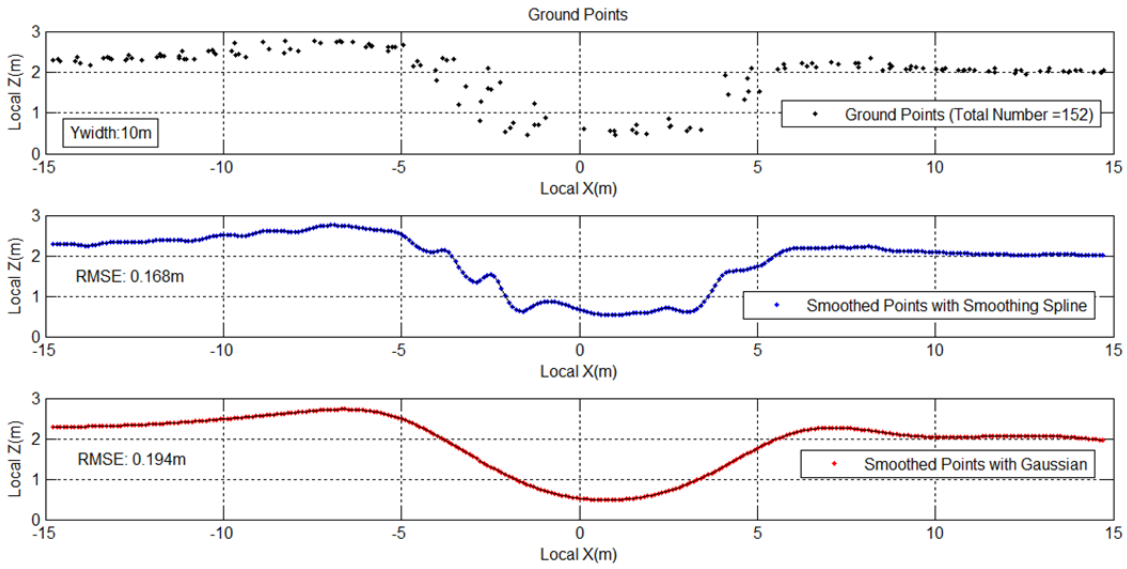

Figure 3.13 Site 3 Cross Section 5- RMSE with the smoothing spline fit and the Gaussian Mixture Model

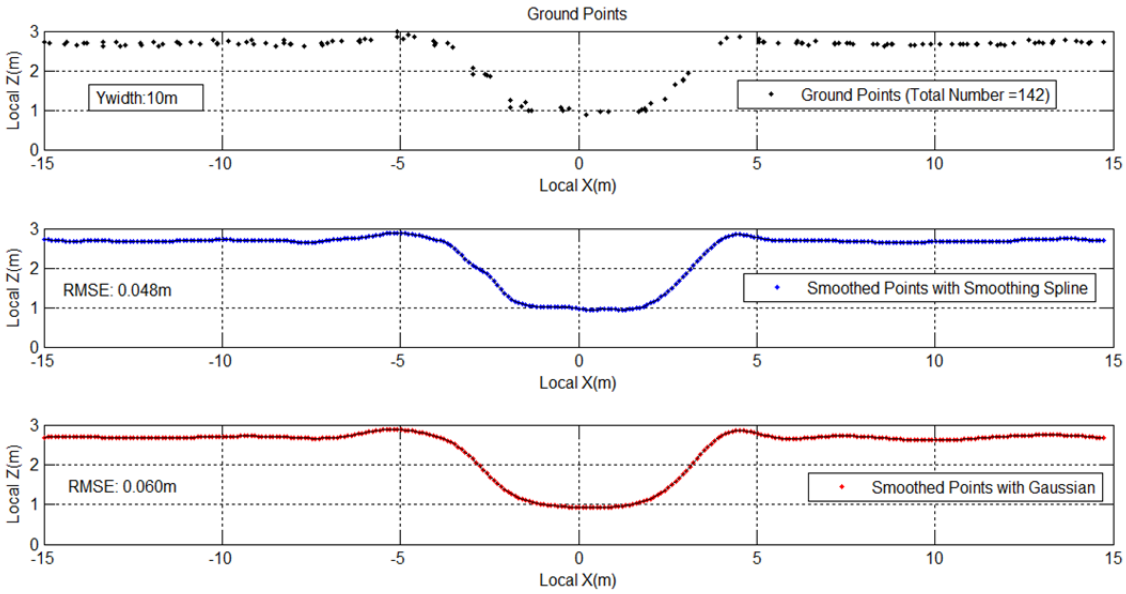

Figure 3.14 Site 4 Cross Section 5 –RMSE with the Smoothing spline fit and the Gaussian Mixture Model

3.3.2 Detection of Top of the bank locations

Every ditch has a different size, slope and height. Automating the process is more complicated when the heights fluctuate along the benches or after top of the bank. Three methods were investigated to detect the top of the bank locations. In some cases, three of the method would indicate same location as a top of the bank; however, in some cases two of the method was showing the same location. Therefore, intermediate and final elimination was applied to obtain final top of the banks.

The center location of the local coordinates was determined by specified stream point as mentioned before. However, the specified stream points may not be in the center of the ditch. The spline is fit to unequally spaced point data from which equally spaced points can be derived from the interpolated data. Prior to detecting the top of the banks, point separation of the negative side and positive side was redefined by using the smoothed points with lowest local Z coordinate. This assured that smoothed points were separated for both side approximately from the center of the ditch. If the digitalized stream point was not placed inside the ditch, the top of the banks could still be detected.

3.3.2.1 Utilizing Derivatives (Slope and Curvature) of the Spline

The first method is based on the first derivative (slope) and second derivative (curvature) of the spline function fit ground points. The goal is to detect the top, which has zero slope and negative curvature. Along the spline, many locations satisfy these requirements. An algorithm was developed to implement rules to both negative and positive sides of the ditch relative to the location on the cross section with the lowest elevation.

Resulted top of the banks were shown in Figure 3.15 and Figure 3.16. The top of the banks (as shown with red arrow) corresponds to zero slope values; however, the function may also have zero slope value in the middle of the ditch area. To select the appropriate value, the locations of the maximum slope on positive side and the minimum slope on the negative of the fitted function were determined. After detecting those locations, which corresponds to the bench most of the time, the candidate locations with zero slope and negative curvature values were searched further away from the center of the ditch in each side (negative side and positive side). On the positive side, the smallest local X coordinate, on the negative side, the location with the largest X coordinate was selected as the top of the banks.

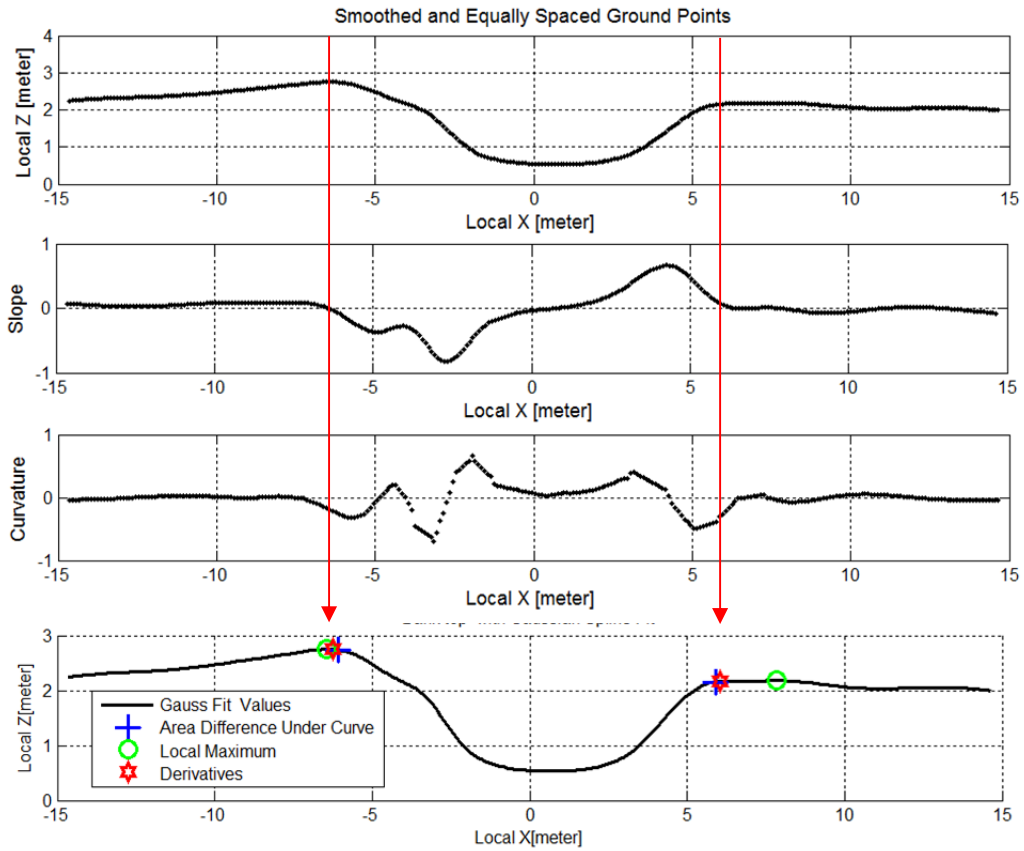

Figure 3.15 Site 3 Cross Section 5 Gaussian Mixture Model, smoothed and equally spaced estimated points and corresponding slope and curvature values, and the top of the bank results

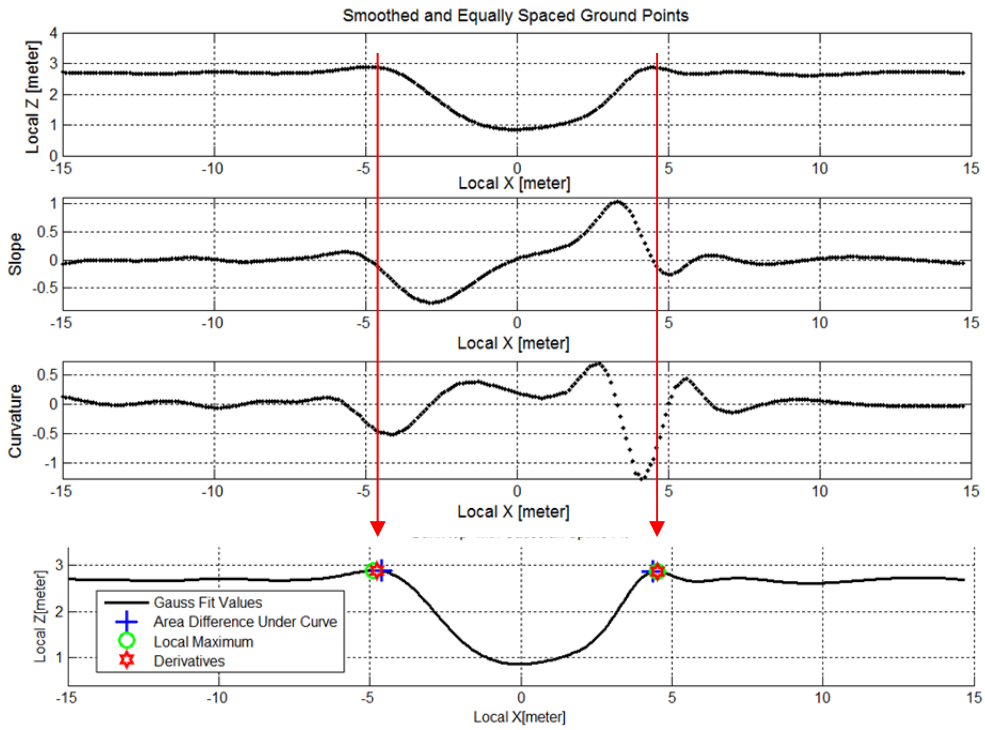

Figure 3.16 Site 4 Cross Section 5 Gaussian fit, smoothed and equally spaced estimated points and corresponding slope and curvature values, and the top of the bank results

3.3.2.2 Utilizing Area Difference under the Spline

The cumulative area (CA) was calculated under the curve for both sides (negative and positive) at each point and successive differences of the CA in each element. On each side, the values where incremental differences were very close to zero (0.001-0.005 is threshold) were identified and the value with the smallest local X coordinate on the positive side and negative side respectively were selected. The Figure 3.17 and Figure 3.18 show CA difference multiplied by 1000 for better visualization. The location of top of the bank typically corresponds to where the CA difference is zero.

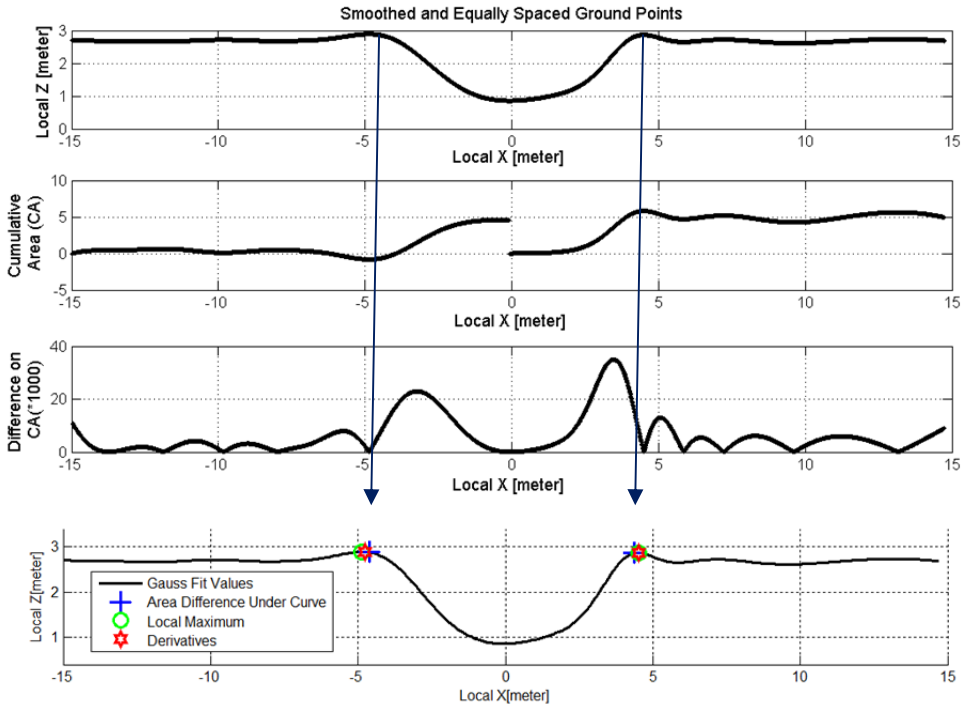

Figure 3.17 Site 4 Cross Section 5 Gaussian Mixture Model, smoothed and equally spaced estimated points, Difference on Cumulative Area

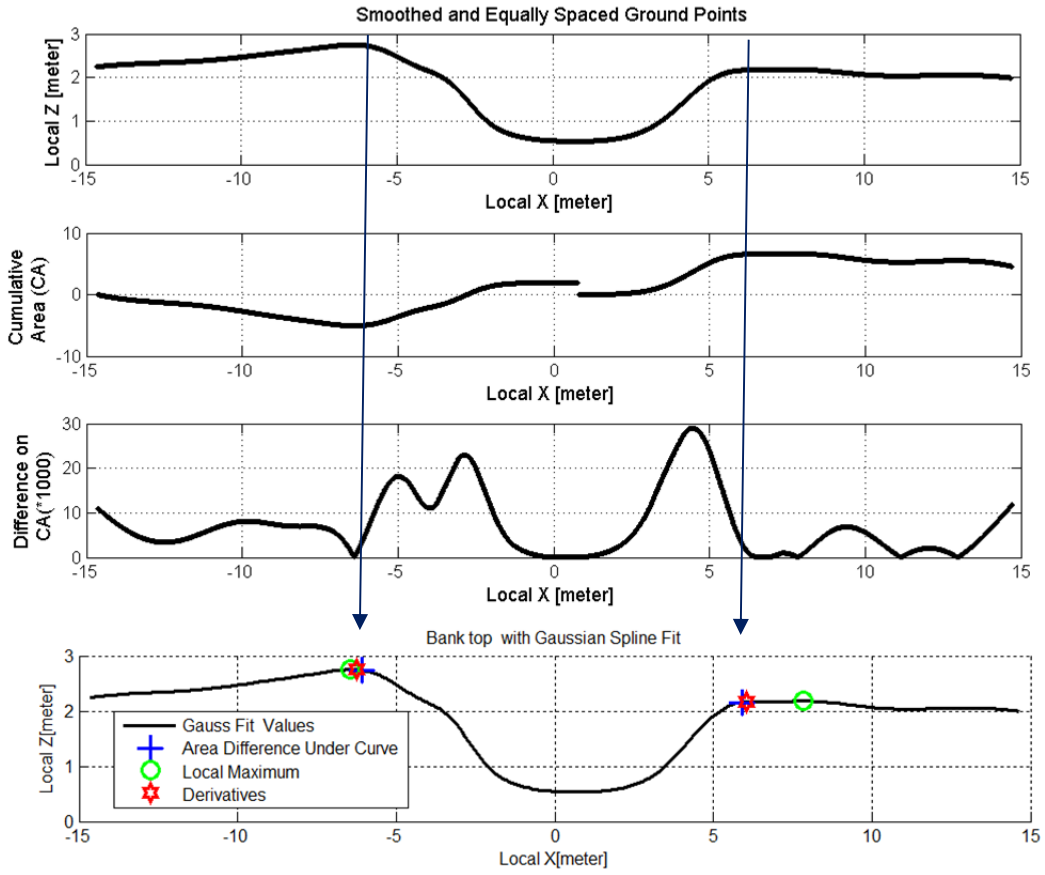

Figure 3.18 Site 3 Cross Section 5 Gaussian Mixture Model, smoothed and equally spaced estimated points, Difference on Cumulative Area

3.3.2.3 Using Local Maximum

The MATLAB commands called **findpeaks** and the function **dat2tp** from WAFO (Wave Analysis for Fatigue and Oceanography) MATLAB-Tool Box (WAFO Group, 2011) were also investigated for finding the top of the bank. The **dat2tp** command finds local extremes by detecting the inflection of the order statistics. As with the other approaches, the largest peaks on positive side and negative side of the lowest elevation reference point were identified. The MATLAB command **findpeaks** also returns the local extremes, the trend, where the difference changes from zero or positives to negative. (Mathworks, 2013). After detecting local extremes, the highest peaks close to the center in both sides were selected as the top of the banks as with **dat2tp**.

This method do not detect the top of the banks stand-alone if the terrain has higher elevations further away from the actual top of the banks (15m limit from the center of the ditch was applied). However, the method assisted during the final elimination to recognize whether there is the large elevation difference between other methods as a last check, which possibly indicates determination of incorrect location of the top of the bank for other methods.

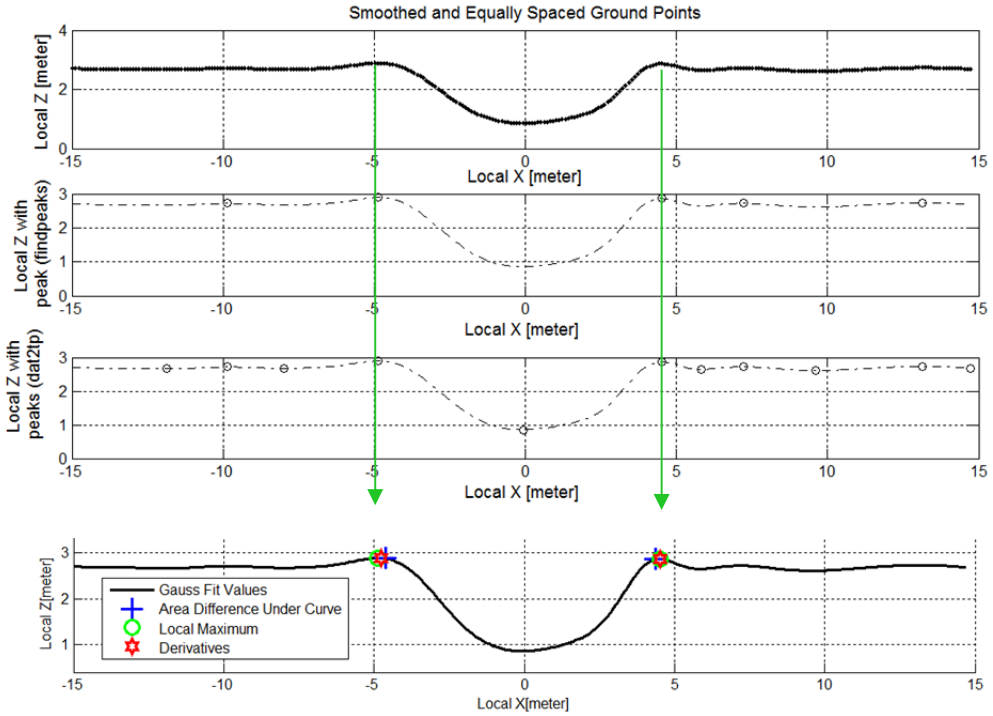

Figure 3.19 Site 4 Cross Section 5 Finding local maximum with the **dat2tp** (WAFO) and the **findpeaks** (MATLAB) commands

Figure 3.20 and Figure 3.19 shows the peaks was returned from the dat2tp function and the findpeaks command. The closest and highest peak to the ditch center were selected from those. In Figure 3.20, is an example in which, the top of the bank on the right side (positive side) is not the highest location, and the local extreme resulted further away from the top of the bank.

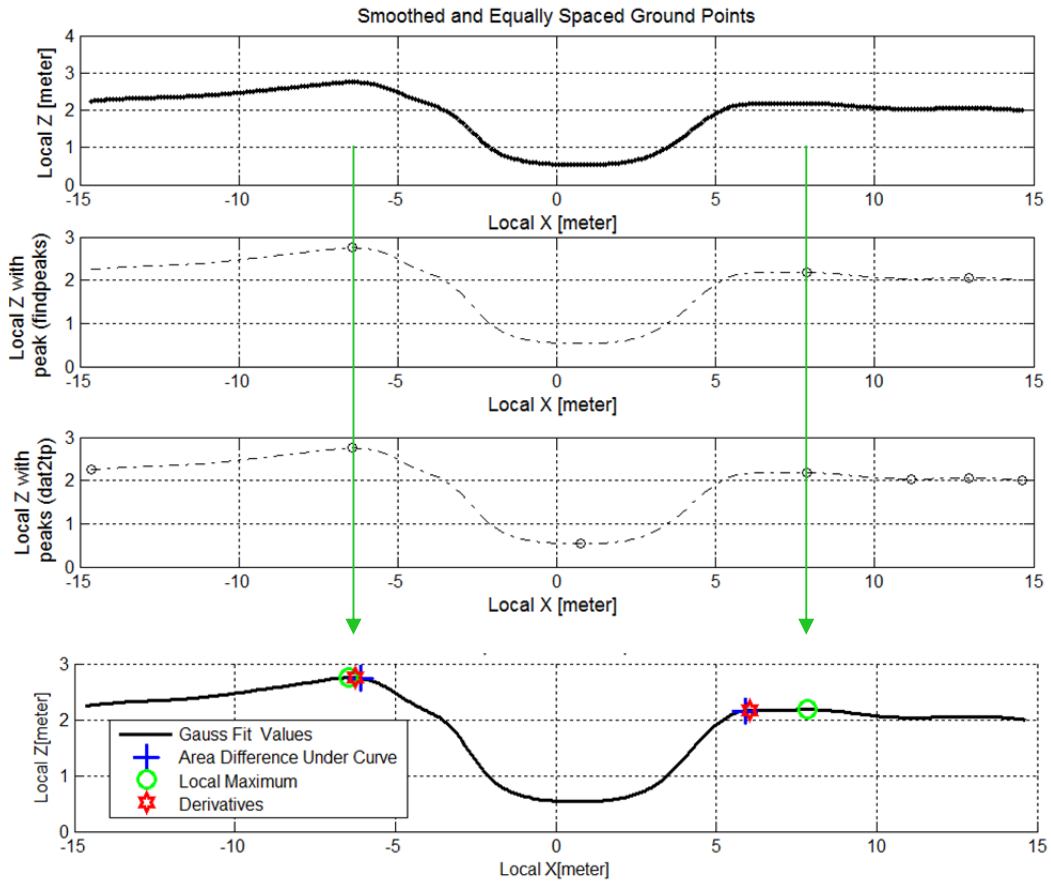

Figure 3.20 Site 3 Cross Section 5, Finding local maximum with the **dat2tp** (WAFO) and the **findpeaks** (MATLAB) commands

3.3.2.4 Evaluation of Top of the Banks Candidates and Selecting a Final Estimate

When the ground data are extracted with a large cross section box, the smoothed spline can have local increases and decreases that depend on the terrain features. These variations are problematic for computing the area difference under curve method. In some cases, after the first fitting, using the spline methods to the ground points, the data were not smoothed adequately because of the RMSE selection criterion. Applying smoothing to the smoothed curves often improved results. Figure 3.21 shows three consecutive fits with smoothing spline option and results for the top of the banks. On the positive side of the first smoothing (Figure 3.21 B), the results were apart from each other due to oscillations on spline. For the second (Figure 3.21 C) and third (Figure 3.21 D)

smoothing, the results indicated more similar. In some location, additional smoothing may improve the location detected as the top of the bank results.

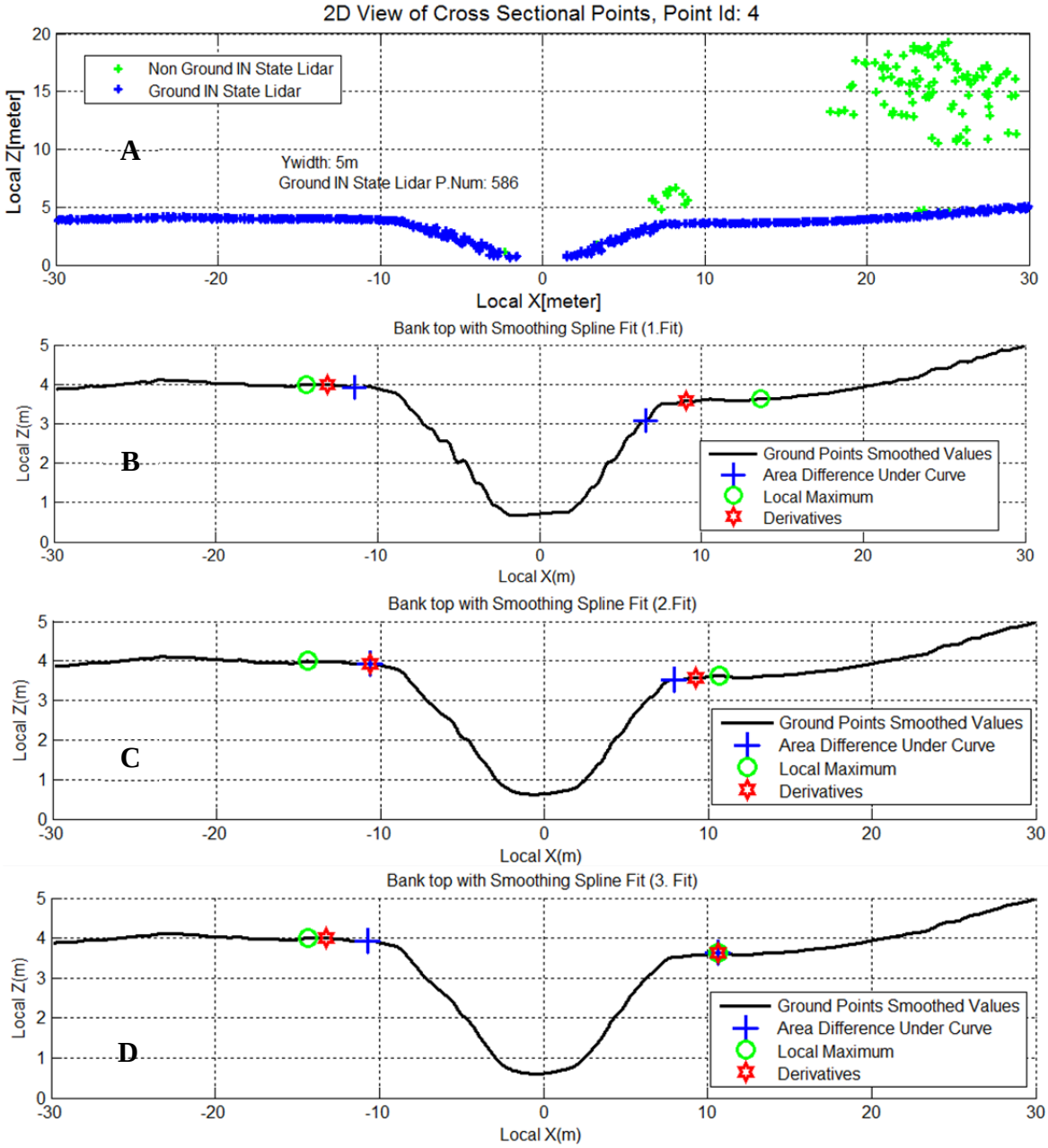

Figure 3.21 Site 1, Top of the bank results with multiple smoothing with smoothing spline fit method

The locations identified using various approaches were compared, and evaluation and selection process of final estimate were implemented in two steps. The first step is to select between top pairs, which are the tops of the bank from same methods, but resulted from different spline fits. The first step reduces the number of candidates to 3 from 6 for each top of the bank by focusing results from 2 spline fits. The following rules determined one of the top pairs by looking proximity of their local coordinates.

1. If the local X coordinate difference, and the local Z coordinate difference is less than 1m, use the mean value of the coordinates in both sides of the ditch.
2. If the local X coordinate difference is less than 1m, and the local Z coordinate difference is larger than 1m, select the highest top in both sides of the ditch.
3. If the local X coordinate difference is larger 1m and the local Z coordinate difference is less than 1m, use the minimum local X value for the positive side and the maximum local X value for the negative side, and the highest value of the Z coordinates in both sides.
4. If the local X coordinate difference is larger than 1m and the local Z coordinate difference is larger than 1m, select the highest estimate of the top selected in both sides of the ditch.

Figure 3.22 C shows the first elimination results between the top of the banks results in Gaussian Fit (Figure 3.22 A) and in Smoothing Spline Fit (2.Fit) (Figure 3.22 B). In the second step, the three tops which was left (Figure 3.22 C) from the first step was evaluated similarly by looking to proximity of their coordinates with the following rules,

1. If the local X coordinate and the local Z coordinate difference between the three values on each side of the ditch is smaller than 1m, use the mean value of coordinates.
2. If the local X coordinate difference less than 1m, and the local Z coordinate difference is larger than 1m between three values, select the highest estimate.
3. If the local X coordinate difference larger than 1m and the local Z coordinate difference is less than 1m between three values, select two of them, which have

local X coordinate closer to each other, then use the minimum local X value for the positive side and the maximum local X value for the negative side.

4. If the local X coordinate difference is larger than 1m and the local Z coordinate difference is larger than 1m between three values, select two which have local X values closer to each other, then
    a. If the local X coordinate difference, and the local Z coordinate difference is less than 1m, use the mean value of the coordinates in both sides of the ditch (step 1-1)
    b. If the local X coordinate difference is less than 1m, and the local Z coordinate difference is larger than 1m, select the highest top in both sides of the ditch (step 1-2)
    c. If the local X coordinate difference is larger 1m and the local Z coordinate difference is less than 1m, use the minimum local X value for the positive side and the maximum local X value for the negative side, and the highest value of the Z coordinates in both sides of the ditch(step 1-3)

In Figure 3.22 D, the final estimate shown between results of the three top of the bank methods was shown.

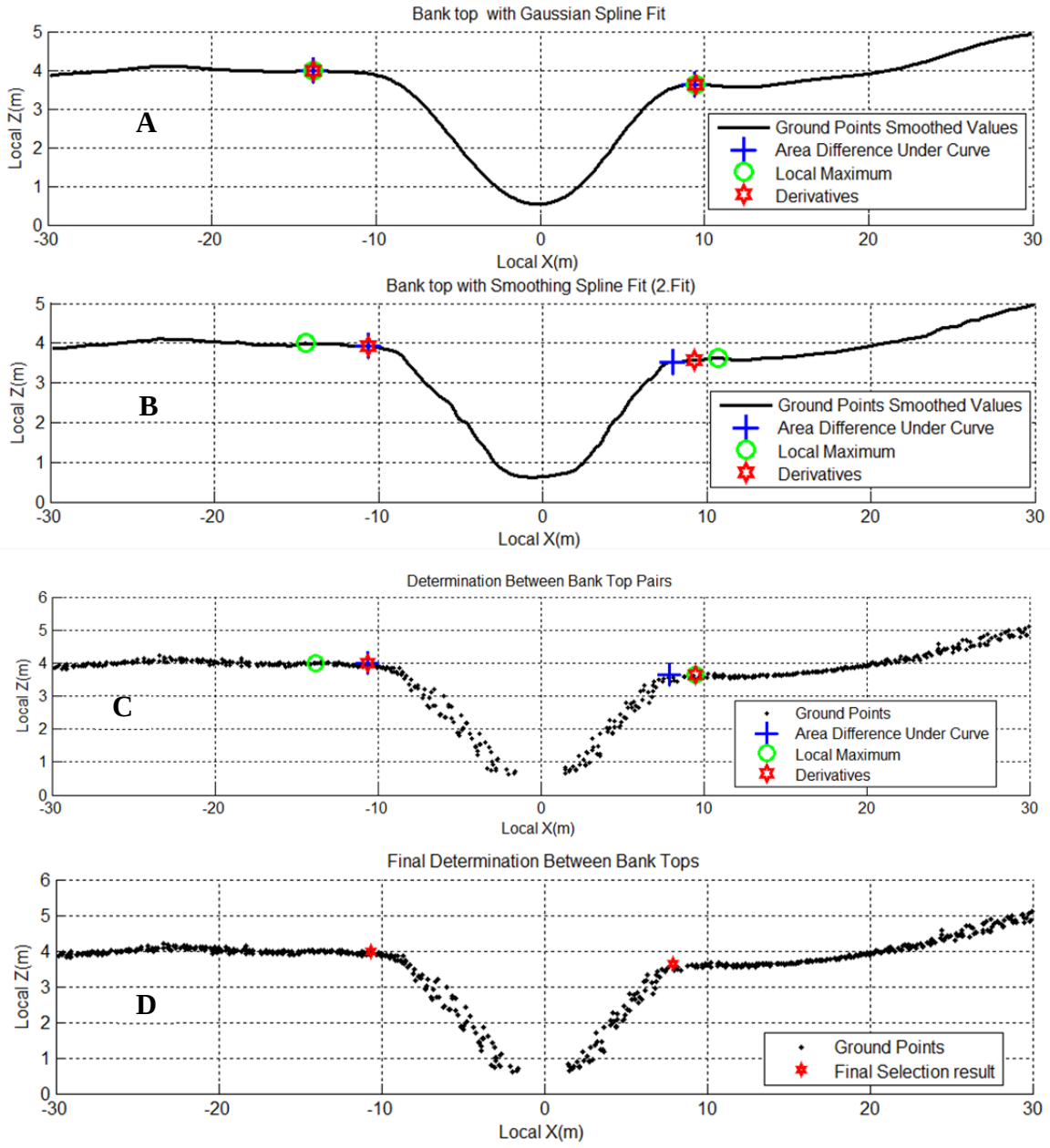

Figure 3.22 Determination of the top of the banks; Gaussian Mixture Model (1. fit) results (A), smoothing spline fit ((1. fit) results (B), Determination Between Bank Top Pairs(C), Final Result for Bank Tops (D)

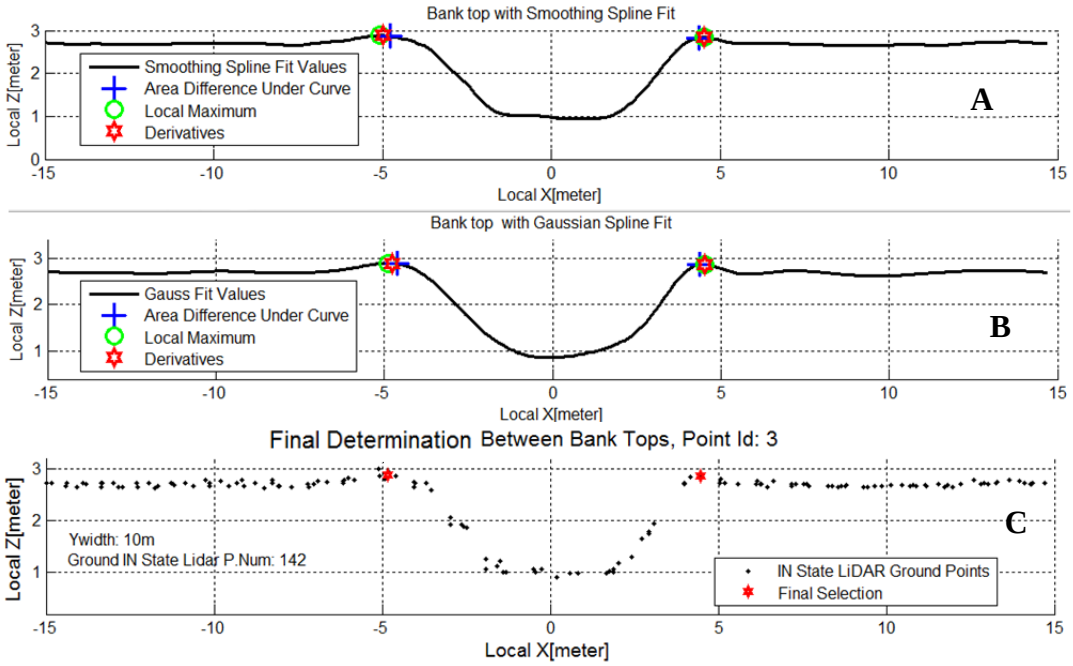

Figure 3.23 Site 4 Cross Section 5, Top of the bank determination(C), between Gauss fit (A) and smoothing spline fit (B) on ground point (LASTOOLS ultrafine ground classification)

Figure 3.23 shows the final results of the top of the banks from site 4 and cross section 5. The top of the bank results from both spline indicates similar locations. In Figure 2.24, the local maximum shows a location further than other methods. The determination steps helps to determine the top of the banks, which are close to the ditch.

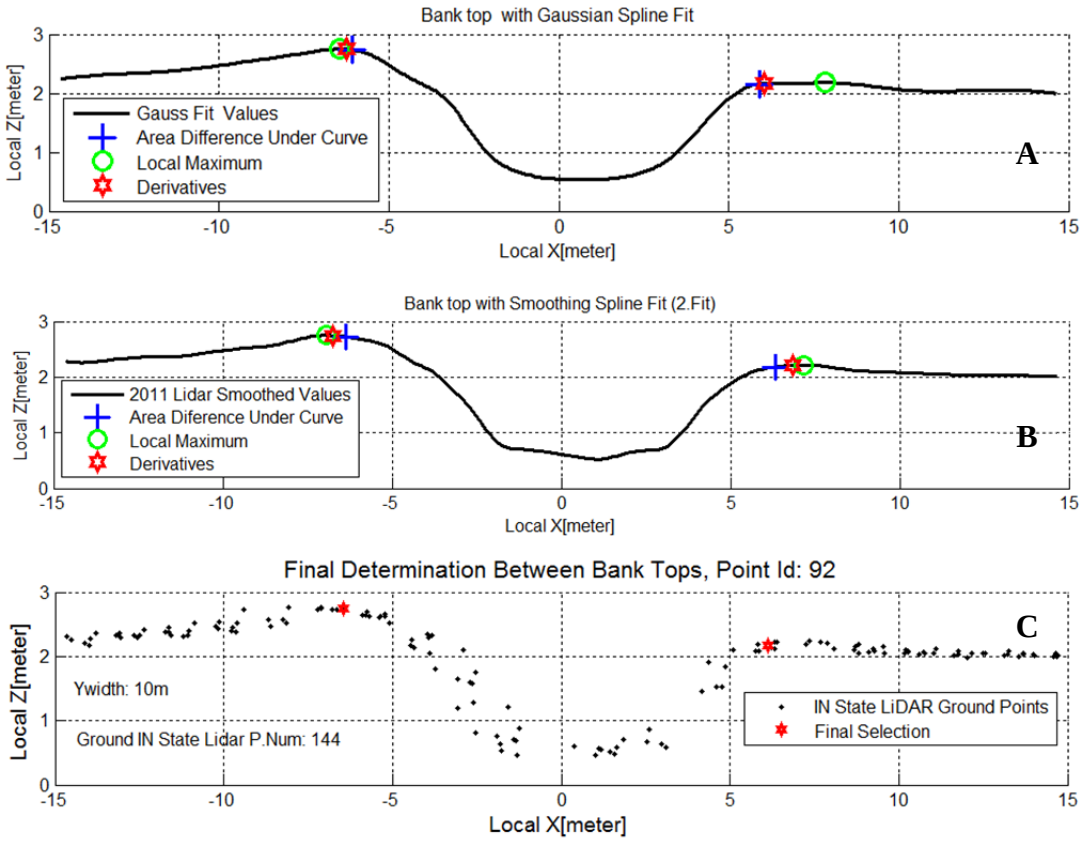

Figure 3.24 Site 3 Cross Section 5, Top of the bank determination between Gauss fit and smoothing spline fit

3.4 Transformation of Local Coordinates to Global Coordinates

By using the same rotation angle k (see Section 3.2.2), the global coordinates was calculated according to;

$$\begin{bmatrix} X \\ Y \\ Z \end{bmatrix} = \begin{bmatrix} \cos(k) & \sin(k) & 0 \\ -\sin(k) & \cos(k) & 0 \\ 0 & 0 & 1 \end{bmatrix}^{-1} \left(\begin{bmatrix} X_t \\ Y_t \\ Z_t \end{bmatrix} + \begin{bmatrix} X_s \\ Y_s \\ Z_s \end{bmatrix} \right) \qquad 3.10$$

This transformation applied to smoothed shape of the ditch points (from Gaussian Mixture Model), to the top of the banks after final elimination, ground and non-ground points (since the data in extend of stream was being transformed to local coordinate, to visualization purpose during iteration, points were transformed back to global coordinates. To prevent this, algorithm should transform the corner coordinates of the cross section box to global and then select points inside those cross section boxes from original data. For small data sets in this study, transforming does not take processing time, for larger data sets, transforming the cross section box corner coordinates should be preferred). The local Y coordinates of the smoothed shape the ditch and the top of the bank values was assigned as 0 which is local Y coordinate of the specified stream point or points.

3.5 Extracting Cross Section Geometry from Surveyed RTK GPS Points

The same method was also applied to smooth the surveyed RTK GPS points of the cross section transect and determine top of the banks as LiDAR points used to extract the top of the bank. Figure 3.25 shows RTK GPS points (in red) and Indiana State LiDAR points (in blue for ground) extracted with 80m by 6m cross section box (Figure 3.25 B). The figure also shows images of the RTK GPS cross section transect area (Figure 3.25 A), right by the tree on left side of the ditch. The final top of the bank results were shown overlaid with Gaussian Mixture Model fits of LiDAR ground points compared to results of same method with RTK GPS points (Figure 3.25 C). The resultant top of the banks was shown in Figure 3. 25 D in local coordinate, and in Figure 3.26 in global coordinates after transformation of local coordinates to global coordinates in 3D view. The green star represents result from RTK GPS points and the dark star represents results from the LiDAR points.

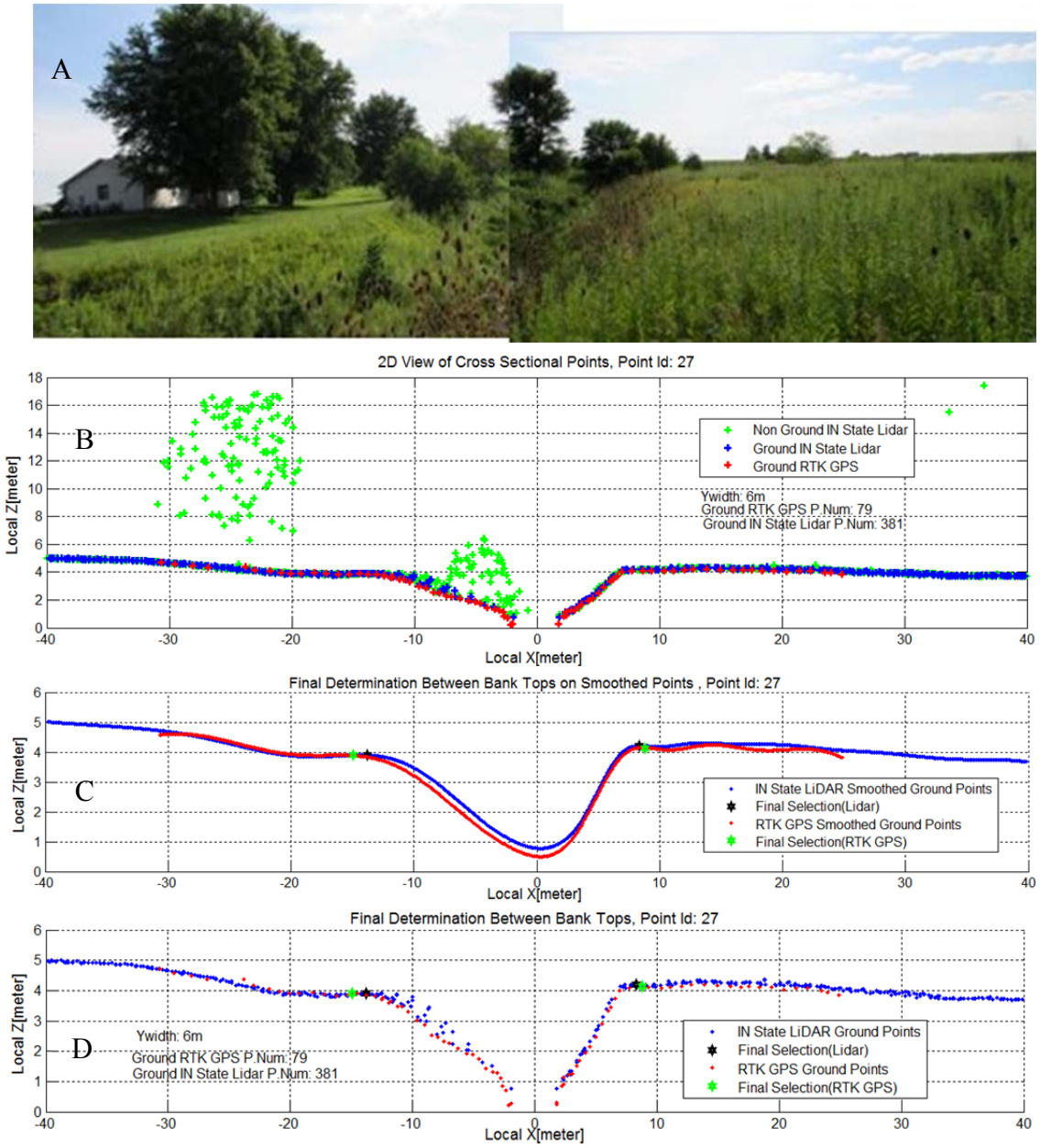

Figure 3.25 Extraction of cross section geometry from the RTK GPS points and results compared to LiDAR points

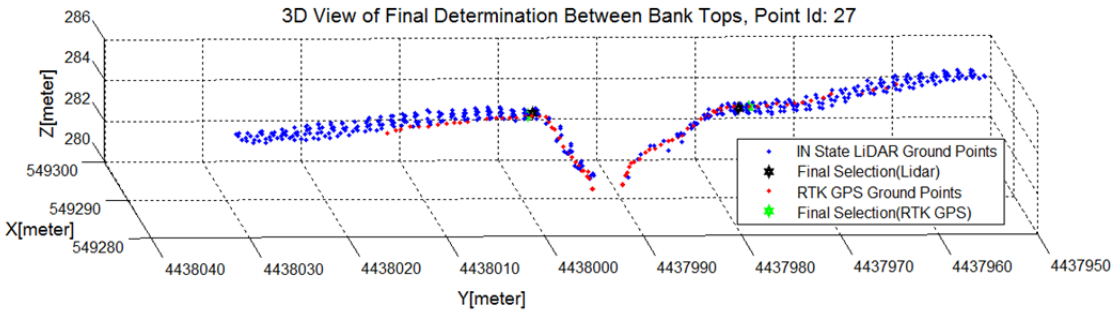

Figure 3.26 The final top of the bank results in NAD83 UTM Zone 16 coordinate system The cross section transect of RTK GPS points (red) overlaid with the LiDAR points (blue) with 6m by 80m cross section box, top of the banks in blue for LiDAR, in green RTK GPS

3.6 Application of the Method to Entire Ditch Section

Field surveyed areas of the ditches were digitized in MATLAB and the method of the identifying top of the bank was implemented to entire ditch section. Figure 3.27 shows surveyed area zoomed in from orthoimagery tile from Site 1. This image was clicked on the curving location of the stream with cursor. The coordinates were obtained and interpolated approximately 5m distance by using a MATLAB script (Fukushima, 2005) called **curvspace**. The method decried in Section 3.1-3.5 was applied to along the length of the stream and transformed to global coordinates. Figure 3.28 shows cross sections in 3D view. Figure 3.29 shows the top of the banks as overlaid with Indiana State Ortho Imagery. The cross section on the curve where the stream points 8 and 10 were located, the top (Figure 3.29 -on left) appeared closer to the ditch than adjacent tops. Figure 3.30 shows the individual cross section points and smoothed line of that particular top of the bank located at the point 9, and shows that top actually located before the tree as it was expected. Figures belong to other surveys sites were included in the appendix. Table 3.1 shows coordinates of the resultant cross sections in UTM NAD83 Zone 16 coordinate system.

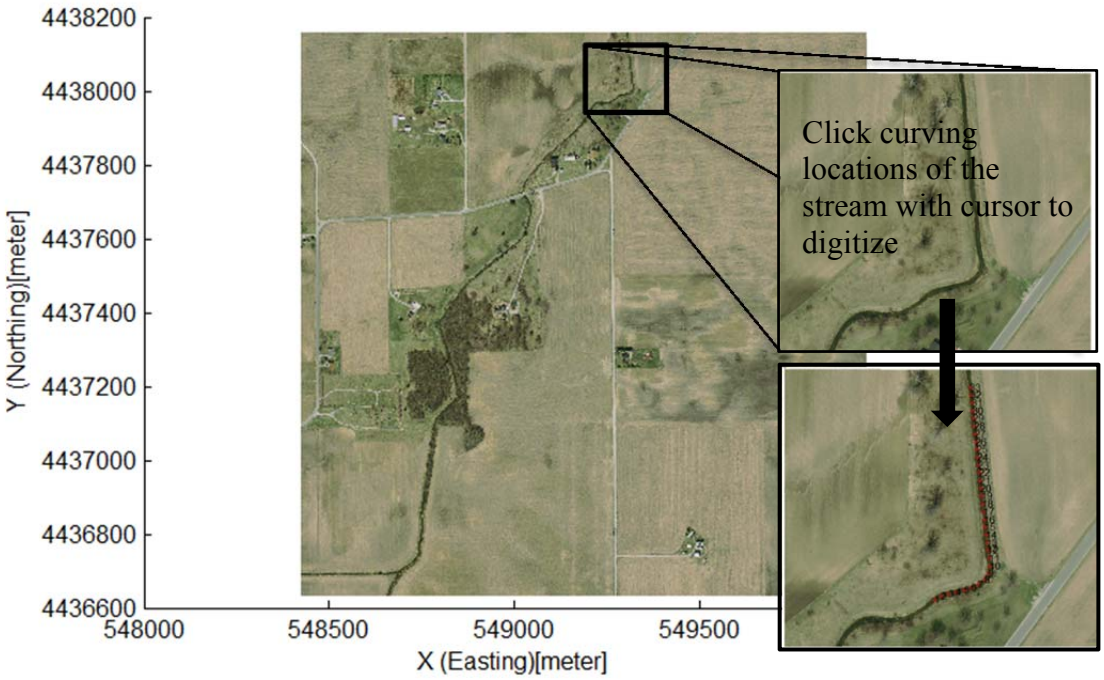

Figure 3.27 Zoomed to surveyed location of the stream and digitized stream by clicking curving location of the stream

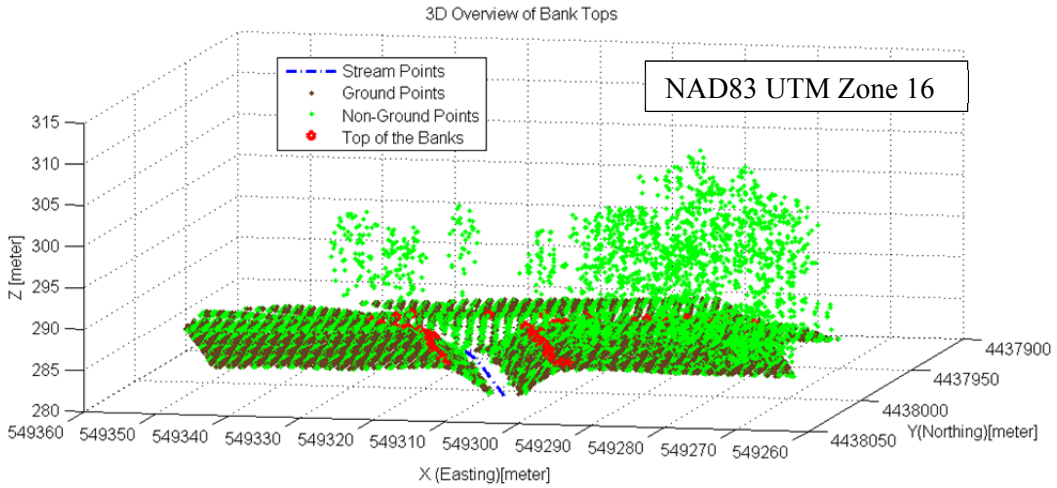

Figure 3.28 Top of the banks over 3D view of Site 1, ground (brown) and non-ground(green) points

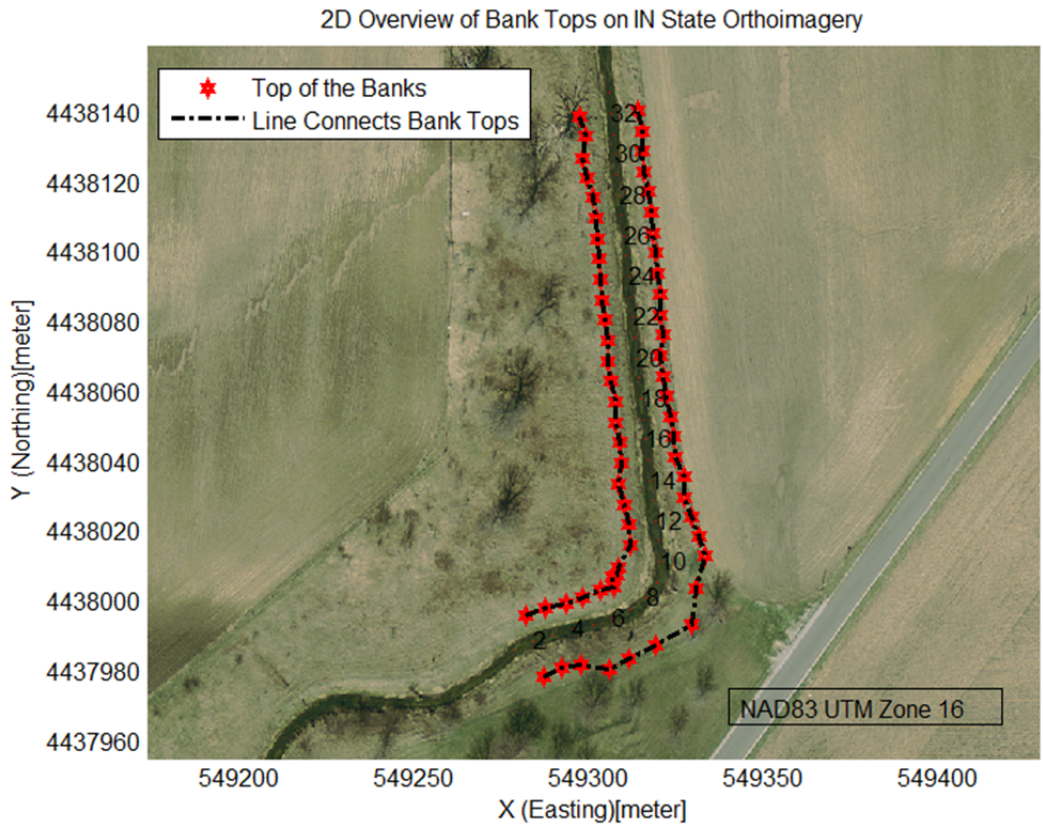

Figure 3.29 Bank Tops over Indiana State Imagery in Site 1

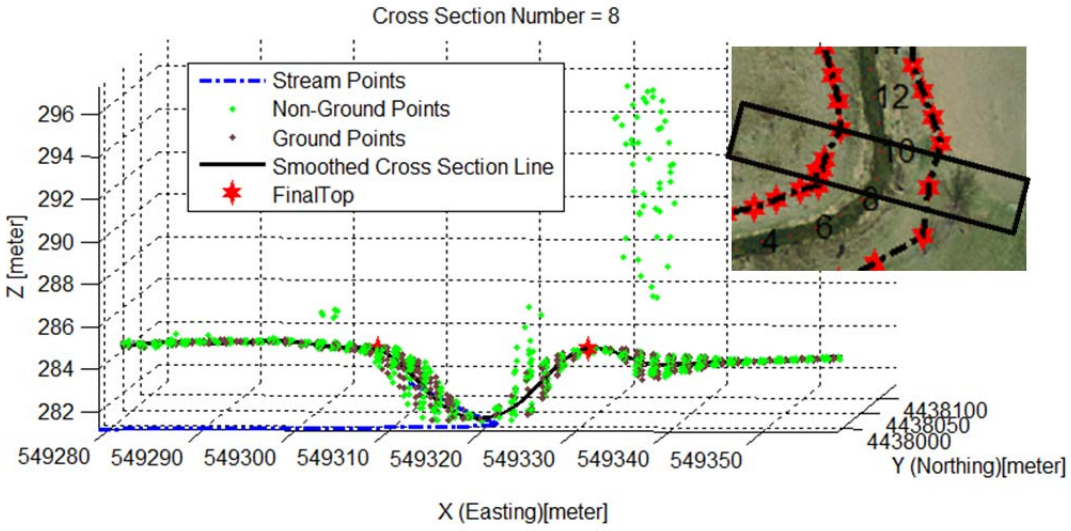

Figure 3.30 Individual cross section can be viewed (the number of cross sections are 1 less than the number of the stream points)

Table 3.1 Bank Top Coordinates for Site 1

Top of the Bank Coordinates (NAD83 UTM Zone 16)						
Site 1	North-West Side of the Stream			South-East Side of the Stream		
	X(m)	Y(m)	Z(m)	X(m)	Y(m)	Z(m)
CR1	549281.94	4437996.41	284.85	549287.12	4437978.64	284.80
CR2	549287.72	4437998.14	284.89	549292.25	4437981.25	284.72
CR3	549293.72	4437999.75	284.94	549297.64	4437982.10	284.65
CR4	549298.21	4438001.45	284.92	549305.79	4437980.70	284.72
CR5	549303.28	4438003.32	284.83	549311.72	4437983.60	284.84
CR6	549307.40	4438004.30	284.70	549319.15	4437987.66	284.79
CR7	549306.91	4438007.18	284.74	549329.33	4437993.52	284.87
CR8	549308.00	4438007.90	284.77	549330.71	4438003.87	284.83
CR9	549308.61	4438009.92	284.73	549333.41	4438013.31	284.68
CR10	549312.04	4438016.32	284.64	549331.78	4438019.01	284.52
CR11	549311.68	4438022.19	284.81	549329.31	4438024.60	284.45
CR12	549310.22	4438028.07	284.64	549327.31	4438030.08	284.49
CR13	549308.65	4438033.87	284.65	549327.38	4438035.92	284.65
CR14	549309.29	4438039.85	284.75	549324.85	4438041.55	284.82
CR15	549308.88	4438045.71	284.59	549324.18	4438047.38	284.91
CR16	549307.75	4438051.49	284.56	549323.45	4438053.21	284.89
CR17	549307.51	4438057.40	284.67	549322.40	4438058.98	284.92
CR18	549306.53	4438063.21	284.49	549321.18	4438064.74	284.96
CR19	549305.74	4438069.03	284.68	549320.61	4438070.58	285.04
CR20	549305.67	4438074.92	284.54	549321.18	4438076.55	285.12
CR21	549304.53	4438080.71	284.55	549320.47	4438082.38	285.04
CR22	549303.77	4438086.53	284.54	549320.41	4438088.27	285.10
CR23	549303.30	4438092.38	284.46	549319.66	4438094.10	285.09
CR24	549303.20	4438098.28	284.44	549319.22	4438099.95	285.07
CR25	549302.43	4438104.10	284.43	549318.30	4438105.76	285.01
CR26	549301.95	4438109.95	284.43	549317.91	4438111.62	285.00
CR27	549301.45	4438115.80	284.46	549317.28	4438117.46	284.99
CR28	549299.52	4438121.50	284.47	549315.99	4438123.23	284.89
CR29	549298.17	4438127.27	284.50	549315.52	4438129.08	284.79
CR30	549299.32	4438133.29	284.62	549315.22	4438134.95	284.80
CR31	549297.59	4438139.01	284.72	549314.31	4438140.76	284.65

CHAPTER 4. RESULTS: EXTRACTION OF THE TOP OF THE DITCH BANKS

Global coordinates of the top of the bank locations were calculated from both the RTK GPS points and the LiDAR points for each cross section. Individual cross section results for each data source are in Appendix B (figures) and Appendix C (tables of coordinates). This chapter discusses the comparisons among the different data sources.

4.1 Comparison of State LiDAR and RTK GPS

The horizontal coordinate difference between RTK GPS and IN State LiDAR for each top of the bank ranged from 0.04m to 1.83m (Figure 4.3). This represents the Euclidian distance of X (Easting) and Y (Northing)

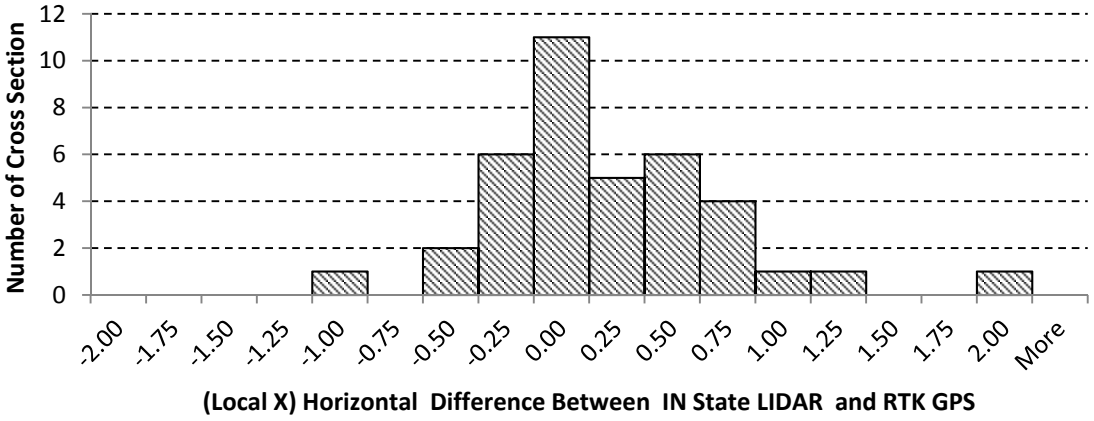

Figure 4.1 Histogram of Local X difference between top of bank locations determined from IN State LiDAR and RTK GPS

The vertical coordinate difference was considerably smaller, ranging only from 0.02 m to 0.41m (Figure 4.2).

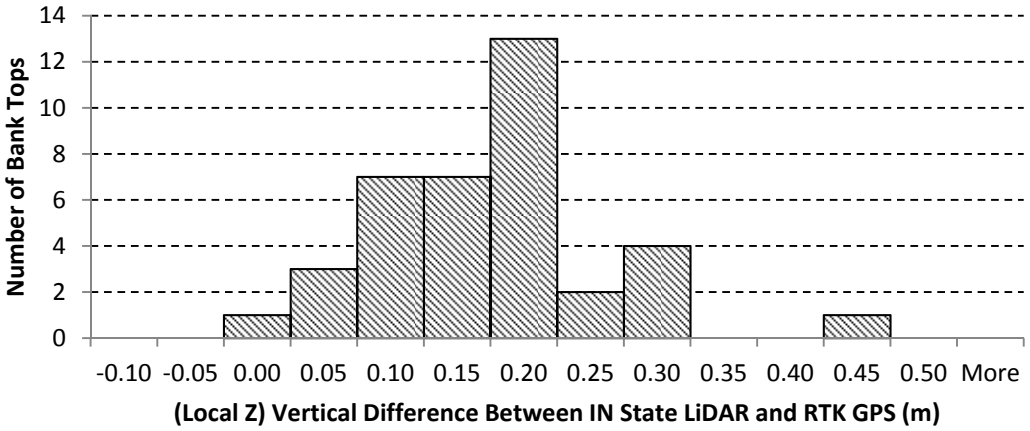

Figure 4.2 Histogram shows Local Z difference between top of bank locations determined from IN State LiDAR and RTK GPS

The largest vertical coordinate difference, 0.41 m, occurred in Site 2 Cross Section 4 (Table 4.1), and was likely due to the high and dense grass vegetation on this site during LiDAR survey. Photos of this site in Appendix B, Figure B9; the high vegetation prevent from obtaining pictures of other cross sections and the high dried vegetation was observed. The largest horizontal coordinate difference, 1.83 m, was observed in Site 1 Cross Section 1, with the likely reason being the smoothness of the spline developed with smoothing spline fit (Figure 5.5). The detected top of bank location from smoothing spline was closer than the tops detected with Gaussian Mixture Model, and because the candidate determination rules are favor of those closer to the ditch center reference, this value was selected. The RMSE of the differences was 0.54m for horizontal and 0.18m for vertical.

Table 4.1 Vertical and horizontal coordinate difference between bank tops

Site and Cross Section	Local Z Difference Between IN State LiDAR - RTK GPS		Local X difference between IN State LiDAR – RTK GPS	
	Positive(P) Sides (m)	Negative (N) Sides (m)	Positive(P) Sides (m)	Negative (N) Sides (m)
Site1-CR1*	0.16	0.10	1.83	-1.16
Site1-CR2*	0.07	-0.02	-0.24	1.23
Site1-CR3	0.02	0.11	-0.20	0.09
Site1-CR4	0.10	0.18	0.07	0.88
Site1-CR5	0.09	0.17	-0.23	-0.58
Site2-CR1	0.30	0.13	0.11	0.08
Site2-CR2	0.27	0.18	-0.72	-0.08
Site2-CR3	0.28	0.19	-0.39	0.32
Site2-CR4	0.41	0.16	0.46	-0.09
Site3-CR1	0.18	0.13	-0.48	-0.22
Site3-CR2	0.27	0.16	0.51	-0.04
Site3-CR3	0.15	0.14	-0.22	0.26
Site3-CR4	0.18	0.15	-0.14	0.53
Site3-CR5	0.17	0.17	-0.08	0.30
Site4-CR1*	0.14	0.01	0.71	0.58
Site4-CR2	0.16	0.25	0.04	-0.42
Site4-CR3	0.08	0.10	-0.36	0.31
Site4-CR4	0.08	0.03	-0.25	-0.47
Site4-CR5	0.16	0.23	0.35	-0.11
RMSE(m)	0.20	0.15	0.55	0.53
RMSE for both sides	0.18		0.54	

The difference in width of the ditch calculated from these values provides more insight into the accuracy of the method for one of its intended purposes. Table 4.2 indicates the width between the corresponding top of the banks for the both data sets and their width difference. Figure 4.3 shows the strong relationship (R^2=0.93) between width from IN State LiDAR and RTK GPS.

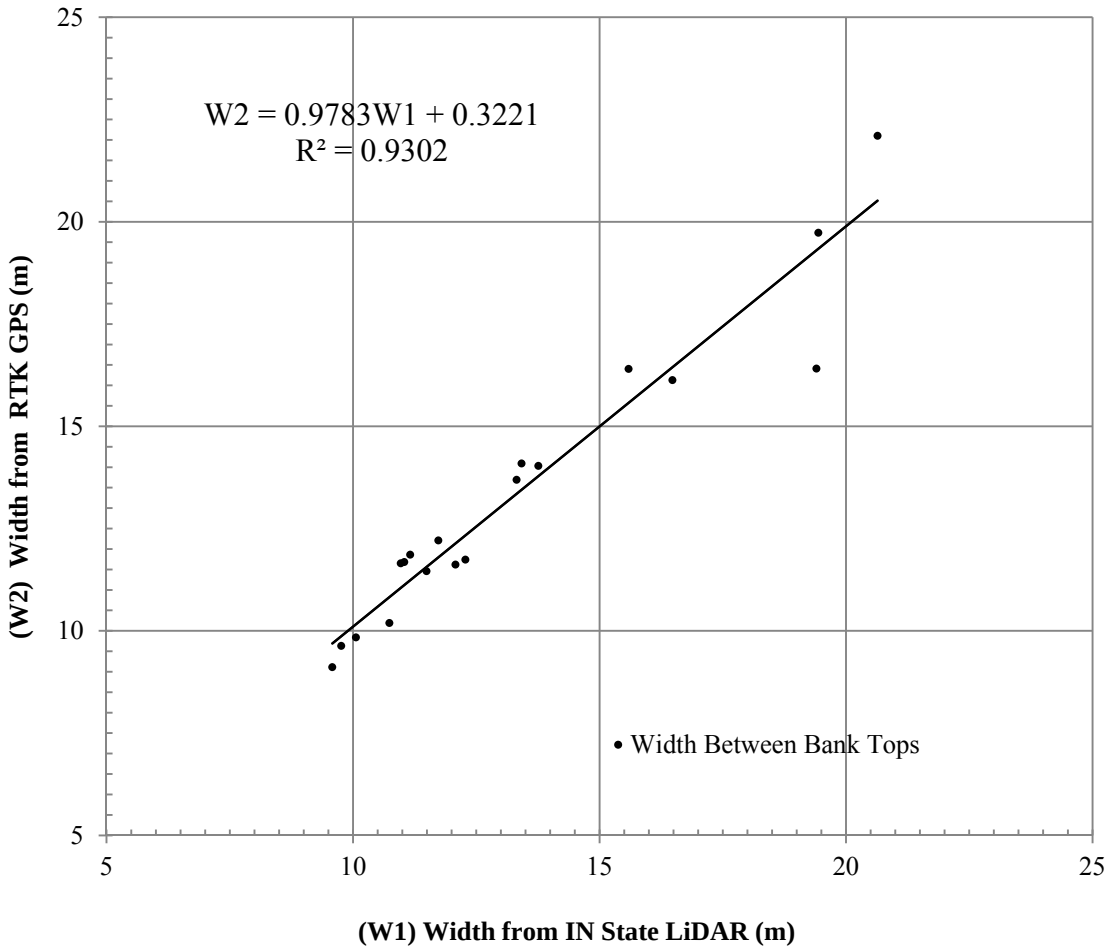

Figure 4.3 Comparison of width between IN State LiDAR and RTK GPS

Table 4.2 Width between the corresponding bank tops of cross sections and width difference between LiDAR and RTK GPS

Width Difference Between Corresponding Bank Tops			
Site and Cross Section	Positive Side –Negative Side		Width Difference
	Width from IN State LiDAR(1) (m)	Width from RTK GPS(2) (m)	(1)- (2) (m)
Site1-CR1*	19.40	16.41	2.99
Site1-CR2*	20.64	22.10	-1.46
Site1-CR3	19.44	19.73	-0.29
Site1-CR4	15.59	16.40	-0.81
Site1-CR5	16.48	16.13	0.35
Site2-CR1	11.49	11.46	0.03
Site2-CR2	11.04	11.68	-0.64
Site2-CR3	11.16	11.86	-0.71
Site2-CR4	10.74	10.19	0.55
Site3-CR1	13.76	14.03	-0.26
Site3-CR2	12.28	11.74	0.55
Site3-CR3	11.73	12.21	-0.48
Site3-CR4	13.42	14.09	-0.67
Site3-CR5	13.32	13.69	-0.37
Site4-CR1*	9.76	9.63	0.13
Site4-CR2	12.08	11.62	0.46
Site4-CR3	10.97	11.65	-0.67
Site4-CR4	10.06	9.84	0.22
Site4-CR5	9.58	9.11	0.46
		RMSE(m):	0.90

4.2 Results from Comparison of State LiDAR and G-LiHT LiDAR with RTK GPS

The last column of Table C.19 and C.24 for height, Table C.20 and Table C.25 for width were used to compare of G-LiHT LiDAR and IN State LiDAR at Site 4 (See Appendix C). Since the absolute accuracy of G-LiHT LiDAR was not as good as IN State LiDAR and of vertical offset explained in section 2.1.2, the difference of H1 and H2 in Table 4.3, the difference of W1 and W2 in Table 4.4 for LIDAR and RTK GPS dataset were used for evaluation of LiDAR data sets. The vertical difference (H1 from LiDAR and H2 from RTK GPS) and horizontal difference (W1 from LiDAR and W2 from RTK

GPS) of the top of the corresponding banks were shown in Figure 4.4. For vertical discrepancy (H1-H2), State LiDAR shows slightly smaller RMSE than G-LiHT LiDAR. For horizontal discrepancy (W1-W2), G-LiHT LiDAR shows slightly smaller RMSE. The initial expectation was that the data with lower NPS would give better results than the data with higher NPS. However, factors such as different seasons of data acquisition, the methods for classification of ground points and the positioning of the LiDAR point cloud due to both IMU and processing of navigation data impacted the results.

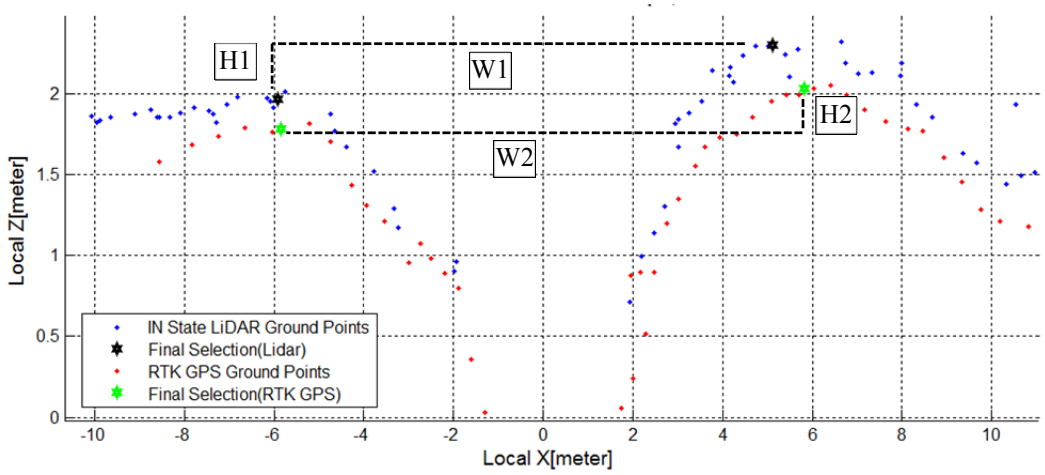

Figure 4.4 Height and Width between corresponding bank tops (Site 2-CR2)

Table 4.3 Comparison for H1 an H2 between IN State LiDAR and G-LiHT LiDAR

Vertical Difference Between Corresponding Bank Tops and Vertical Discrepancy					
Site 4	Positive Side –Negative Side			IN State LiDAR (1)- (2) (m)	G-LiHT LiDAR (1)- (2) (m)
	IN State LiDAR (1)(m)	G-LiHT LiDAR (1)(m)	RTK GPS (2) (m)		
CR1*	-0.27	-0.18	-0.40	0.13	0.22
CR2	0.02	0.09	0.12	-0.10	-0.03
CR3	0.66	0.93	0.67	-0.02	0.26
CR4	0.34	0.29	0.29	0.05	0.00
CR5	0.04	0.13	0.11	-0.07	0.02
			RMSE(m):	0.08	0.15

Table 4.4 Comparison for W1 and W2 between IN State LiDAR and G-LiHT LiDAR

Horizontal Difference Between Corresponding Bank Tops and Horizontal Discrepancy					
Site 4	Positive Side –Negative Side			IN State LiDAR (1)- (2) (m)	G-LiHT LiDAR (1)- (2) (m)
	IN State LiDAR (1)(m)	G-LiHT LiDAR (1)(m)	RTK GPS (2) (m)		
CR1*	9.76	9.39	9.63	0.13	-0.24
CR2	12.08	11.69	11.62	0.46	0.06
CR3	10.97	11.10	11.65	-0.67	-0.54
CR4	10.06	10.37	9.84	0.22	0.53
CR5	9.58	9.28	9.11	0.46	0.17
			RMSE(m)	0.44	0.36

4.3 Additional Issues

During calculation of the top of the banks, one issue was the miscalculation of the top from the RTK GPS points for Site 2 Cross Section 5. Due to occurrence of natural step (bevel) on the bank, shown on negative side in Figure 4.5, the methods detected the step as top of the bank with RTK GPS points (green dot). Thus, that particular cross section was excluded from calculations of the results and tables indicating relations between bank tops.

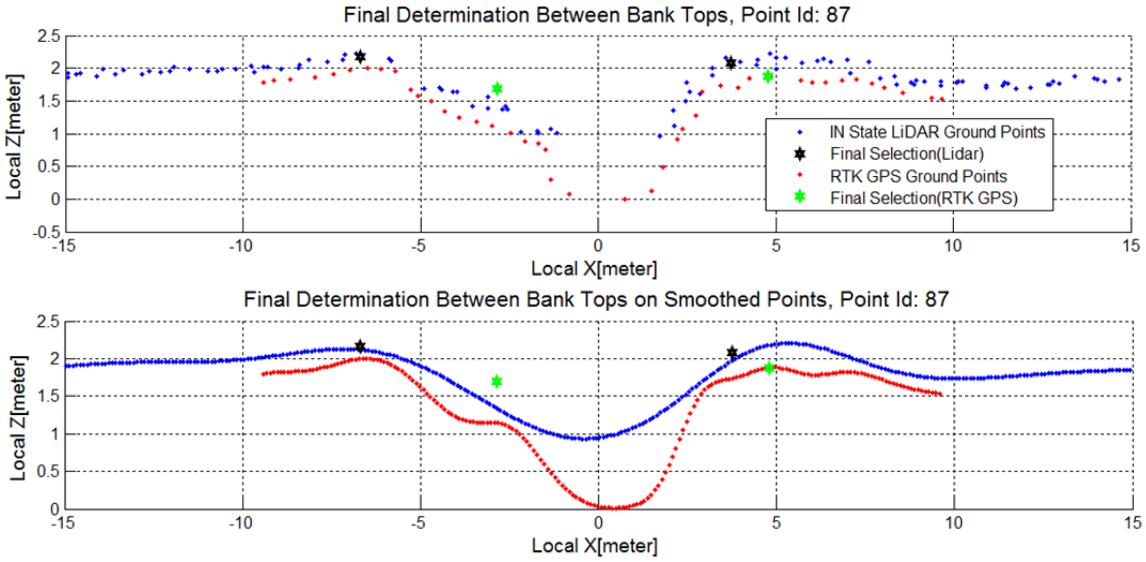

Figure 4.5 Site 2 Cross Section 5, on the left side, the top of the bank from GPS points determined on the small step of the spline

It should be noted that additional smoothing with Gaussian Mixture Model option on smoothed data helped to finding the bank top with RTK GPS points shown in Figure 4.6. In the future algorithm should be extended to handle similar issues. From the standpoint of two stage ditches, the algorithm potentially could be adopted to determine lower and higher stages with settings of less and more smoothing options and some changes in rules of candidate determination of the top of the bank.

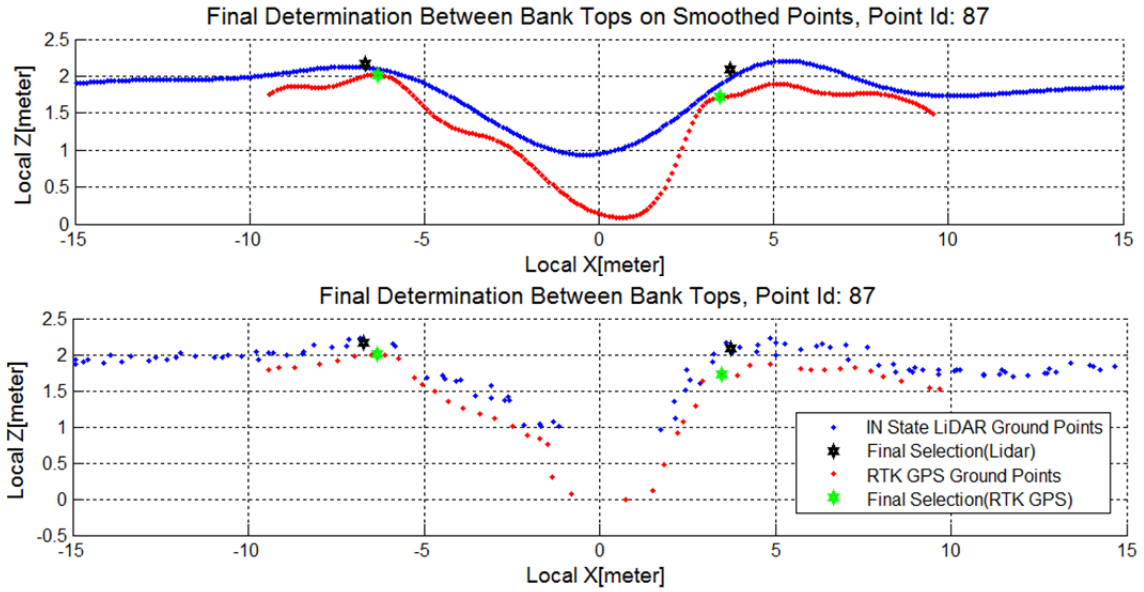

Figure 4.6 Cross Section 5, on the left side, the top of the bank from GPS points determined after double Gaussian Mixture Model Smoothing

CHAPTER 5. CONCLUSIONS AND RECOMMENDATIONS

The goal of this study was to investigate the use of the Indiana Statewide LiDAR data products for identifying the cross sectional shape of agricultural drainage ditches. To accomplish this, A method was developed to identify the top of the banks of the ditches from LiDAR point cloud data. The method includes six steps; 1) Digitize and smooth points along the course of the stream, 2) Transform to local coordinates to position a cross section box for extracting LiDAR data at a given location, 3) Select LiDAR points in the cross section , 4) Smooth LiDAR ground points within the cross section, 5) Identify candidate top of bank points using three methods and select final locations, 6) Convert back to global coordinates. The method was applied to determine the top of the bank of an entire section of the ditch.

A set of NASA Goddard`s LiDAR (G-LiHT) data, was also analyzed to evaluate the impact of lower nominal point spacing on proper characterization of the ditch geometry. Spline fits and mixture of Gaussian models were investigated to smooth the pre-classified ground points.

The locations of the top of the banks obtained using the new method were compared to results from the field surveyed RTK GPS points of 19 cross section transects of four ditches in Howard, Clinton and Boone County, Indiana. The RMSE of orthometric height difference between results from the Indiana Statewide LiDAR and RTK GPS points were ± 0.18m, the RMSE of the difference in horizontal location between the top of the bank results were ± 0.54m.The comparison of results derived from the two LiDAR data sets was performed in 5 cross sections in Howard County.

Issues contributing to errors in the cross section delineation from LiDAR include; 1) misclassification of ground points, 2) stream curvature, 3) the difference in date between collection of field data and LiDAR data, 4) the effects of vegetation

Conclusions from the study included:

- For obtaining top of the bank and similar applications from Indiana State LiDAR, the LiDAR point cloud should be used instead of the DEM; i) accuracy of results improved with reclassification of LiDAR points, ii) the use of point data also enables the user to understand issues such as whether the top of the banks is located under a tree or another object which is not shown in the DEM.

- The vendor`s classification of data was adequate in 3 sites but not in Howard County. The G-LiHT LiDAR point classification was not adequate because points located in bank tops were also classified as non-ground. The Indiana State LIDAR data in Howard County and G-LiHT LiDAR was re-classified. The quality of original data classification varied for several reasons, including presence of vegetation. The classification by the vendor was performed for development of a large scale DEM, and not always appropriate for extracting find scale ditch geometry.

- Ascii format data and MATLAB software worked well for exploration of the algorithm. For operational purposes, the data should to be in LAS format, and the algorithms should be coded in a programming language that can accommodate large data sets in LAS format

- The LiDAR dataset with lower point spacing (NASA G-LiHT) was obtained for purpose of canopy height modeling in June 2012 when the vegetation was high. It was used in this study as a possible alternative with lower point spacing. For ditch geometry analysis, data with tall, dense vegetation resulted in misclassification of LiDAR points

This research provides the foundation for future studies that would utilize the ditch geometry, including 1) Calculation of bankfull area (See appendix B for bankfull area calculation results) and estimating the volume of the ditch section, 2) calculation of an easement buffer area for a ditch section, and 3) the identification of the tops of two stage ditches could be possible future works related to this study.

The cross sections developed during this research could support managers in developing effective strategies for construction and maintenance, as well as researchers seeking to better understand hydrology of the rural areas and related to water quality from areas agricultural areas.

5.1 Issues Related to the Methods

5.1.1 Data Acquisition Dates and Misclassification of Points

As shown in Figure 5.1, Cross Section 4 in Site 4, the G-LiHT point data are quite variable in the summer 2012 data acquisition. However, 2013 surveyed RTK GPS points and 2011 IN State LiDAR points show very smooth terrain in Figure 5.1

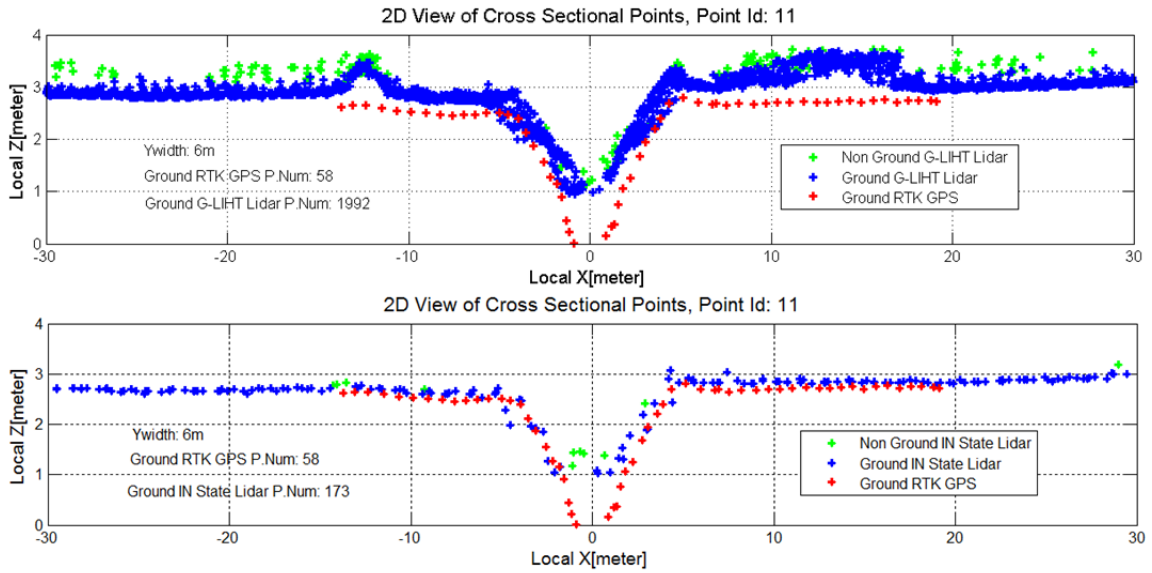

Figure 5.1 Site 4 Cross Section 4, August 2013 RTK GPS points were overlaid with G-LiHT LiDAR- June 2012, (top figure), and with Indiana State LiDAR (bottom figure)- March 2011

Since data acquisition occurred on March 2011, before the vegetation regrew, the small trees in Figure 5.2 in the ditch are not even visible in the State LiDAR, but were observed with the G-LiHT LiDAR on June 2012. Dense vegetation in terrain impacts the LiDAR reaching the ground as can be seen in the left side of Figure 5.3 and on both sides of the Figure 5.1 for G-LiHT LiDAR resulting in vegetation being classified as ground points. The resulting spline fits on those points may negatively affect the resulting identification of the top of the banks.

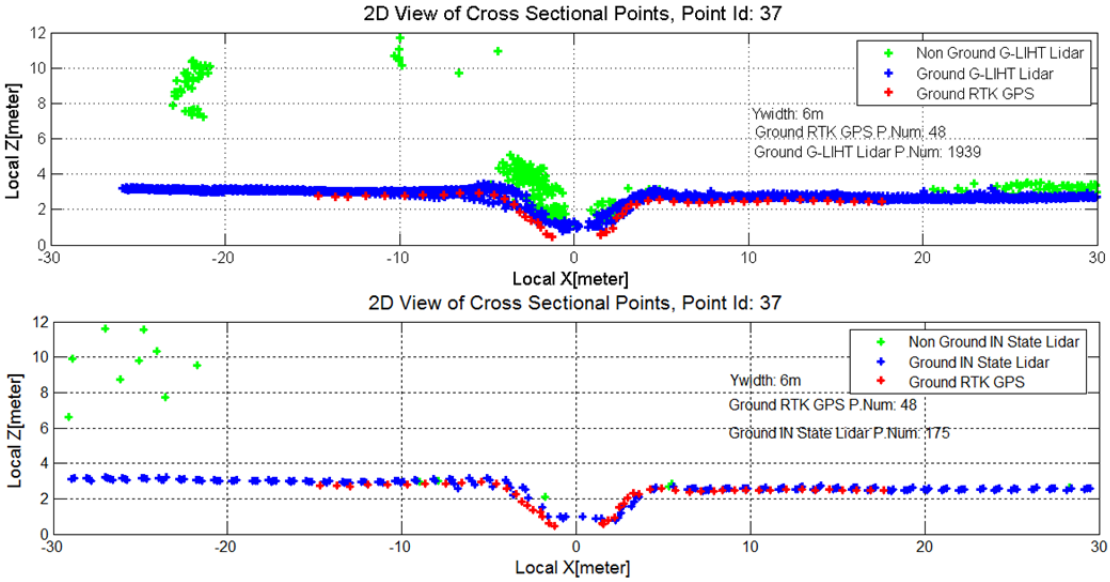

Figure 5.2 Site 4 Cross Section 1, August 2013 RTK GPS points were overlaid with G-LiHT LiDAR- June 2012, (top figure), and with Indiana State LiDAR (bottom figure)- March 2011

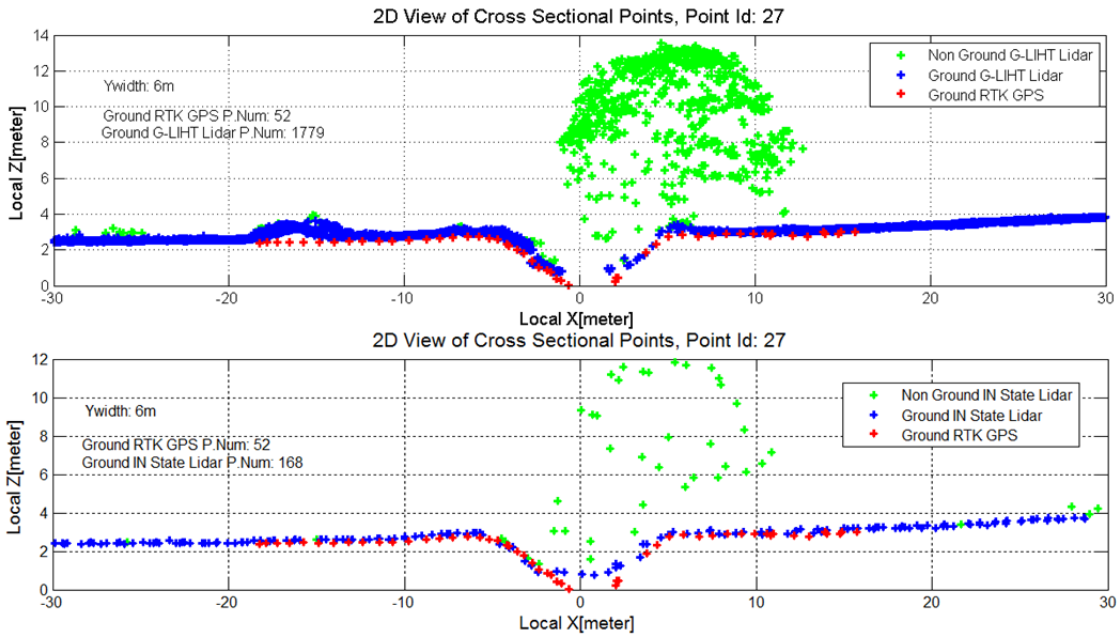

Figure 5.3 Site 4 Cross Section 2, August 2013 RTK GPS points were overlaid with G-LiHT LiDAR- June 2012, (top figure), and with Indiana State LiDAR (bottom figure)- March 2011

For Site 1, Cross Section 2 on the left side, the ground points under the tree were more scattered and less dense, leading to fitting a higher elevation and obtaining a final top of the bank from the State LiDAR points that does not agree with the RTK GPS points (Figure 5.4).

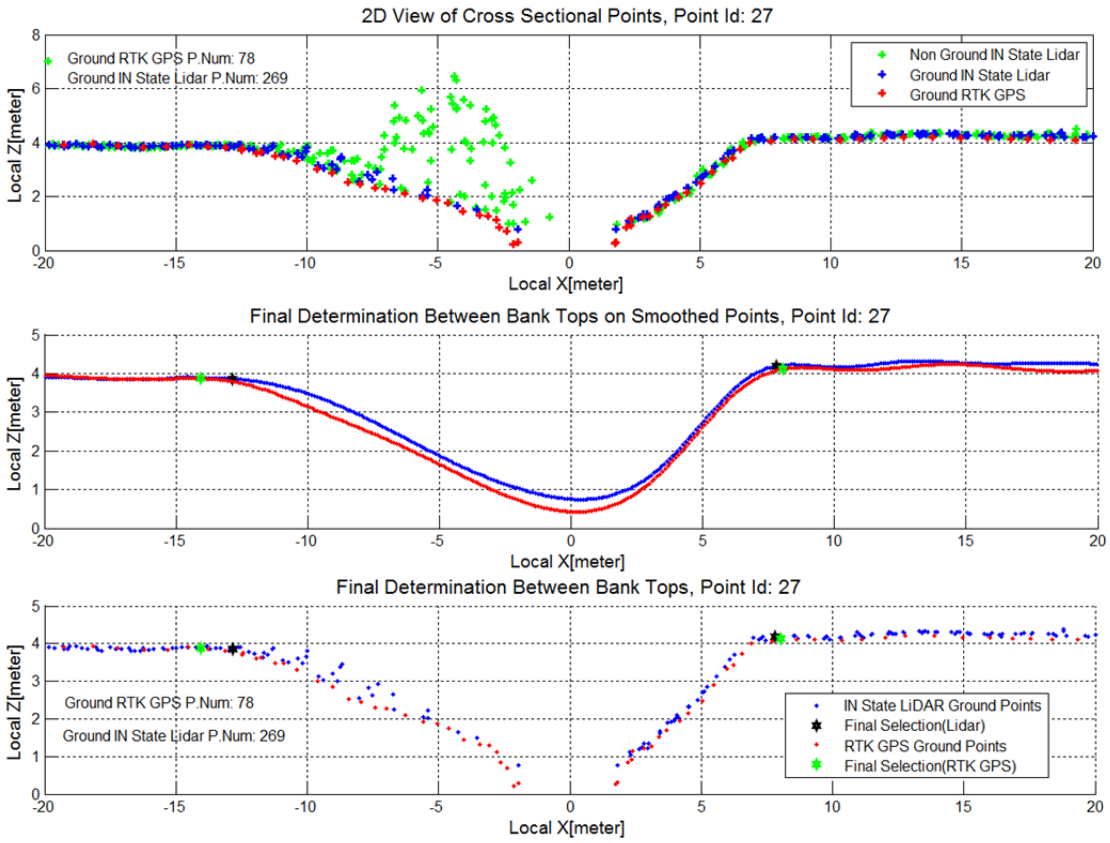

Figure 5.4 Site 1 Cross Section 2, on the left side, the tops of the bank have large horizontal discrepancy due to scattering ground points (blue) under the tree

5.1.2 Determination of Bank Tops between Smoothing Spline and Gaussian Mixture Model

Spline fit parameters were determined by the fit with smallest RMSE for both smoothing methods (see Section 3.3.1.3). During evaluation of candidate locations for the top of the bank, the bank top with the highest value and the closest to the center reference were preferred within the rules summarized in Section 4.3.2. The smoothing spline fits generally exhibit more curvature than the Gaussian fit. In several cases, when the rules selected the top of the bank using the smoothing spline, the values were higher elevation than the actual ground RTK points.

The final estimate of the bank top was about 10 cm above the RTK GPS points in the example shown in Figure 5.5. The selection process and the spline fits contribute uncertainty in final top of the estimate.

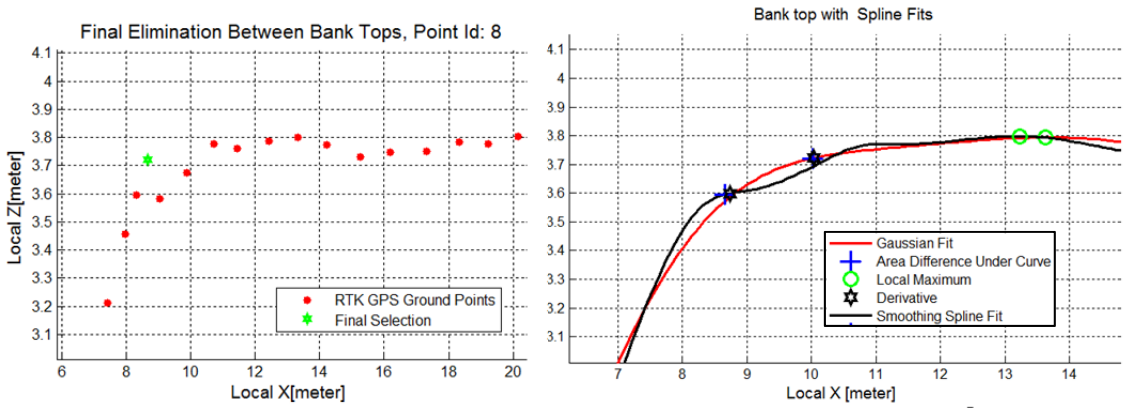

Figure 5.5 Site 1 Cross Section 1 (Positive Side) Effect of candidate evaluation rules on final top of the estimate

5.2 Recommendations

Several issues should also be considered relative to methodology.

- The cross section box size should be adaptive to sinuosity of stream points and NPS of the data. The stream curvature affected the location of the resultant top of the bank. The algorithm should be adapted to automatically reduce the size of the width when data are being extracted from curving sections of the stream. The method should also assure that an adequate number of points are included to represent the banks and the benches representing the tops of the banks.. Changes between rotation angles also can be used as an indicator of stream curving in the adaptation process.
- Choice of spline impacted the resultant location of the top of the bank. Automatic selection of the spline fit parameters and goodness of fit should be reviewed, possibly by putting restrictions on potential parameter values. The grid search with a minimum RMSE objective function results in the best fit of the spline to

the ground points, but not necessarily the best representation of the ditch cross section shape. The top of the bank locations obtained using the Gaussian fit option, were sometimes impacted by over smoothing. However, the smoothing spline fit option did not always provide adequate smoothing using parameters derived from grid search with RMSE.

- The process selecting for the final tops of the banks from candidate locations needs further investigation. When the top of the bank locations from the various methods were close to each other on the edge of the banks, the top of the banks were detected above actual ground points due to the simplification of using the mean value of local coordinates in the rules. For example, the mean x value along with its corresponding z coordinate value could be selected. The smoothing spline could also contribute to exaggerated height of the top of the banks.
- In two stage ditches or ditches with natural benches, the algorithm may detect the first stage as the top of the bank, if the spline shape is not adequately smooth (example: site 2- cross section 5, Figure B.14 and B.15). To handle this issue, the algorithm could be applied first to the data with less smoothing to find the lower stage, and then adapted with more smoothing to obtain the higher stage as the top of the bank.

Several issues should also be considered relative to software and processing methodology

- Reading data from LAS format instead of ASCII format in MATLAB would be necessary when large size data need to be processed. During the reclassification process, the LAS format files were converted to ASCII format via LASTOOLS software, which is not an open source software package for large data sets. The open source MCC_LIDAR could be used for reclassification of the LiDAR points for large datasets and reading large dataset in binary format in MATLAB would also eliminate the need to obtain a subset of the data via FUSION software (but limited to MATLAB handling capability).

Several other technical issues impacted the analysis. For future studies it is recommended that for fieldwork:

- The difference between Geoid12A and Geoid09 should be considered. The Indiana State LiDAR was referenced to Geoid09 and RTK GPS points acquired via the In-CORS Network were referenced to Geoid12A height model; the comparison of the height difference from the two models could create about 5cm height difference in orthometric height (Roden, 2013). Referencing same geoid model for large size (> 1km due to grid resolution of geoid models) ditch analyses may improve accuracy.
- The RTK GPS and LiDAR data collection should be as concurrent as possible, and when minimal water is in the ditches.
- For cross sections with high-level trees, the RTK GPS accuracy becomes very low due to interference, and sometimes a solution cannot be obtained via the data collector.
- To determine the error of the method itself, the top of the banks could be measured via RTK GPS on sites with limited vegetation. Determination of the top of the bank itself also can be an issue with high-level grass vegetation covering the ditch site as in Site 2.The ditches used to obtain model accuracy should be chosen from less vegetated areas to reduce the impact of the vegetation.
- Effect of the NPS and improvement needs further study.

REFERENCES

LIST OF REFERENCES

Abbitt, R. J., Ellison, E., & Rakovan, M. (2011). Stream Channel Mapping In Southwest Ohio Using LiDAR [ESRI Conference Presentation]. Retrieved from http://www.units.muohio.edu/geography/wp-content/uploads/abbitt_esri_2011.pdf

ASPRS (2010). American Society for Photogrammetry & Remote Sensing LAS Specifications Version 1.3. Retrieved from http://asprs.org/a/society/committees/standards/LAS_1_3_r11.pdf

ASPRS (2013). *LASer (LAS) File Format Exchange Activities*. Retrieved October 6, 2013, from http://asprs.org/Committee-General/LASer-LAS-File-Format-Exchange-Activities.html

Axelsson, P. (2000). DEM generation from laser scanner data using adaptive TIN models. *Remote Sensing and Spatial Information Sciences*.

Bater, C. W., & Coops, N. C. (2009). Evaluating error associated with lidar-derived DEM interpolation. *Computers & Geosciences*, *35*(2), 289–300

Cantu, O. R. (2011). *Topcon Hyperlite and FC-236 RTK Network Webinar Presentation*. http://ftp://ftp.hayeshelp.com/TechDocs/Topcon_HiPer_II_with_FC-236_in_a_Real_Time_Network.pdf

CBBEL - Christopher B. Burke Engineering, Ltd (1999). *DNR: Indiana Drainage Handbook*. 338

Chapra, S. C. (2012). *Applied numerical methods with MATLAB for engineers and scientists*. New York: McGraw-Hill., 371

Cleveland, W. S. (1979). Robust Locally Weighted Regression and Smoothing Scatterplots. *Journal of the American Statistical Association*, *74*(368).

Cook, B. D., Corp, L. A., Corp, R. F., Middleton, E. M., Morton, D. C., McCorkel, J. T., Masek, J. G., Ranson, K. J., Ly, V., & Montesano, P. M. (2013). NASA Goddard?s LiDAR, Hyperspectral and Thermal(G-LiHT) Airborne Imager. *Remote Sensing* **2013**, *5*, 4045-4066

CSAbrochure ,2010. *Indiana County Surveyor Brochure*. Retrieved from County Surveyors Association of Indiana website: http://www.indianacountysurveyors.org/docs/CSAbrochure2010.pdf

Deuflhard, P. (2011). *Newton Methods For Nonlinear Problems: Affine Invariance And Adaptive Algorithms*. Berlin: Springer. 174

Dietterick, B. C., White, R., & Hilburn, R. (2012). Comparing LiDAR-Generated to Ground- Surveyed Channel Cross-Sectional Profiles in a Forested Mountain Stream. *General Technical Reports of the Pacific Southwest Research Station-PSW-GTR-238*. 639 http://www.fs.fed.us/psw/publications/documents/psw_gtr238/psw_gtr238_639.pdf

Evans , J. S., & Hudak, T. H. (2007). A Multiscale Curvature Algorithm for Classifying Discrete Return LiDAR in Forested Environments. *IEEE Transactions on Geoscience And Remote Sensing*, *45*(4).

Fan , J., & Yao , Q. (2005). *Non-Linear Time Series, Non Parametric and Parametric Methods*. Secaucus,NJ/USA: Springer. 251

Faux, R. N., Buffington, J. M., Whitley, M. G., Lanigan, S. H., & Roper, B. B. (2009). Use of Airborne Near-Infrared LiDAR for Determining Channel Cross-Section Characteristics and Monitoring Aquatic Habitat in Pacific Northwest Rivers: A Preliminary Analysis. *PNAMP Special Publication: Remote Sensing Applications for Aquatic Resource Monitoring*. 43

FGCD (2013). *Geospatial Positioning Accuracy Standards Part 3: National Standard for Spatial Data Accuracy*. Retrieved June 2, 2013, from http://www.fgdc.gov/standards/projects/FGDC-standards-projects/accuracy/part3/chapter3

Fox , J. (2002). Nonparametric Regression, Appendix to An R and S-PLUS Companion to Applied Regression. Retrieved from http://cran.r-project.org/doc/contrib/Fox-Companion/appendix-nonparametric-regression.pdf

Fukushima, Y. (2005). *MATLAB Center-curvspace*. Retrieved October 25, 2013, from http://www.mathworks.com/matlabcentral/fileexchange/7233-curvspace/content/curvspace.m

Greenville County (2013). Greenville County Storm Water Management Design Manual,South Carolina. Retrieved from http://www.greenvillecounty.org/land_development/pdf/designmanual/DesignManual_revJan_2013.pdf

Guo , Q., Li , W., Yu , H., & Alvarez , O. (2010). Effects of Topographic Variability and Lidar Sampling Density on Several DEM Interpolation Methods. *Photogrammetric Engineering & Remote Sensing*, *76*(6).

Habib , A. F., Chang , Y. C., & Lee , D. C. (2009). Occlusion-based Methodology for the Classification of Lidar Data,. *Photogrammetric Engineering & Remote Sensing*. 703-712

Haugerud, R. A., & Harding , D. J. (2001). Some Algorithms for Virtual Deforestation (Vdf) Of Lidar Topographic Survey Data. Retrieved from http://pugetsoundlidar.ess.washington.edu/vdf4.pdf

Hofmann-Wellenhof , B., Lichtenegger , H., & Wasle, E. (2008). *GNSS-Global Navigation Satellite Systems: GPS, GLONASS, Galileo & More*. Springer WienNewYork., 315

IN LiDAR Metadata (2011). *Indiana state 2011 metadata*. Retrieved October 8, 2013, from https://spatialdata.iu.edu/DOQQS/state/2011/metadata/

The Indiana Drainage Code (2003). *Indiana Code 36-9-27*. Retrieved October 7, 2013, from http://www.in.gov/legislative/ic/code/title36/ar9/ch27.html

Indiana University Spatial Data Portal (2011). *2011-2013 Indiana Orthophotography (RGBI), LiDAR and Elevation*. Retrieved September 13, 2013, from http://gis.iu.edu/datasetInfo/statewide/in_2011.php

Indiana University Spatial Data Portal (2011). *Indiana 2011-2013 LiDAR Source Dates and NPS*. Retrieved September 24, 2013, from http://gis.iu.edu/files/images/dataset/2011-2013inmap_las_source_date.jpg

Isenburg, M. (2013). *LAStools: converting, filtering, viewing, processing, and compressing LIDAR data in LAS format*. Retrieved July 20, 2013, from http://www.cs.unc.edu/~isenburg/lastools/

Karp , S., & Stotts , L. B. (2012). *Fundamentals of Electro-Optic Systems Design: Communications, Lidar , and Imaging*. Cambridge University Press, 170.

Korzeniowska , K., Mandlburger , G., & Klimczyk , A. (2013). Experimental evaluation of ALS point cloud ground extraction over different land cover in the Małopolska Province. *Geophysical Research Abstracts*, *15*.

LASRead (2008). *LASRead - File Exchange - MATLAB Central*. Retrieved October 8, 2013, from http://www.mathworks.com/matlabcentral/fileexchange/21434-lasread

LASTOOLS (2013). *Lasclassify_README*. Retrieved from http://www.cs.unc.edu/~isenburg/lastools/download/lasclassify_README.txt

Ma, R. (2005). DEM Generation and Building Detection from Lidar Data. *Photogrammetric Engineering & Remote Sensing* , *71*(7). 847-854

Martin, E. C. (2011). Measuring Water Flow in surface irrigation Ditches and Gated Pipe. *Arizona Water Series*, *31*(2011).

Mathworks (2013). *Filtering and Smoothing Data - MATLAB & Simulink*. Retrieved September 12, 2013, from http://www.mathworks.com/help/curvefit/smoothing-data.html

Mathworks (2013). *Gaussian Models - MATLAB & Simulink*. Retrieved August 22, 2013, from http://www.mathworks.com/help/curvefit/gaussian.html

Mathworks (2013). *Smoothing Splines - MATLAB & Simulink*. Retrieved August 22, 2013, from http://www.mathworks.com/help/curvefit/smoothing-splines.html?searchHighlight=smoothingspline

MCC-LIDAR (2013). *MCC-LIDAR | Free Science & Engineering software downloads at SourceForge.net*. Retrieved August 2, 2013, from http://sourceforge.net/projects/mcclidar/

McGaughey, R. J. (2013). USDA FUSION/LDV: Software for LIDAR Data Analysis and Visualization, United States Department of Agriculture, Forest Service Pacific Northwest Research Station, FUSION Manual. Retrieved from http://forsys.cfr.washington.edu/fusion/FUSION_manual.pdf

ODNR DSWC (2008). *Rural Drainage Systems*. Retrieved from Ohio State Department of Natural Resources, Divison of Soil and Water Conservation website: http://www.dnr.state.oh.us/portals/12/CE/RuralDrainage/Drainage_Report.pdf

OpenTopography (2013). *NSF OpenTopography Facility | About*. Retrieved September 14, 2013, from http://www.opentopography.org/index.php/about/

OPUS (2013). *Online Positioning User Service*. Retrieved May 23, 2013, from http://www.ngs.noaa.gov/OPUS/

Passalacqua , P., Belmont, B., & Foufoula-Georgiou, E. (2012). Automatic geomorphic feature extraction from lidar inflat and engineered landscapes. *Water Resources Research*, *48*(3).

Pérez-García, J. L., Delgado, J., Cardenal, J., Colomo, C., & Ureña , M. A. (2012). Progressive Densification And Region Growing Methods For Lidar Data Classification. International Archives of the Photogrammetry, Remote Sensing and Spatial Information Sciences,Volume XXXIX-B3, 2012 XXII

Roden, S. (2013). New York State Association of Professional Land Surveyors Conference Presentation. Retrieved from NYSDOT Design Services Bureau, Land Surveying Section website: https://www.dot.ny.gov/divisions/engineering/design/design-services/land-survey/repository/NYSAPLS2013.pdf

Roley , S. S., Tank, J. L., Stephen, M. L., Johnson, L. T., Beaulieu , J. J., & Witter, J. D. (2010). Floodplain restoration enhances denitrification and reach-scale nitrogen removal in an agricultural stream. *Ecological Applications*, *22*(1).281-297

Schmid , K. (2008). An Introduction Lidar Technology, Data, and Applications. *National Oceanic and Atmospheric Administration (NOAA) Coastal Services Center Lidar 101*. Retrieved from http://www.csc.noaa.gov/digitalcoast/_/pdf/lidar101.pdf

Sofia, G., Tarolli , P., Cazorzi, F., & Dalla Fontana, G. (2013). Automatic Measurement Of Bankfull Widths From High Resolution Lidar Dtms. Retrieved from http://www.cirgeo.unipd.it/geomatics4risk/papers/Sofiaetal.pdf

Soininen , A. (2011). *TerraScan User Guide*. Retrieved from Terrasolid Ltd website: https://www.terrasolid.com/download/user_guides.html

Soininen , A. (2009). Retrieved September 24, 2013, from ftp://terrasolid.fi/pub/terrasolid.fi/ground_classification_0.ppt

Terrio , J. E., & Nazimek , P. J. (1997). Changes in Cross-Section Geometry and Channel Volume in Two Reaches of the Kankakee River in Illinois. US Geological Survey,Water Resources Investigation Reports 96-4261

Topcon (2012). Topcon Magnet Field Help. Retrieved from http://www.topcontotalcare.com/files/8513/3123/1727/MAGNET_Field_v1.0_-_Help_Manual_Rev._A_1000411-01.pdf

WAFO Group (2011). *A Matlab Toolbox for Analysisof Random Waves and Loads, Tutorial for WAFO version 2.5*. Retrieved from Lund University, Faculty Of Engineering Centre For Mathematical Sciences website: http://www.maths.lth.se/matstat/wafo/documentation/wafotutor25.pdf

Wang, Y. (2011). *Smoothing splines: Methods and applications*. Boca Raton, FL: CRC Press. 5

Ward, A., & Mecklenburg, D. (2005). Two-Stage Ditch Design. Retrieved from http://www.glc.org/basin/pubs/projects/wi_WtSedCoBs_pub1.pdf

Wehr, A., & Lohr, U. (1999). Airborne laser scanning -an introduction and overview. *ISPRS Journal of Photogrammetry & Remote Sensing*, *54*(68-82).

Wilkinson , R. W., & Wilkinson , R. N. (2013). Conference Presentation: An independent vertical accuracy assessment on Indiana Statewide LIDAR Data. *IGIC Geographic Information Conference, Muncie,* Retrieved from http://www.igic.org/training/pres/conf/2013/3.Accuracy_LiDAR_IGIC_May2013_rwilkinson.ppt

Williams , A. P. (1986). River Meanders And Channel Size. *Journal of Hydrology*, *88*(1-2).

Wilson, J. P., & Gallant, J. C. (2000). *Terrain analysis: Principles and applications*. New York: Wiley. 75

Woolpert Inc. (2011). *Indiana Statewide Imagery and Lidar Program ,Airborne Task Order Report*. Woolpert Inc./ Brain Foster.

Zhang , K., Chen , S. C., Whitman, D., Shyu, M. L., Yan, J., & Zhang, C. (2003). A Progressive Morphological Filter for Removing Nonground Measurements From Airborne LIDAR. *IEEE Transactions on Geoscience and Remote Sensing*, *41*(4).

APPENDICES

A. Appendix -Survey Sites and Maps

Table A.1 Information for survey sites used in the study

Site	1	2	3	4
Ditch Name	Browns Wonder Creek	Murphy Family Trust-Man Ditch	Anderson Family-Little Potato Creek	Honey Creek (Matthew Howell)
LiDAR NPS (m)	1	1.5	1.5	1.5
Cross Section Number	5	5	5	5
GPS Survey Date	8/15/2013	7/22/2013	7/22/2013	8/1/2013
Description	North of intersection between Ellizaville Road and N250E	About 600m North of intersection between County Road 330E and Road 150S, east side	About 400m North of intersection between County Road 300S and Road 200W , west side	East of intersection between Country Round E 500N and N900E
County	Boone	Clinton	Clinton	Howard
Watershed	Wabash	Wildcat	Wildcat	Sugar
Latitude (Degree)	40.090621	40.269772	40.246103	40.550386
Longitude (Degree)	-86.422631	-86.446723	-86.543606	-85.95009
IN State Data Tile Number	31351760_12	31301825_12	31001820_12	02451930_12
Data Web Page	http://webdb.iu.edu/spatial/scripts/isdp/filelist.cfm?xmin=548730&xmax=549950&ymin=4437854&ymax=4439074	http://webdb.iu.edu/spatial/scripts/isdp/filelist.cfm?xmin=547530&xmax=548750&ymin=4457355&ymax=4458575	http://webdb.iu.edu/spatial/scripts/isdp/filelist.cfm?xmin=538995&xmax=540215&ymin=4453707&ymax=4454927	http://webdb.iu.edu/spatial/scripts/isdp/filelist.cfm?xmin=588491&xmax=589728&ymin=4488358&ymax=4489595

Table A.2 Indiana State LiDAR Class Codes in Las 1.2 Format

Class 1	Unclassified Data
Class 2	Bare-earth /Ground
Class 9	Water
Class 7	Noise
Class 10	Ignored Ground
Class 12	Overlap points
Class 13	Bridges

RTK GPS Field Survey Sites

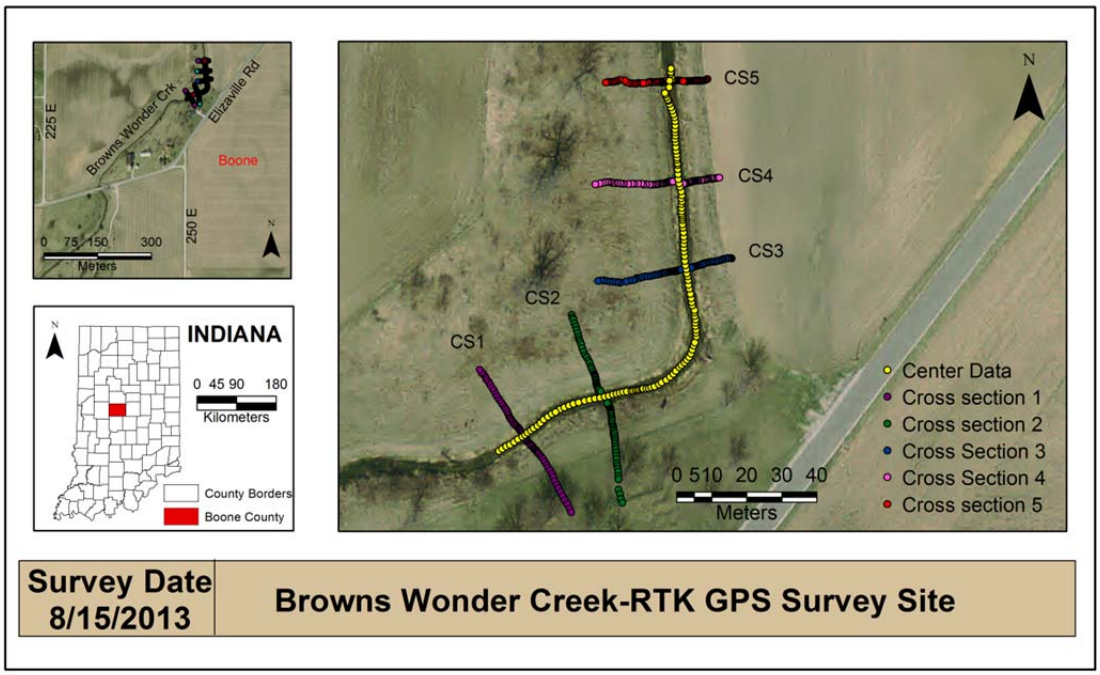

Figure A.1 Site 1

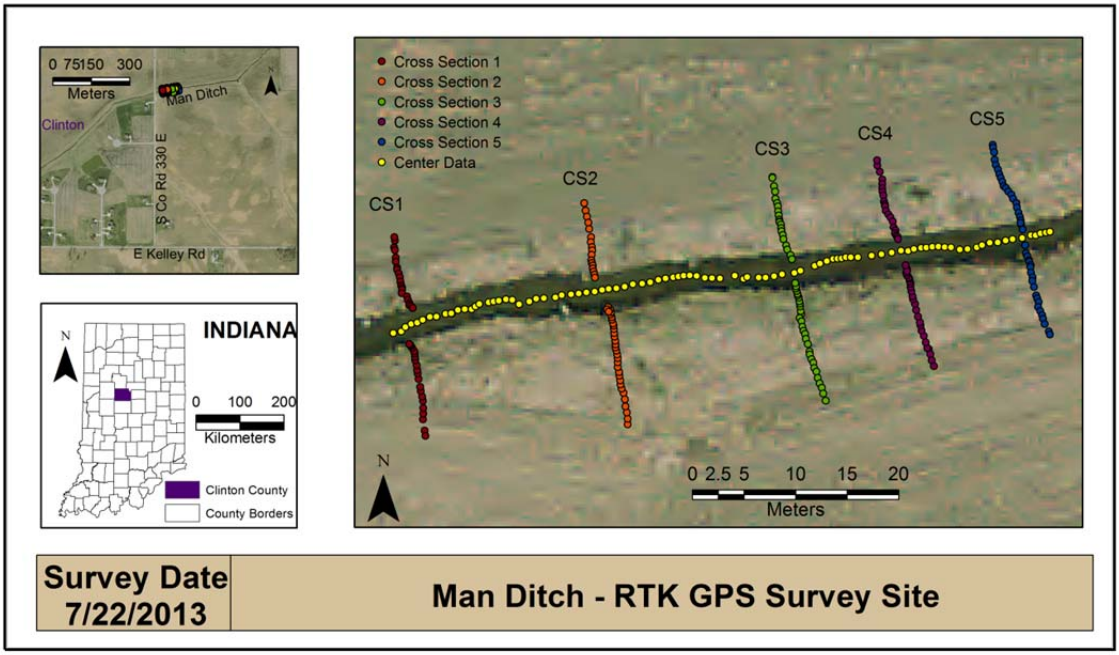

Figure A.2 Site 2

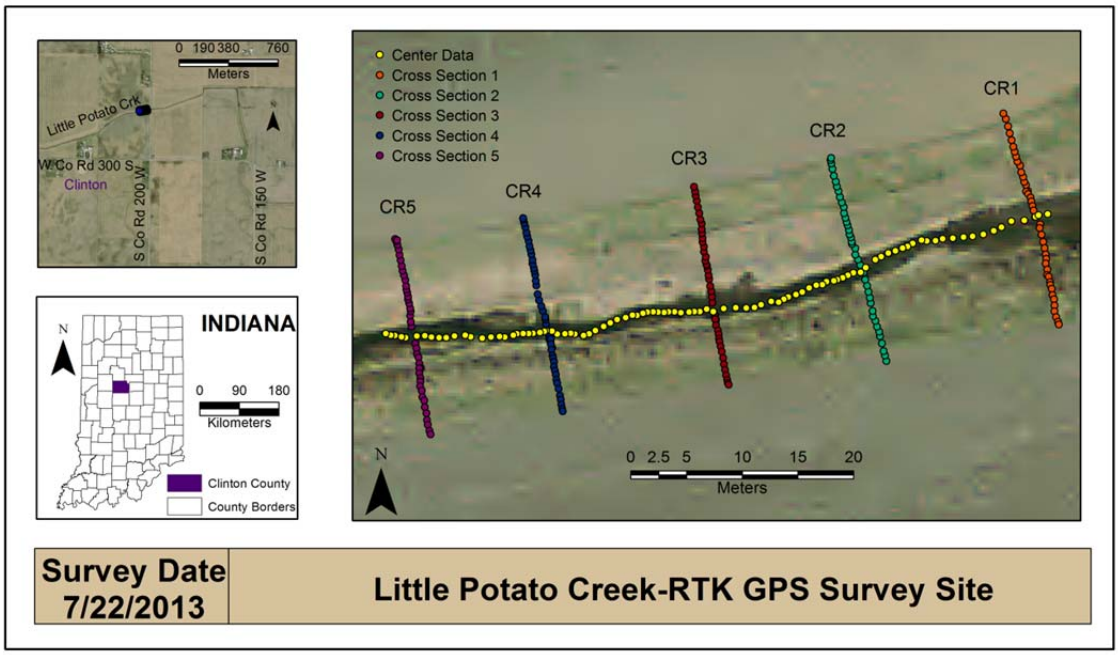

Figure A.3 Site 3

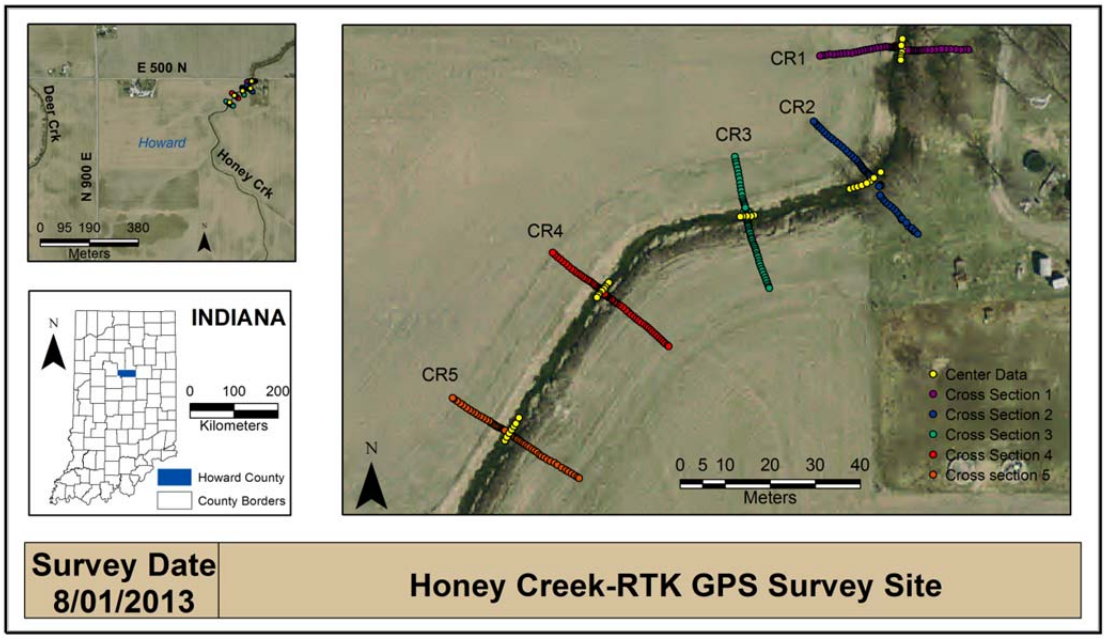

Figure A.4 Site 4

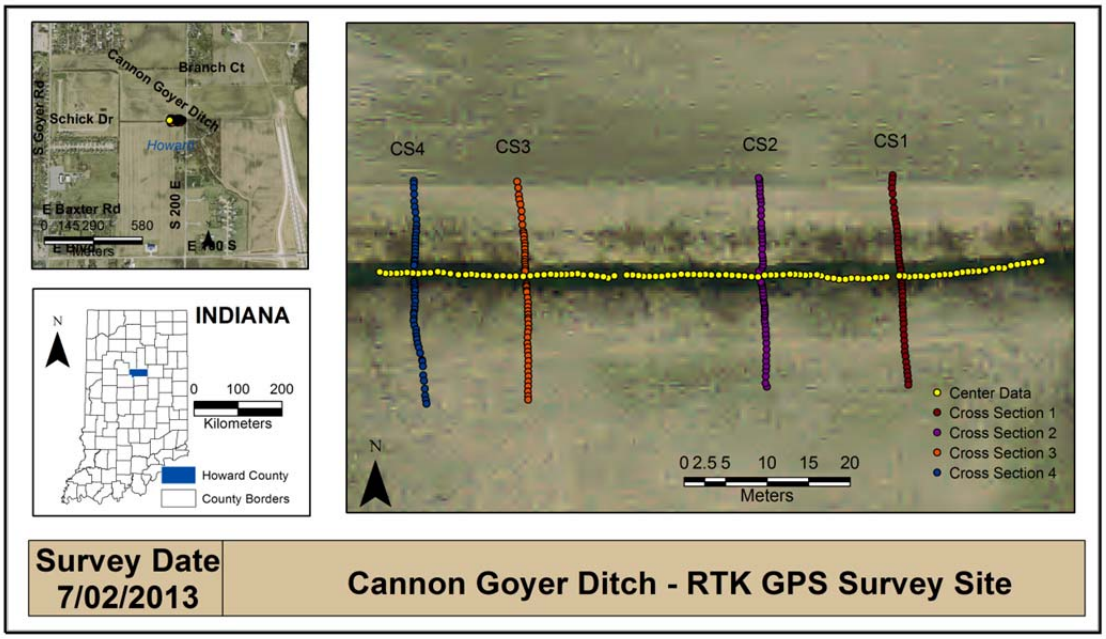

Figure A.5 Site 5

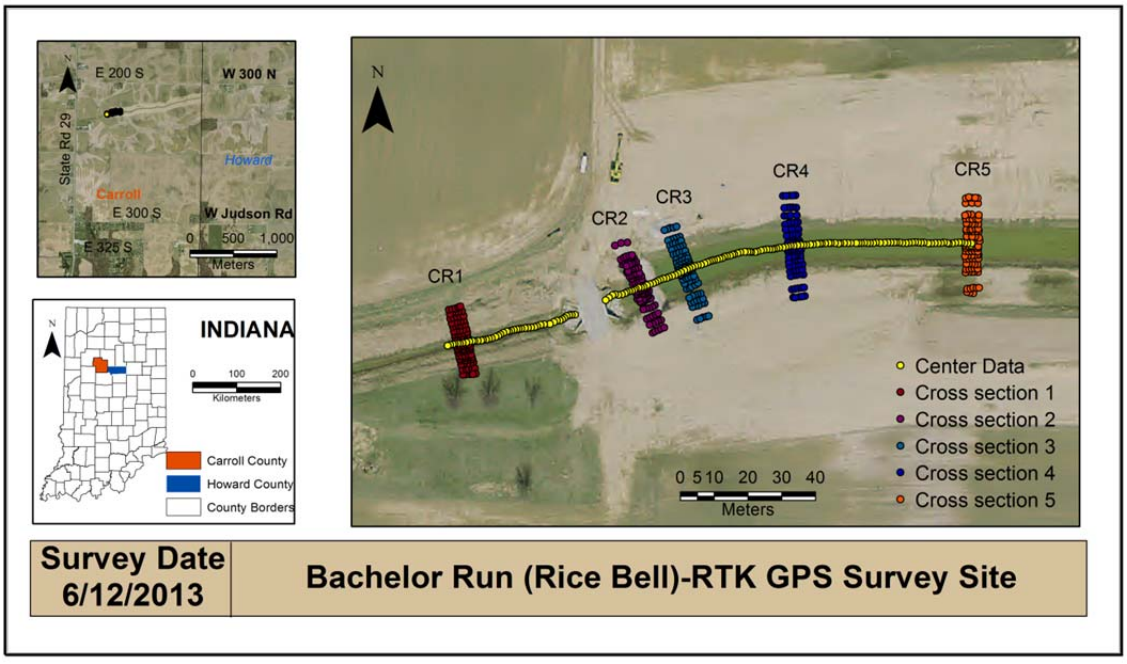

Figure A.6 Site 6

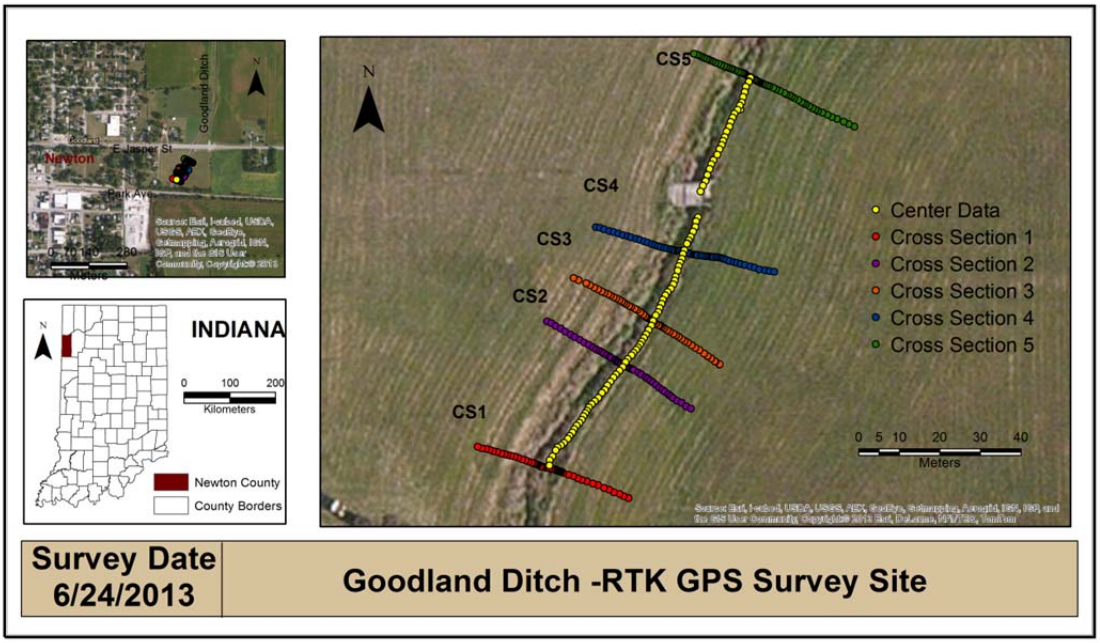

Figure A.7 Site 7

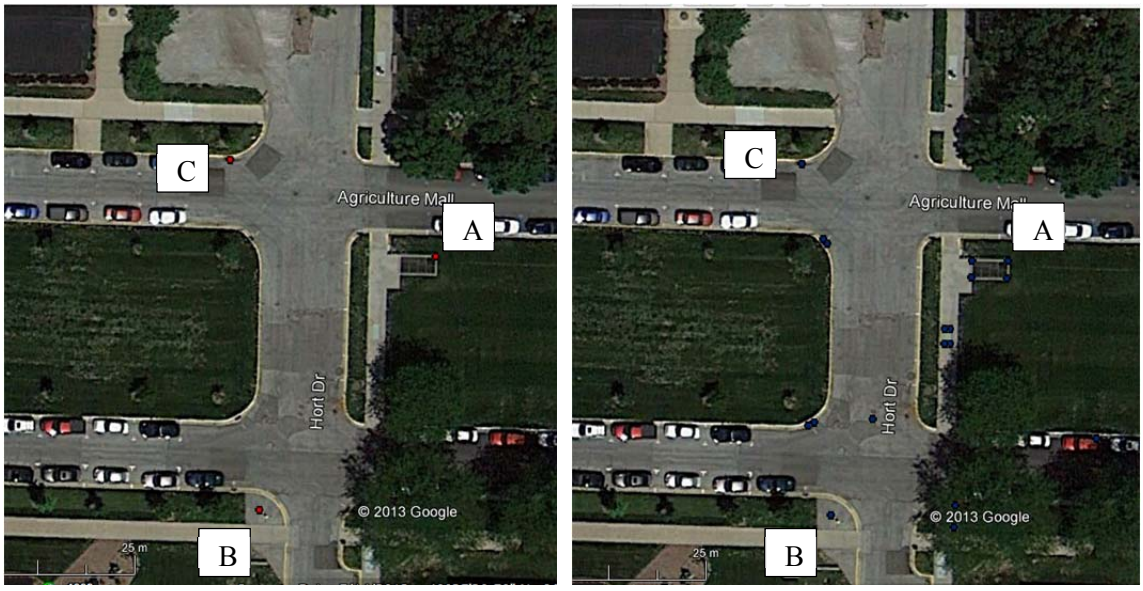

Figure A.8 Measured Points in both rapid static GPS (red) and RTK GPS (blue) methods

Table A.3 NAD83 UTM Zone 16 Coordinates of Test Points

	Rapid Static (s)			RTK GPS (r)		
	X (m)	Y(m)	Z(m)	X (m)	Y(m)	Z(m)
A	4474634.772	507226.215	188.046	4474634.771	507226.222	188.032
B	4474634.791	507221.544	188.068	4474634.781	507221.528	188.040
C	4474647.313	507199.378	187.863	4474647.304	507199.388	187.828

Table A.4 RMSE Calculation (FGDC,2013)

$X_s - X_r$(m)	$Y_s - Y_r$(m)	$Z_s - Z_r$(m)	$(X_s - X_r)^2 + (Y_s - Y_r)^2$ (m^2)	$(Z_s - Z_r)^2$ (m^2)
0.001	-0.007	0.014	0.000050	0.000196
0.010	0.016	0.028	0.000356	0.000784
0.009	-0.010	0.035	0.000181	0.001225
		Sum	0.000587	0.002205
		Average	0.000196	0.000735
		RMSE(m)	0.014	0.027

Horizontal error at 95%= 1.73xRMSEr

Vertical error at 95%= 1.9600xRMSEz

95 % Confidence Interval	NASSDA(m)	0.024	0.053

Figure A.9 Rapid Static Points Measured in Agriculture Mall at Purdue University Campus to check RTK GPS System accuracy

B. Appendix -Top of The Bank Figures For Each Surveyed Cross Section

Each Cross Section Figure consists of four subfigures. The top figure is ground and non-ground LiDAR points overlapped with RTK GPS points. The next figure is Gaussian fit smoothed and equally spaced interpolated ground points with top of the bank from final determination results. The next one shows top of the bank result with ground LiDAR points overlapped with RTK GPS points. The final subfigure shows calculation of bankfull area under lower top of the bank. Area calculation was implemented as future reference and statistic for area calculation was not represented for this study due to uncertainty of water levels.

Figures belong to Site 1 Cross Section 1and Cross Section 2 and Site 4 Cross Section 1 were processed with 180° rotation to match with existent pictures of the cross section.

Site 1 Top of the Bank Figures

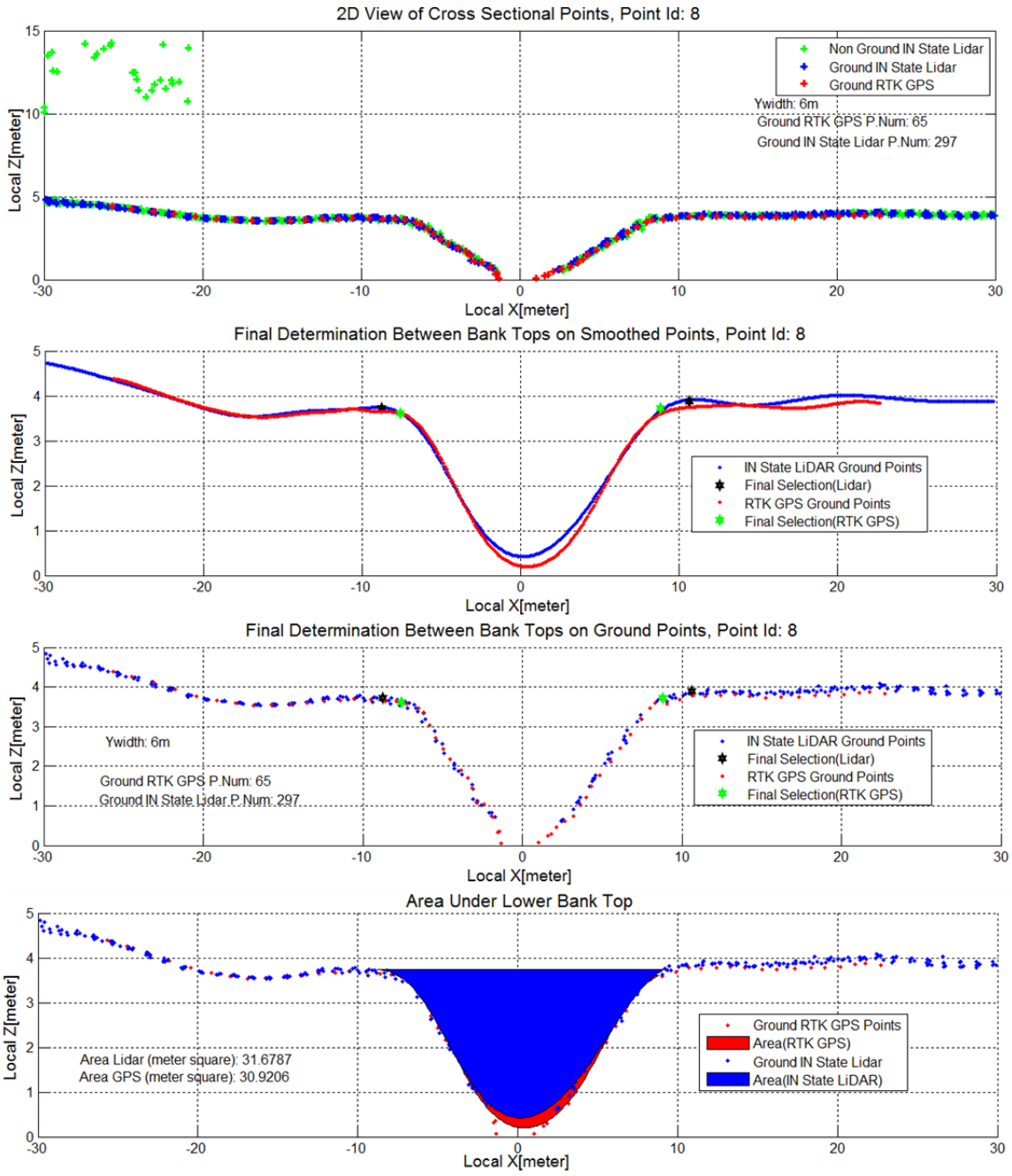

Figure B.1 Site 1 Cross Section 1 Top of the bank in Local Coordinate (180° Rotated to match with images)

Figure B.2 Site 1 Cross Section 1

Figure B.3 Site 1 Cross Section 2

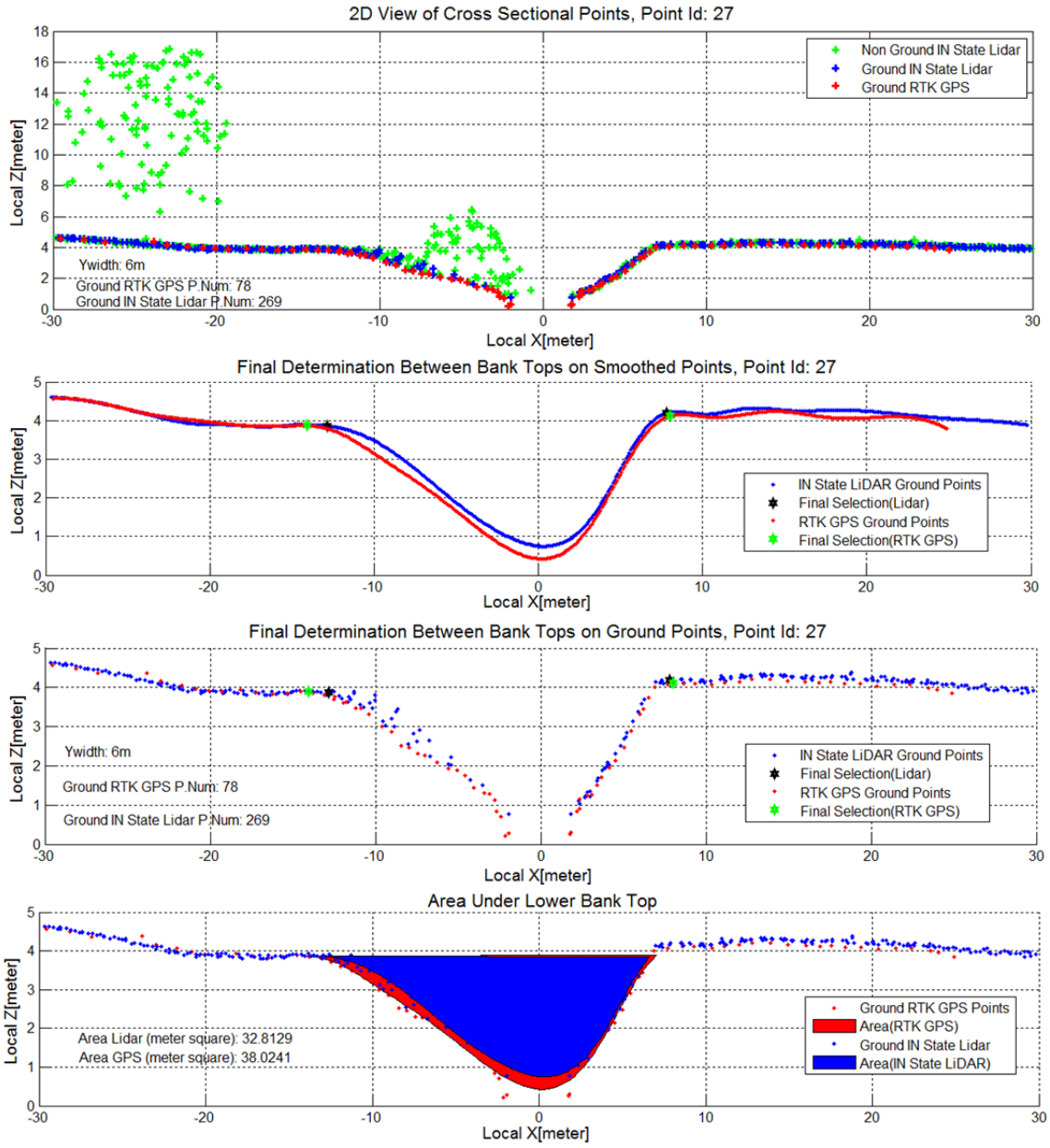

Figure B.4 Site 1 Cross Section 2 Top of the bank in Local Coordinate (180° Rotated to match with images)

Figure B.5 Site 1 Cross sections 3-4-5

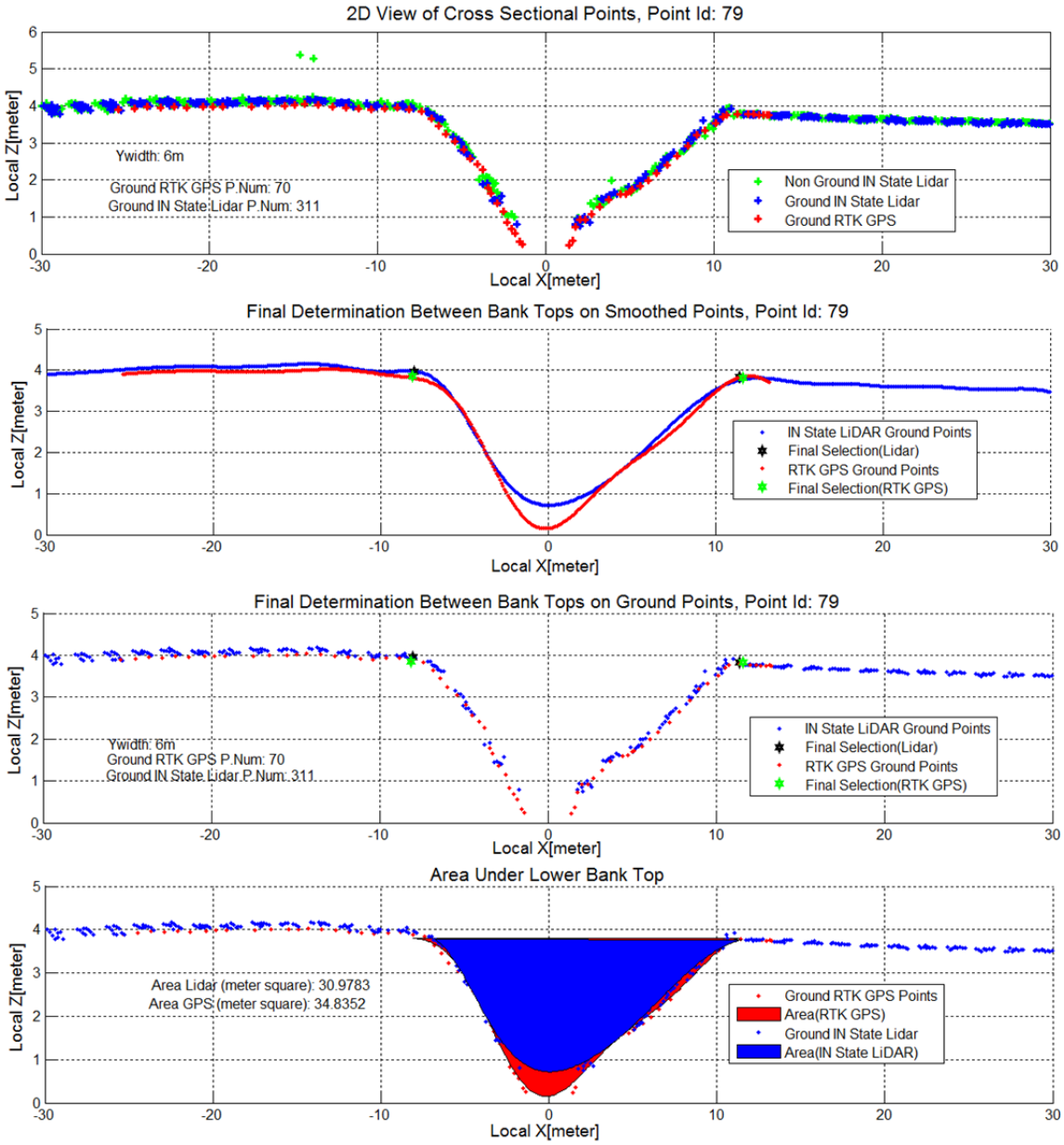

Figure B.6 Site 1 Cross Section 3 Top of the Banks in Local Coordinates

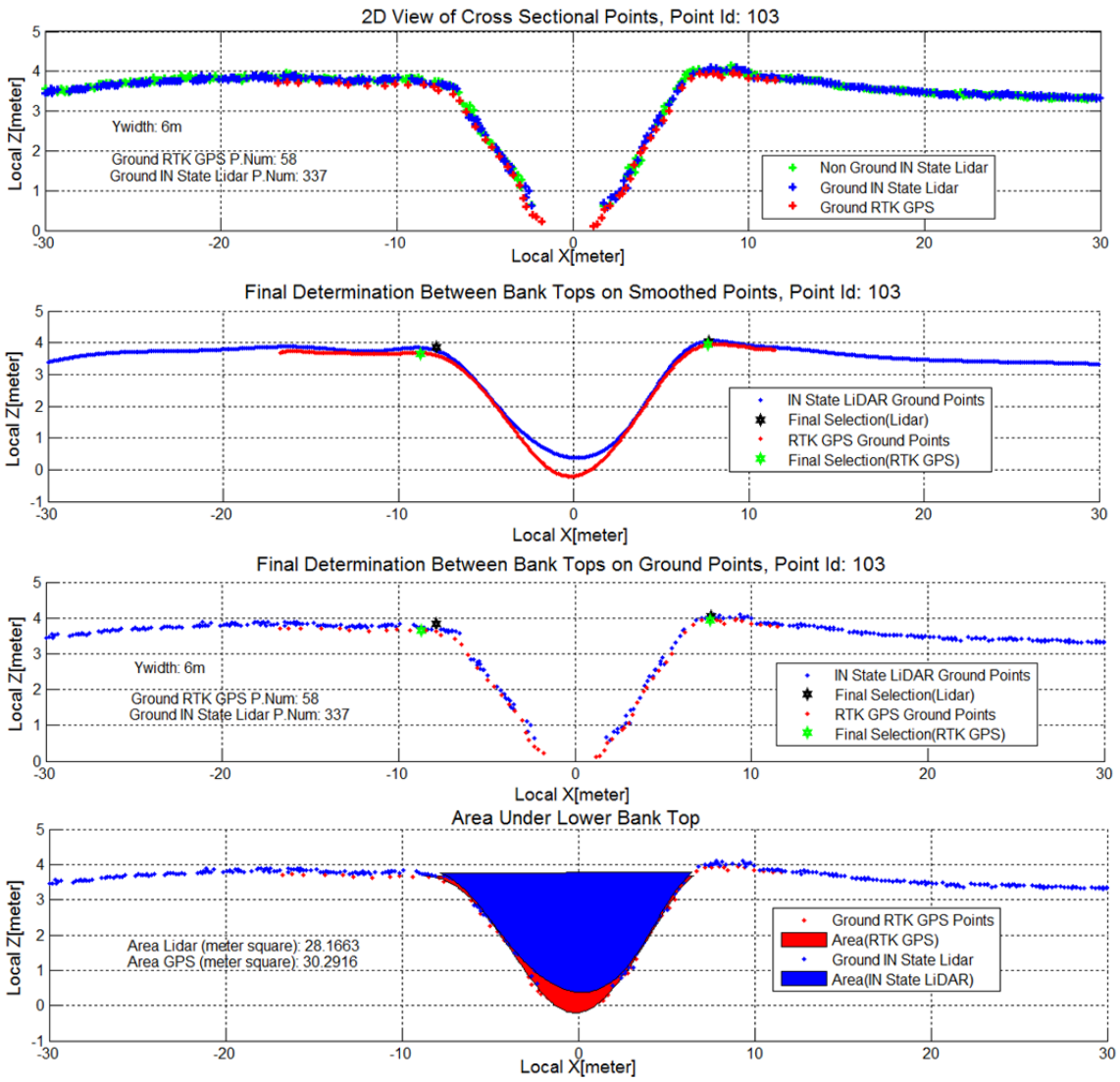

Figure B.7 Site 1 Cross Section 4 Top of the Banks in Local Coordinate

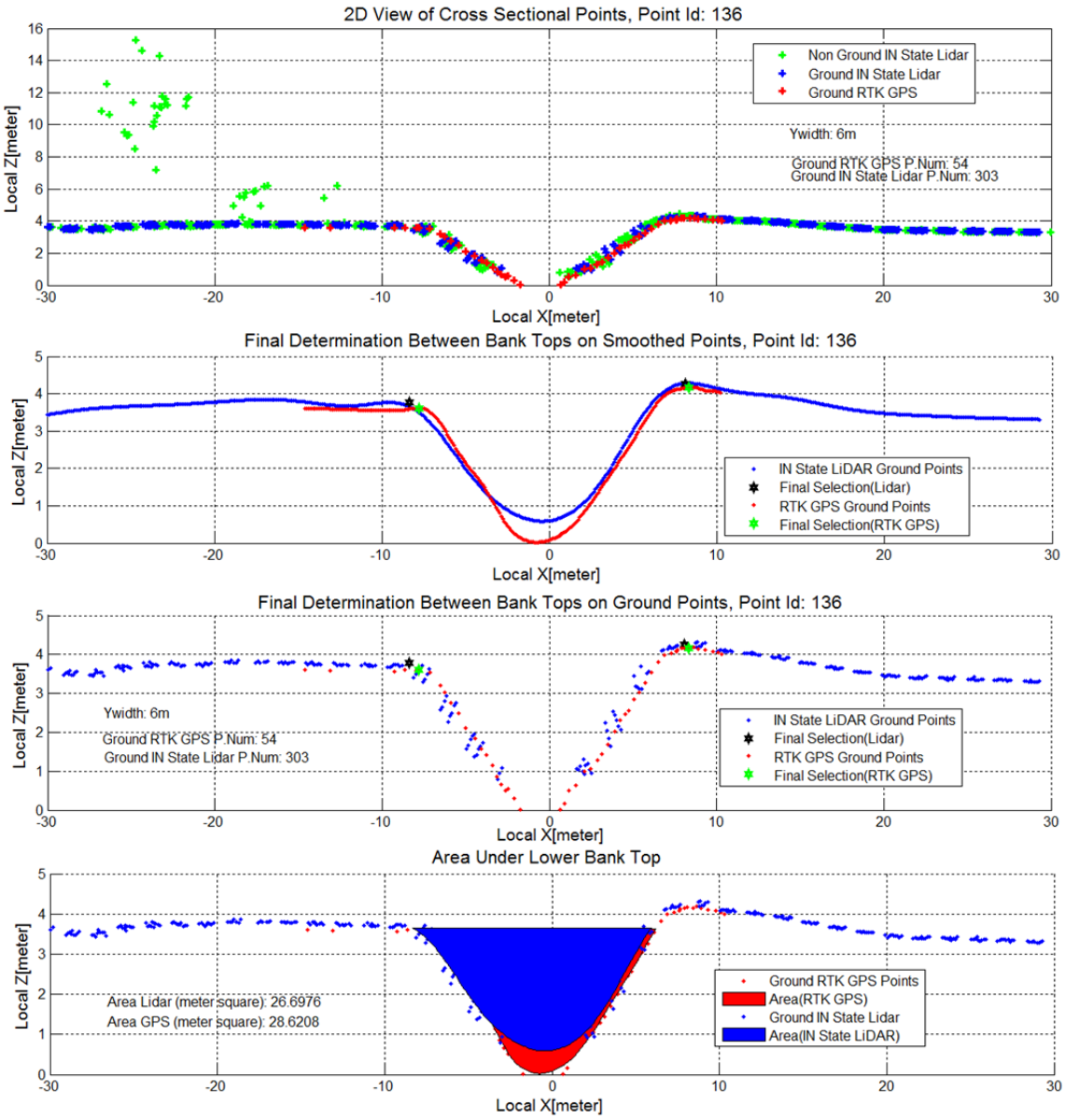

Figure B.8 Site 1 Cross Section 5 Top of the Banks in Local Coordinates

Site 2 Top of the Bank Figures

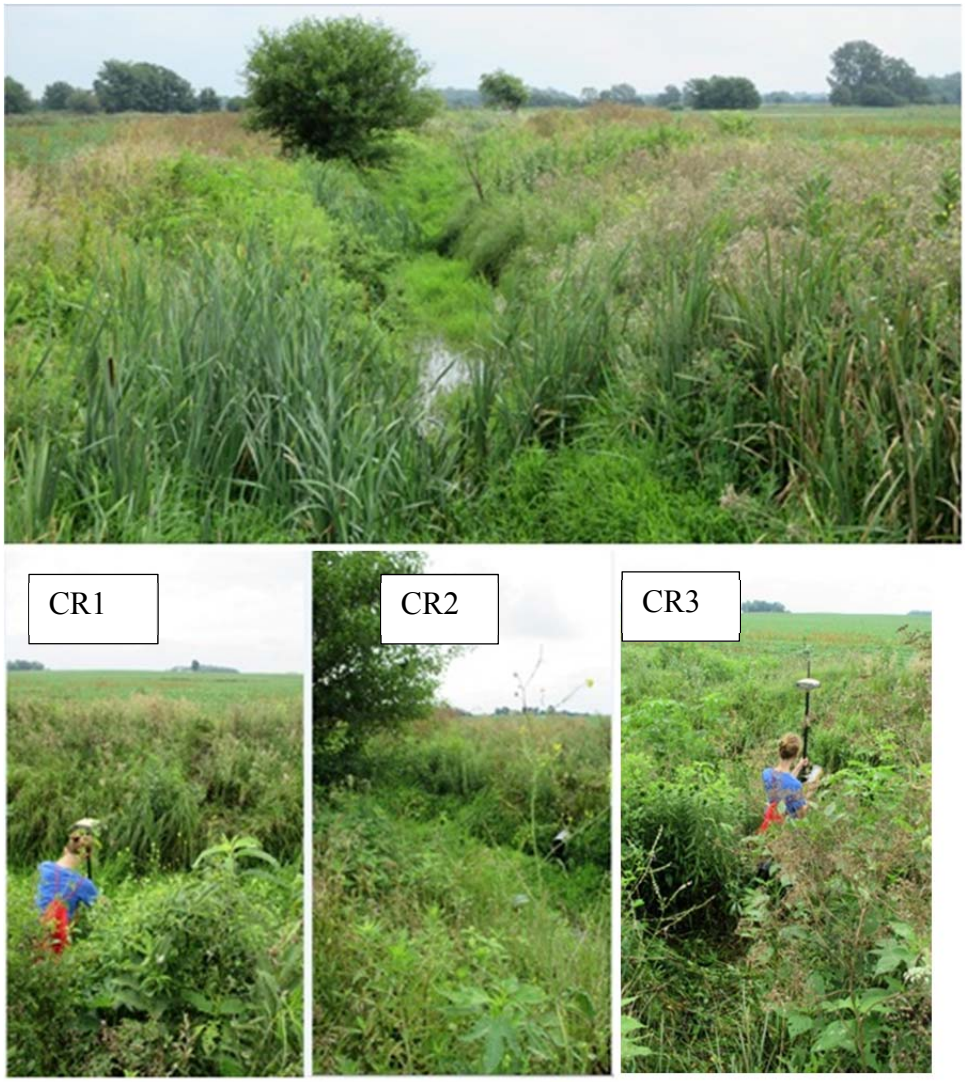

Figure B.9 Site 2 Cross Sections

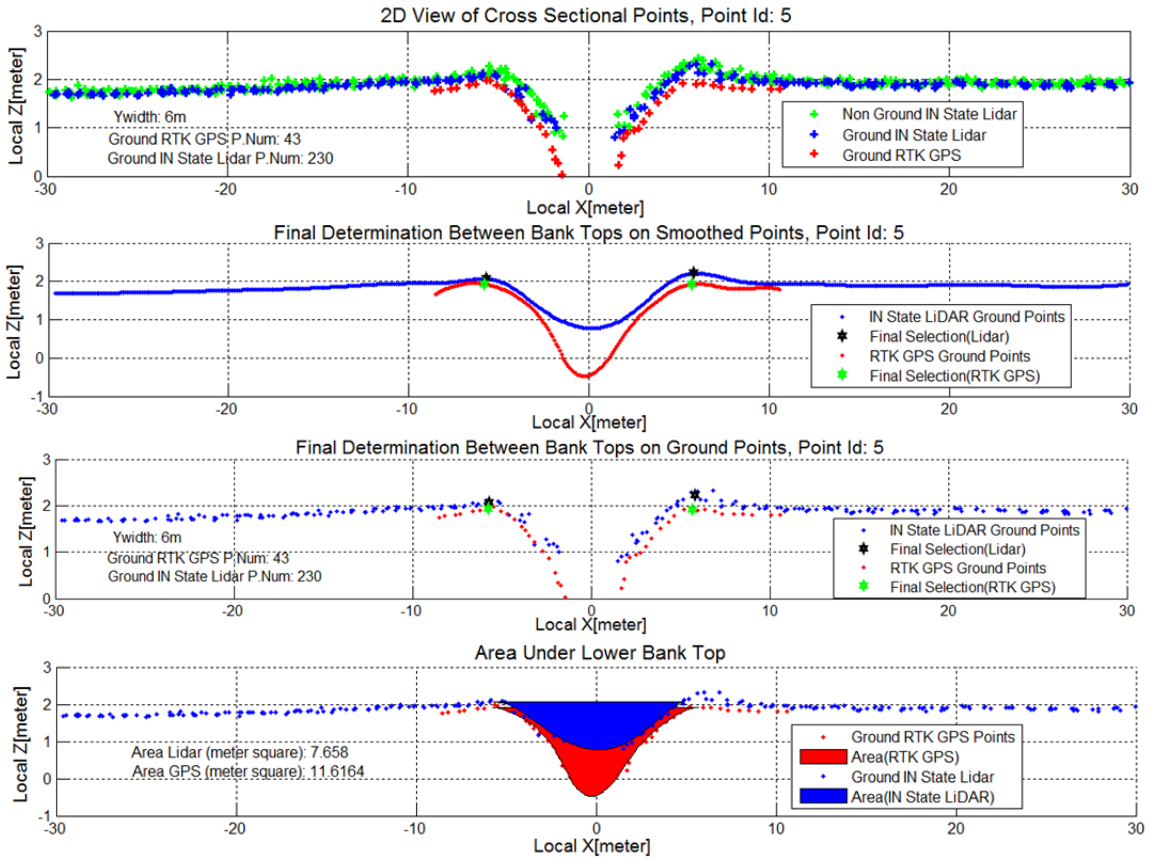

Figure B.10 Site 2 Cross Section 1 IN State LiDAR Top of the Banks in Local Coordinates

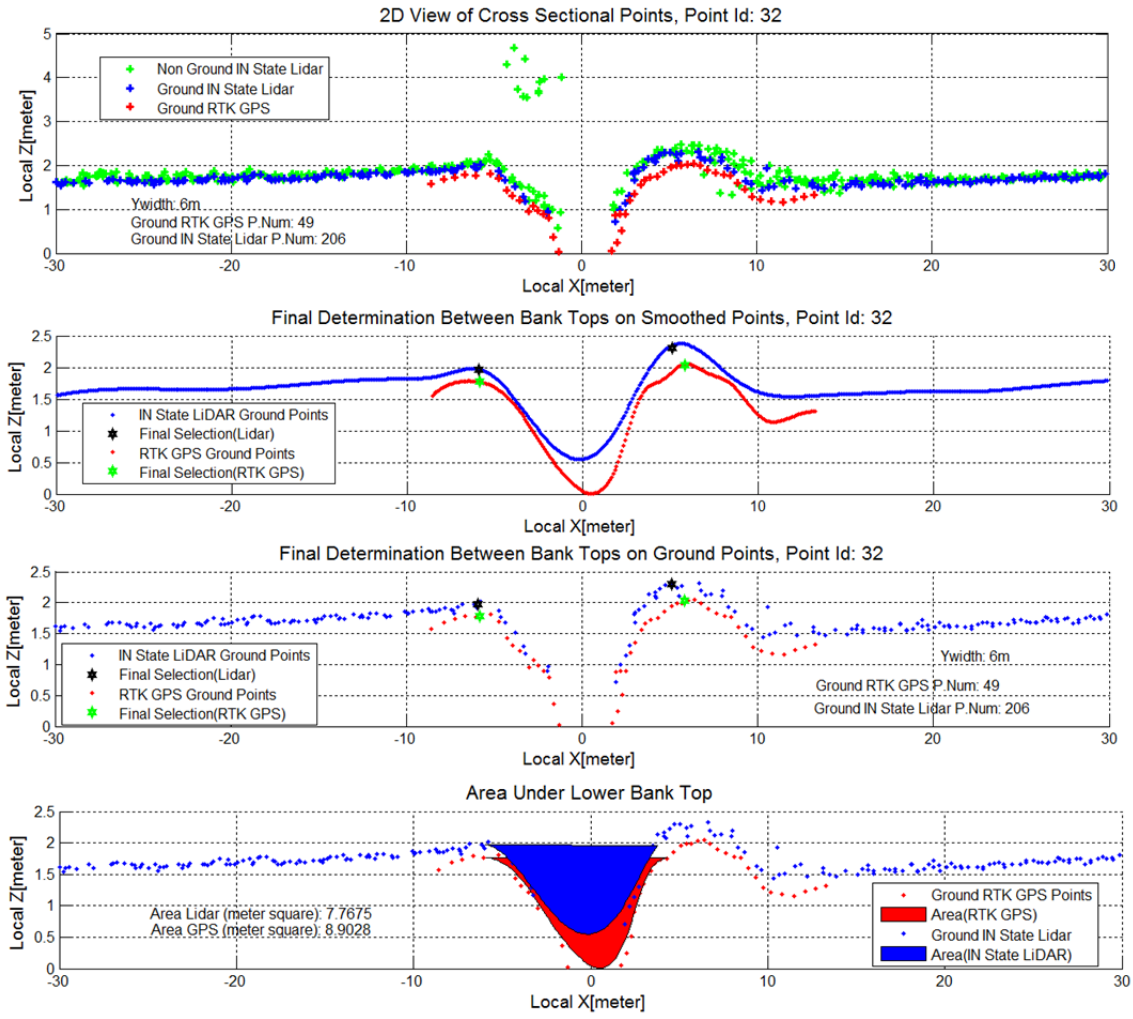

Figure B.11 Site 2 Cross Section 2 IN State LiDAR Top of the Banks in Local Coordinates

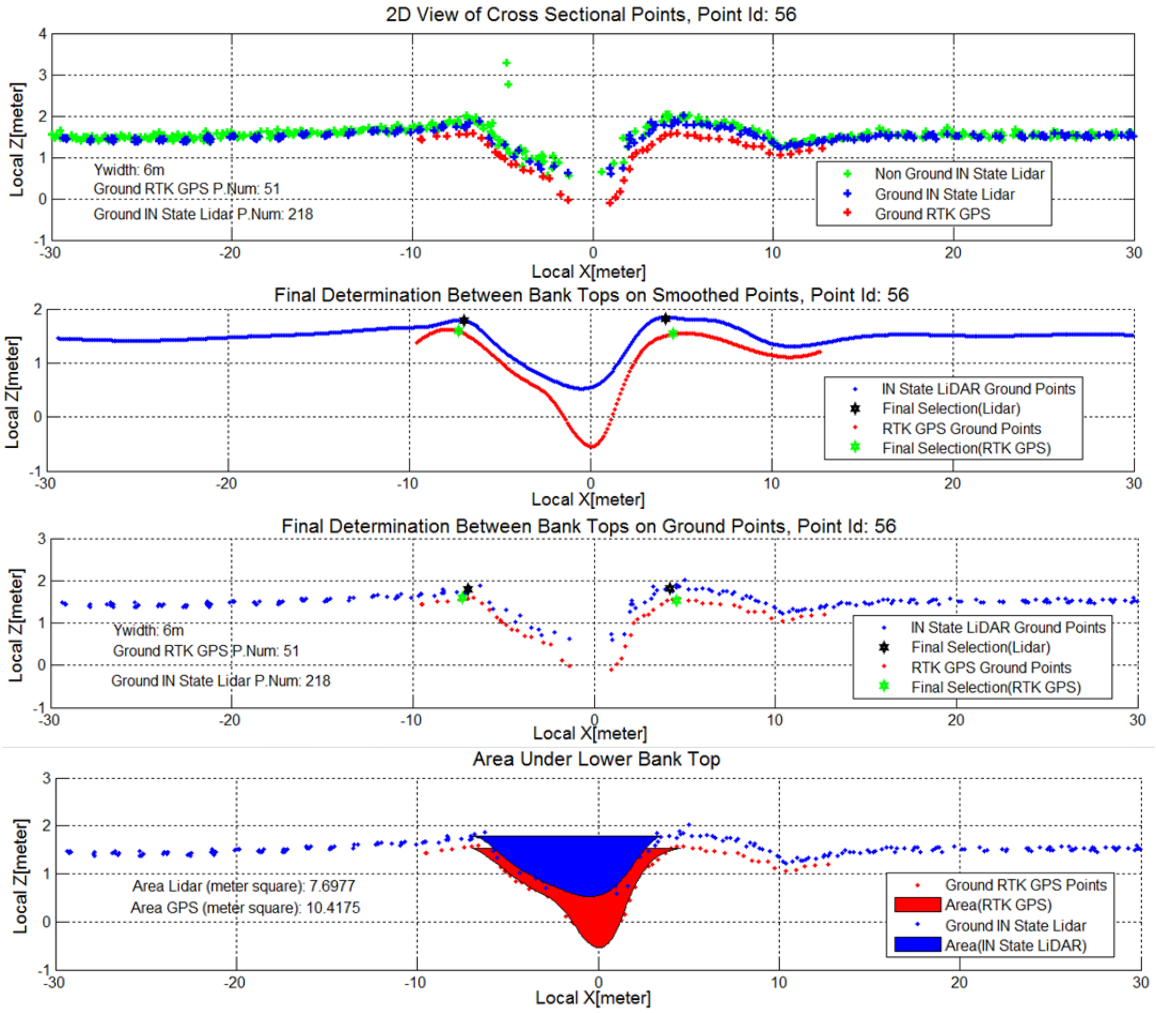

Figure B.12 Site 2 Cross Section 3 IN State LiDAR Top of the Banks in Local Coordinates

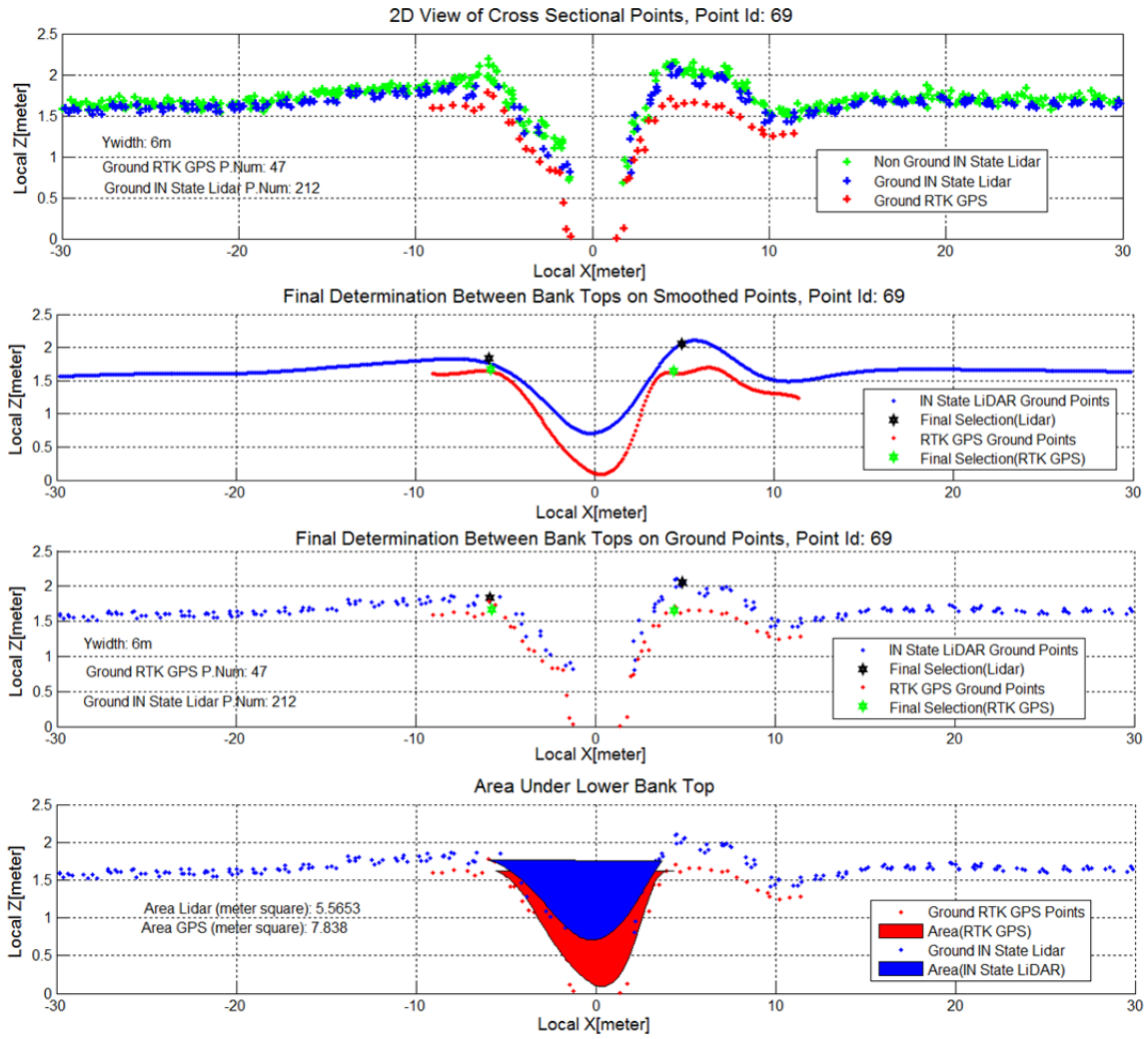

Figure B.13 Site 2 Cross Section 4 IN State LiDAR Top of the Banks in Local Coordinates

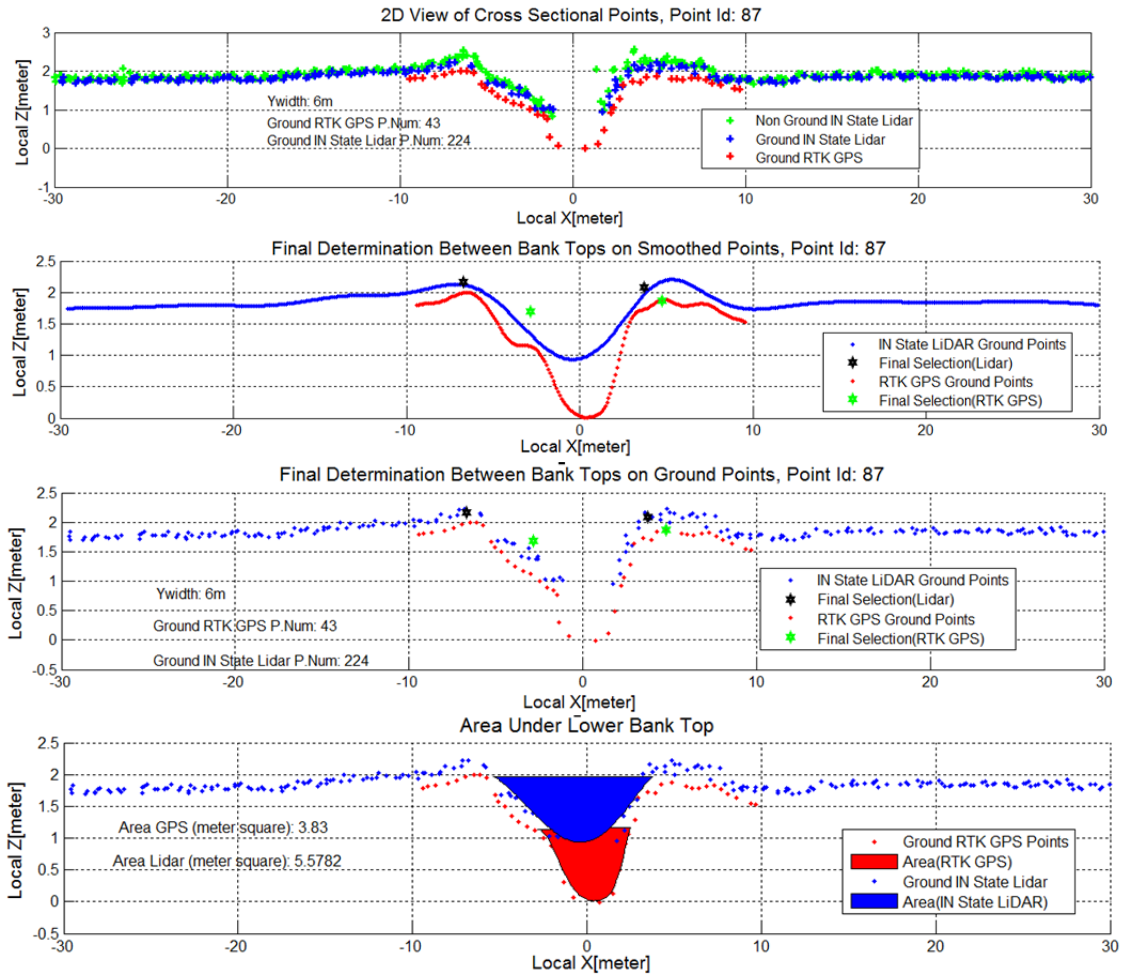

Figure B.14 Site 2 Cross Section 5 IN State LiDAR Top of the Banks in Local Coordinates

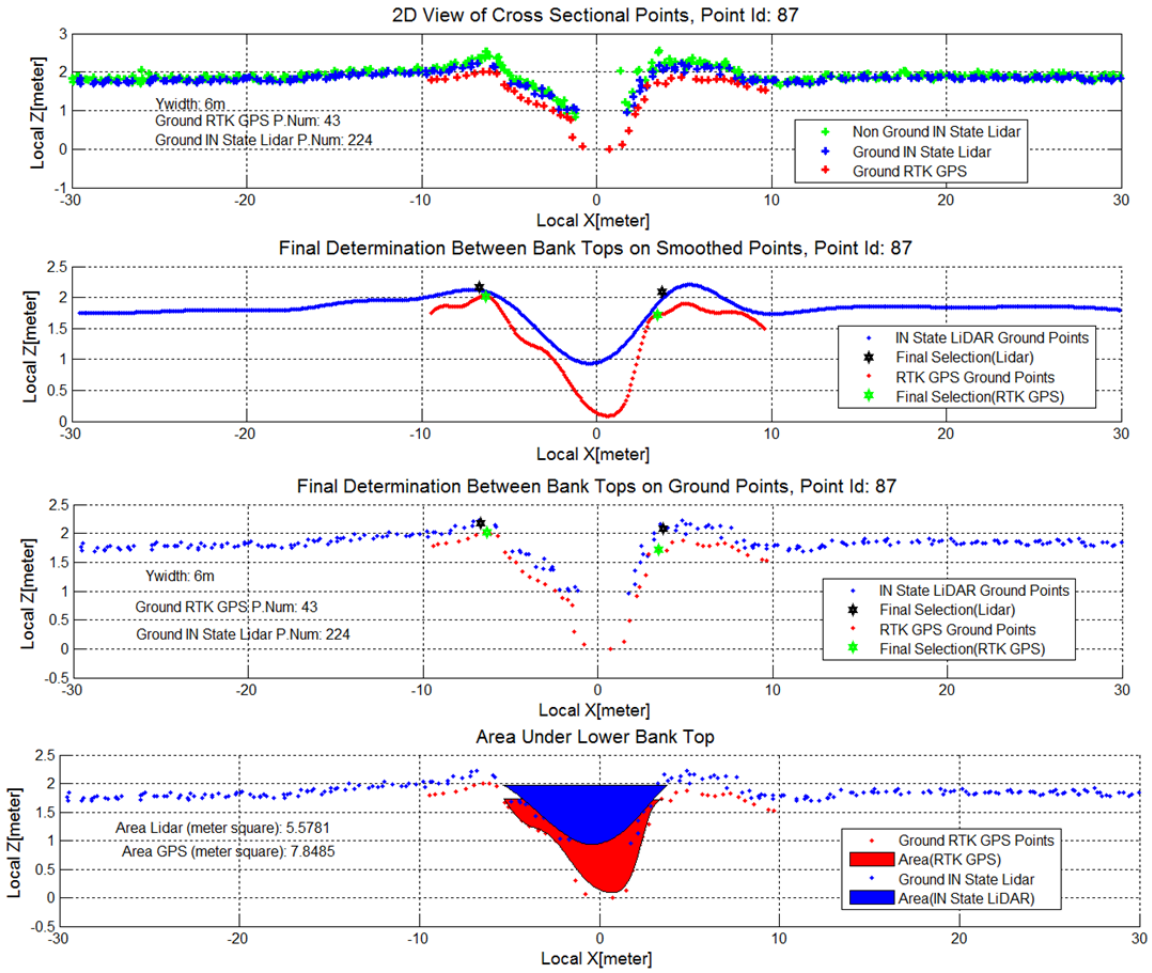

Figure B.15 Site 2 Cross Section 5 IN State LiDAR Top of the Banks in Local Coordinates (exceptionally with double Gaussian Mixture Model smoothing)

Site 3 Top of the Bank Figures

Figure B.16 Site 3 Cross Sections 1 2 3 4 5

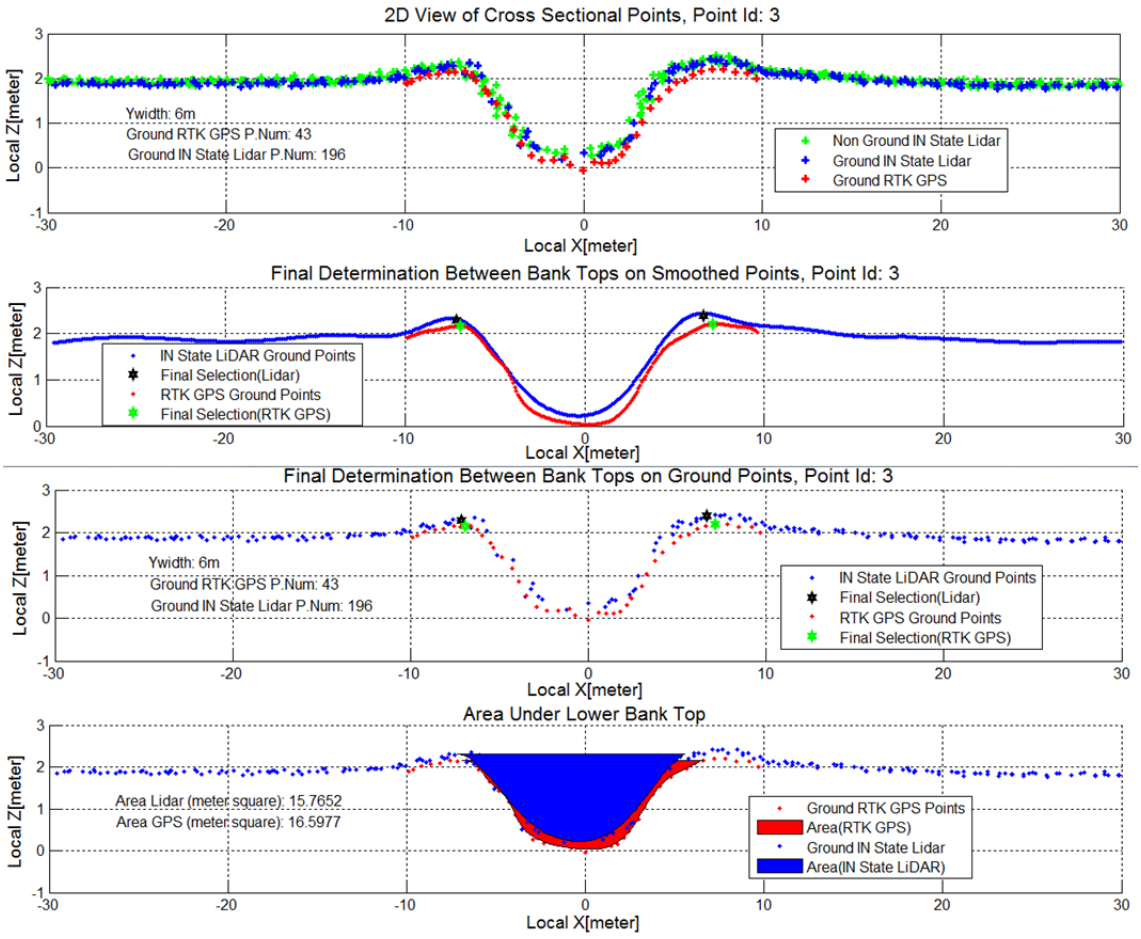

Figure B.17 Site 3 Cross Section 1 IN State LiDAR Top of the Banks in Local Coordinates

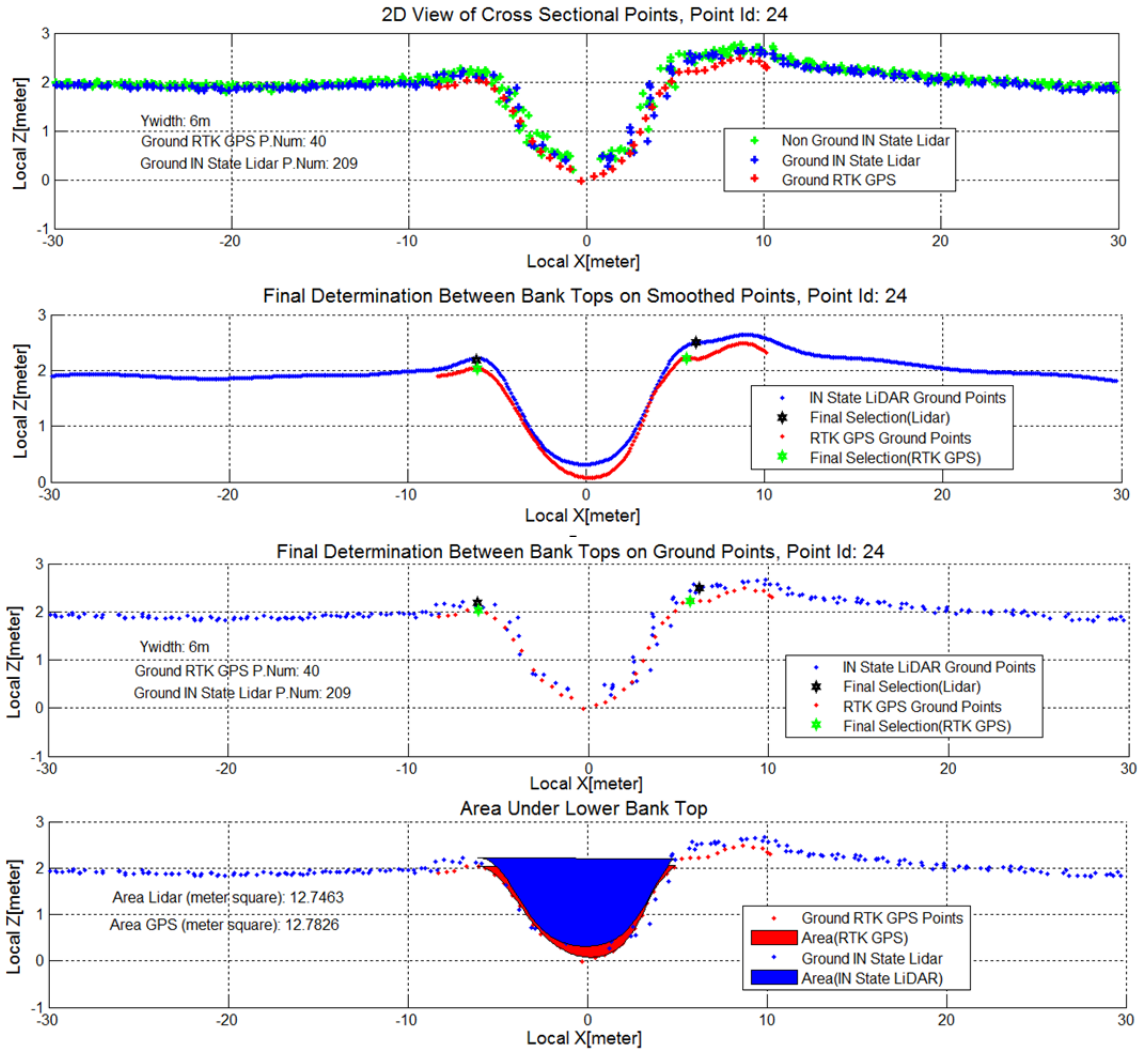

Figure B.18 Site 3 Cross Section 2 IN State LiDAR Top of the Banks in Local Coordinates

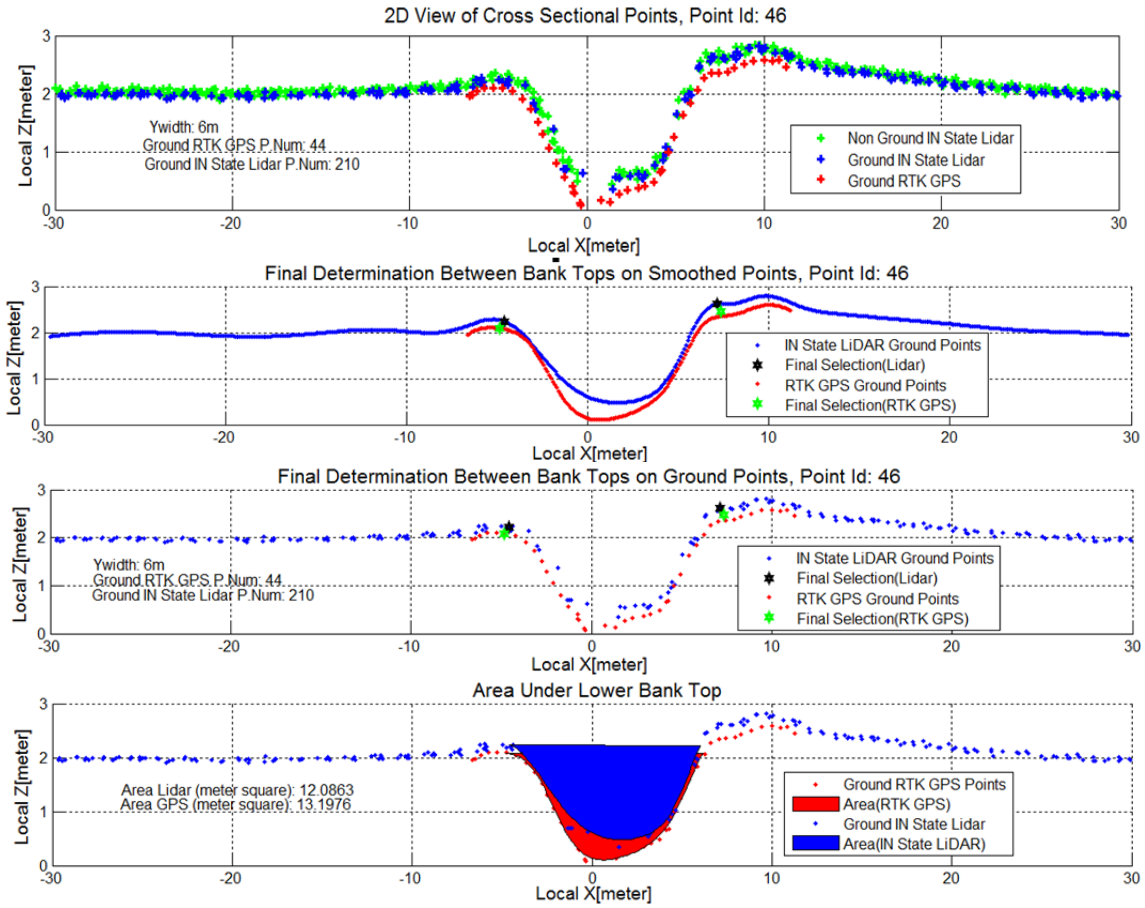

Figure B.19 Site 3 Cross Section 3 IN State LiDAR Top of the Banks in Local Coordinates

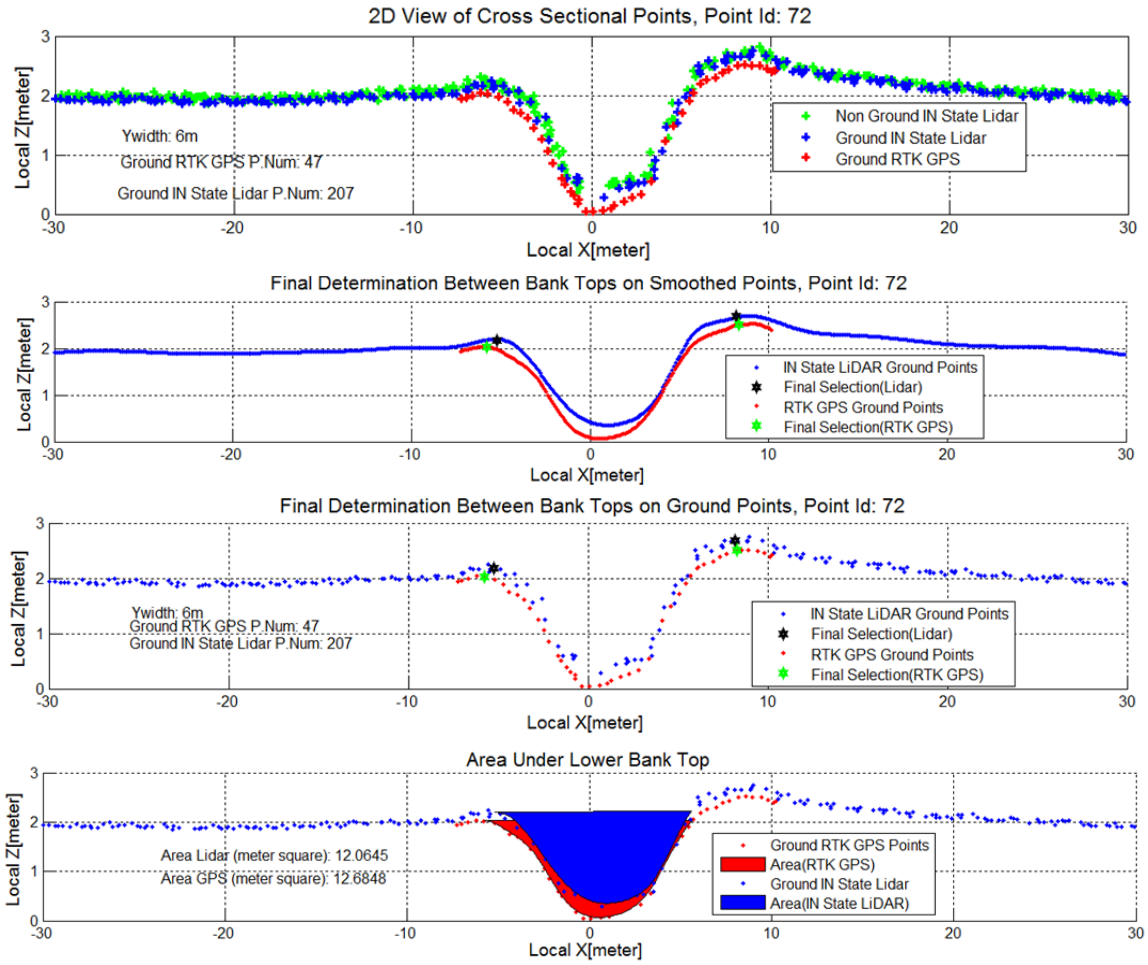

Figure B.20 Site 3 Cross Section 4 IN State LiDAR Top of the Banks in Local Coordinates

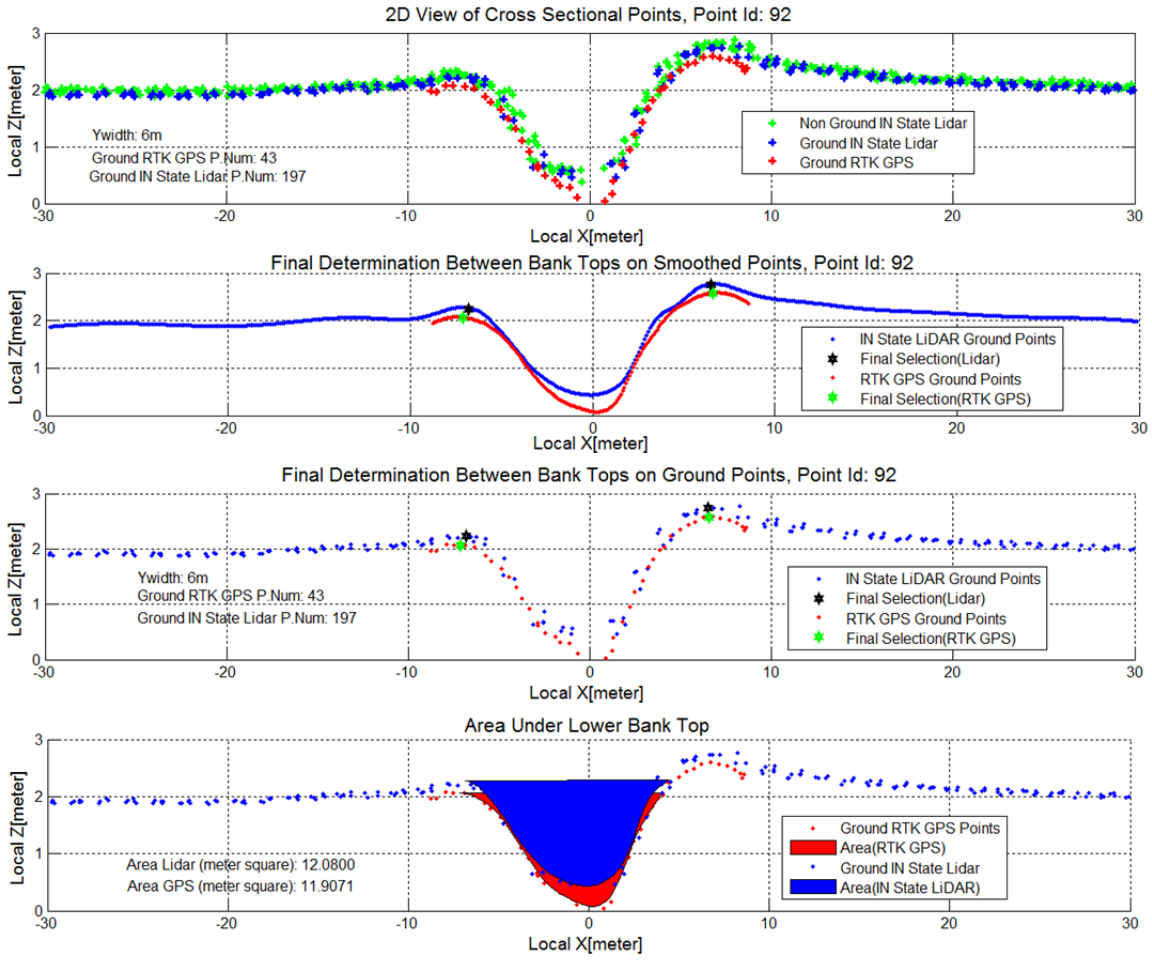

Figure B.21 Site 3 Cross Section 5 IN State LiDAR Top of the Banks in Local Coordinates

Site 4 Top of the Bank Figures

Figure B.22 Site 4 Cross Section 1

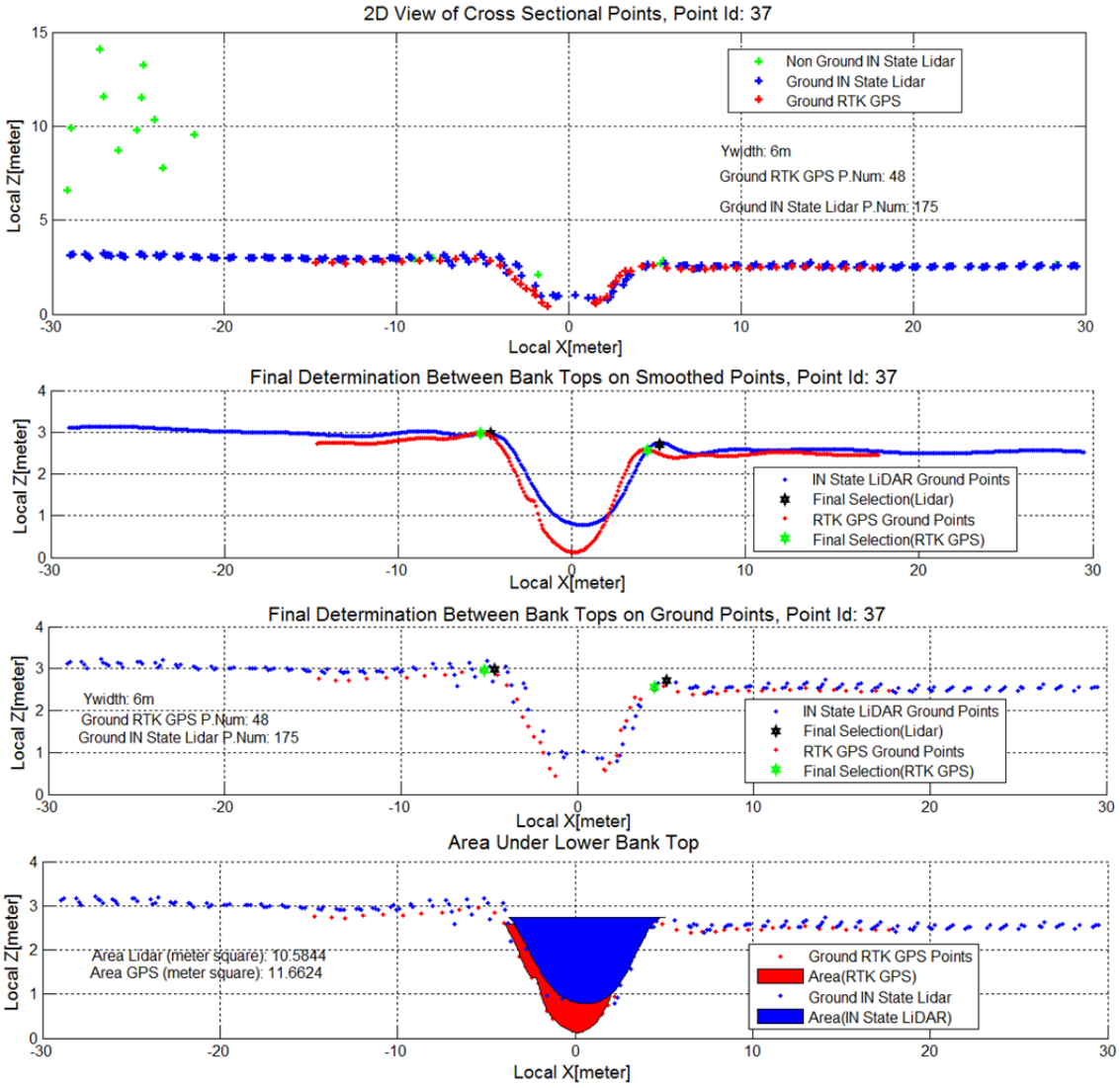

Figure B.23 Site 4 Cross Section 1 IN State LiDAR Top of the Banks in Local Coordinates

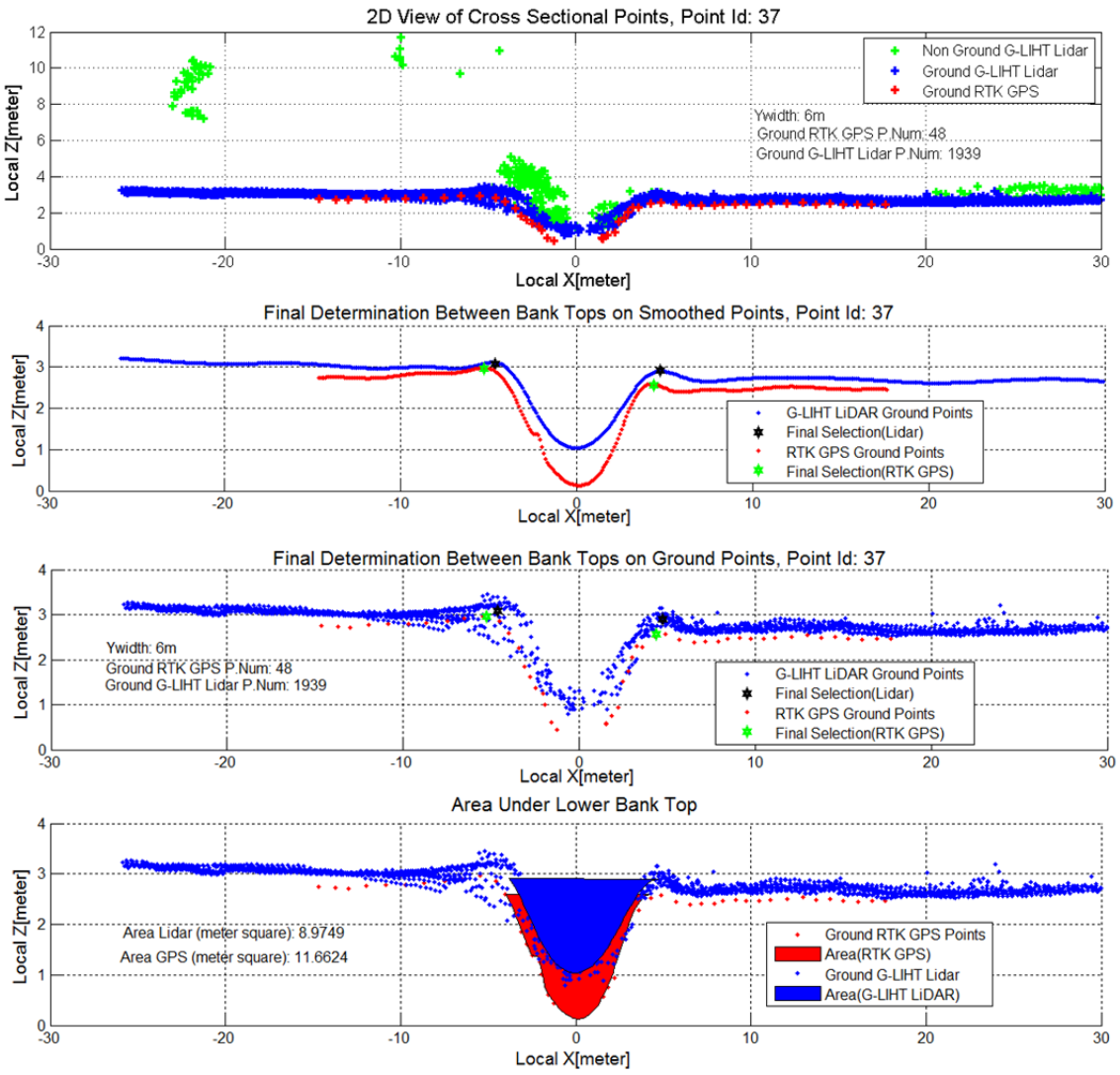

Figure B.24 Site 4 Cross Section 1 G-LiHT LiDAR Top of the Banks in Local Coordinates

Figure B.25 Site 4 Cross Section 2

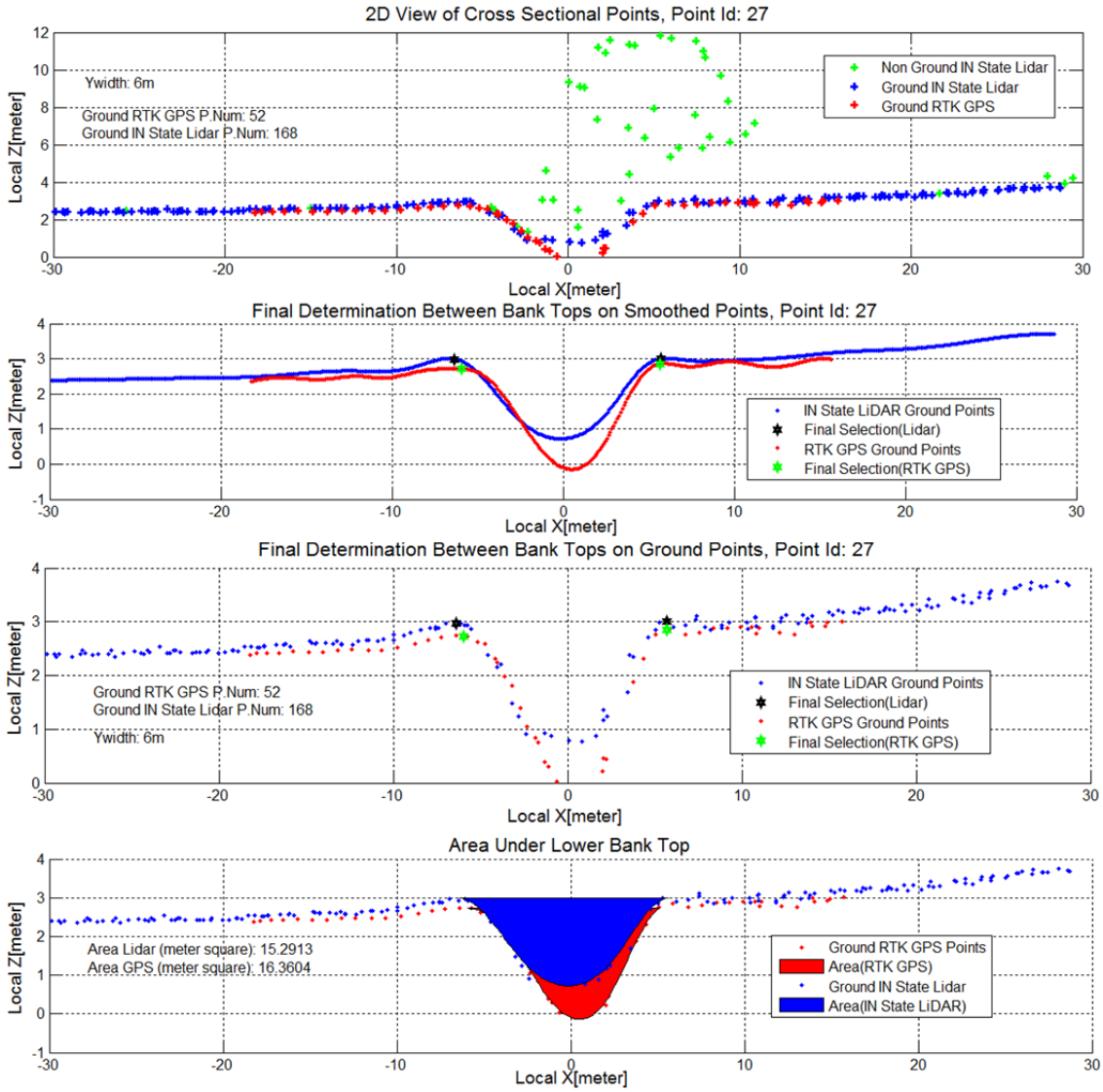

Figure B.26 Site 4 Cross Section 2 IN State LiDAR Top of the Banks in Local Coordinates

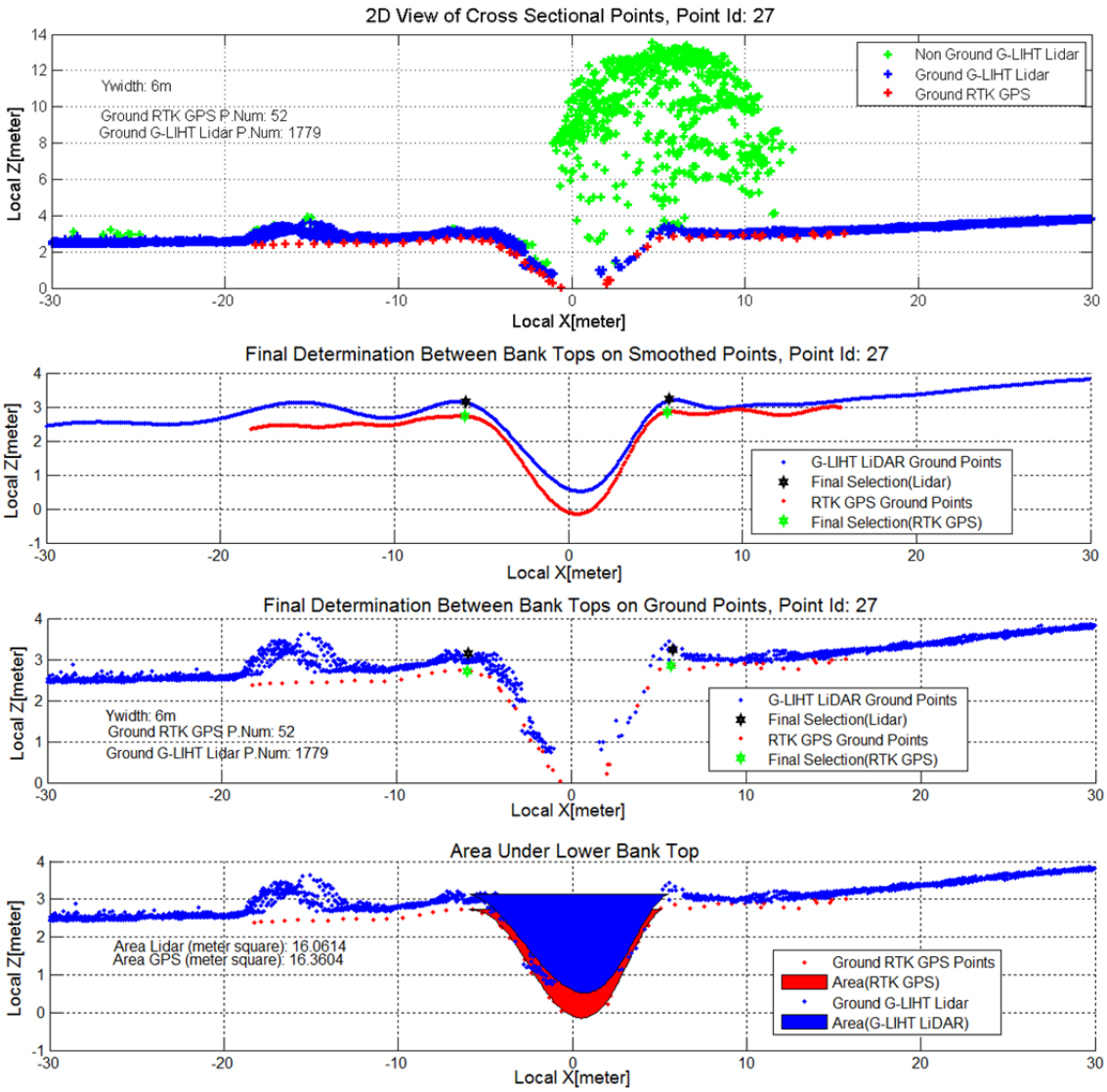

Figure B.27 Site 4 Cross Section 2 G-LiHT LiDAR Top of the Banks in Local Coordinates

Figure B.28 Site 4 Cross Section 3

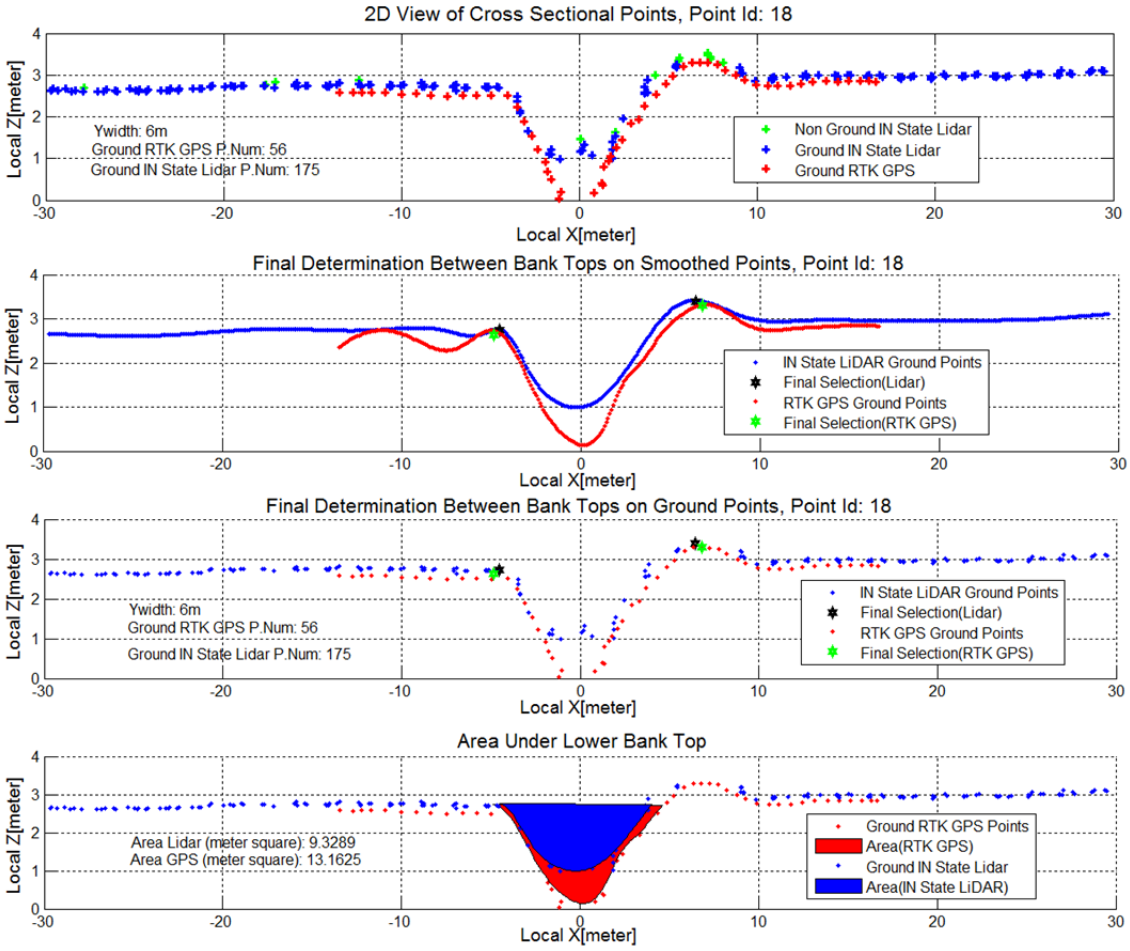

Figure B.29 Site 4 Cross Section 3 IN State LiDAR Top of the Banks in Local Coordinates

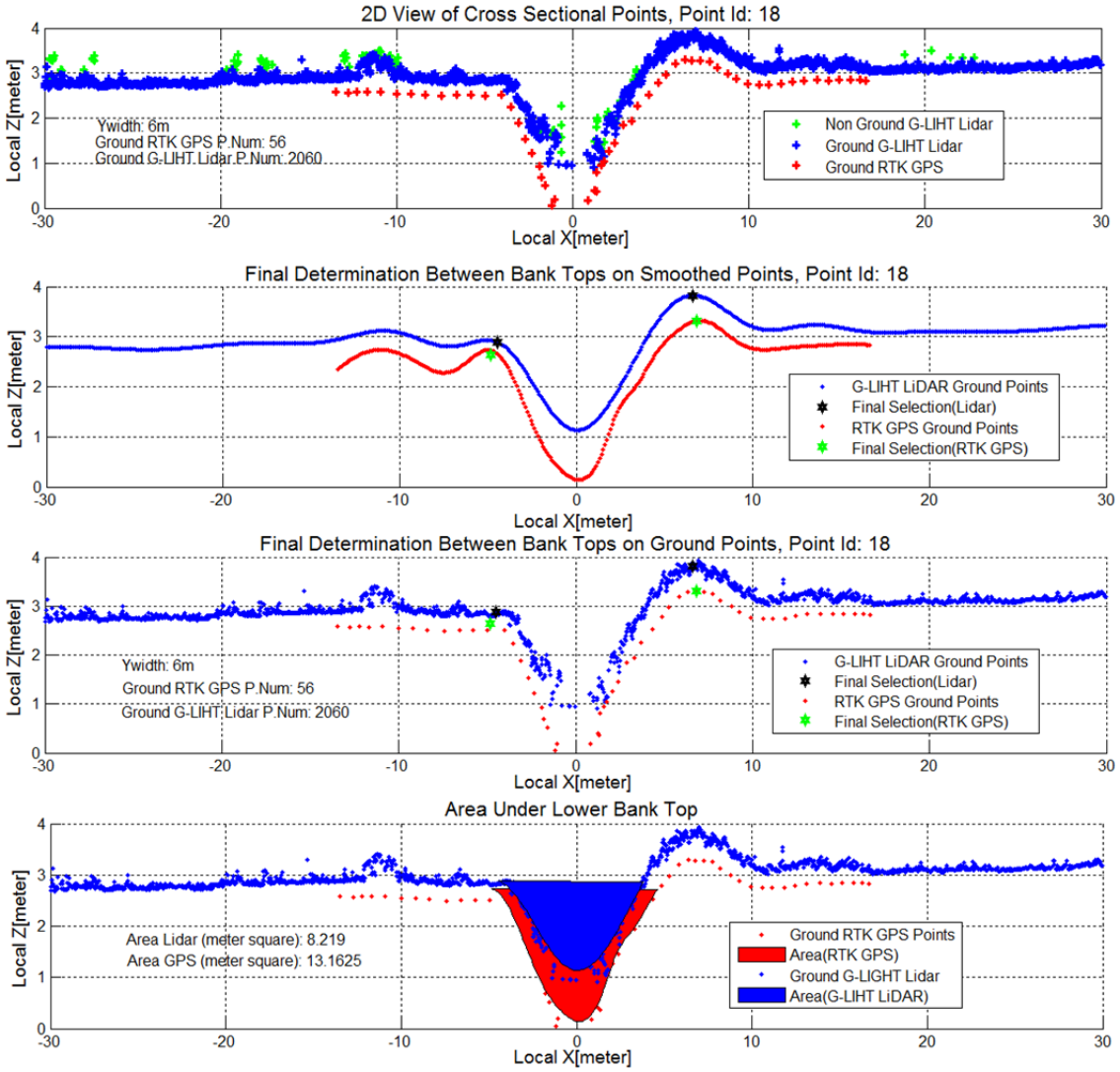

Figure B.30 Site 4 Cross Section 3 G-LiHT LiDAR Top of the Banks in Local Coordinates

Figure B.31 Site 4 Cross Section 4 and 5

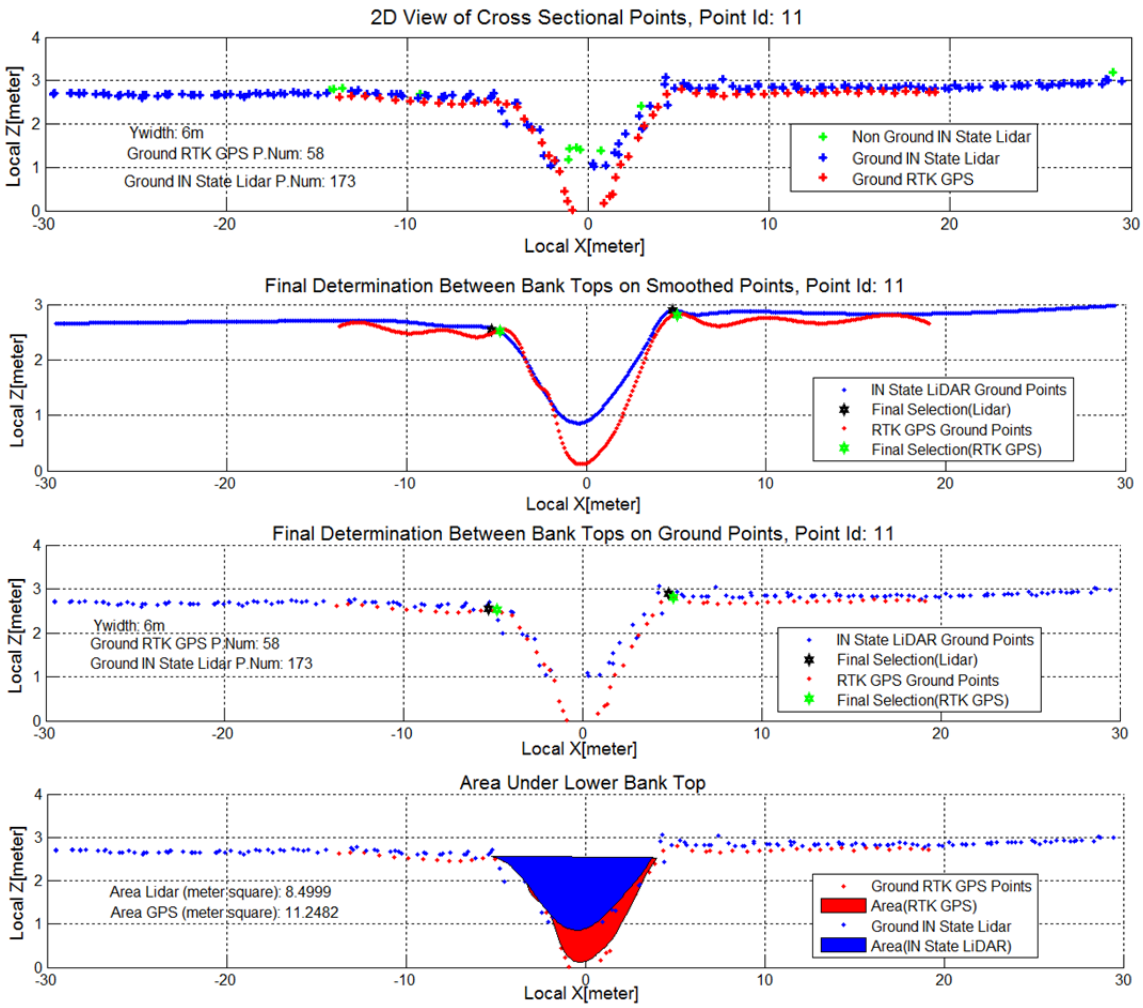

Figure B.32 Site 4 Cross Section 4 IN State LiDAR Top of the Banks in Local Coordinates

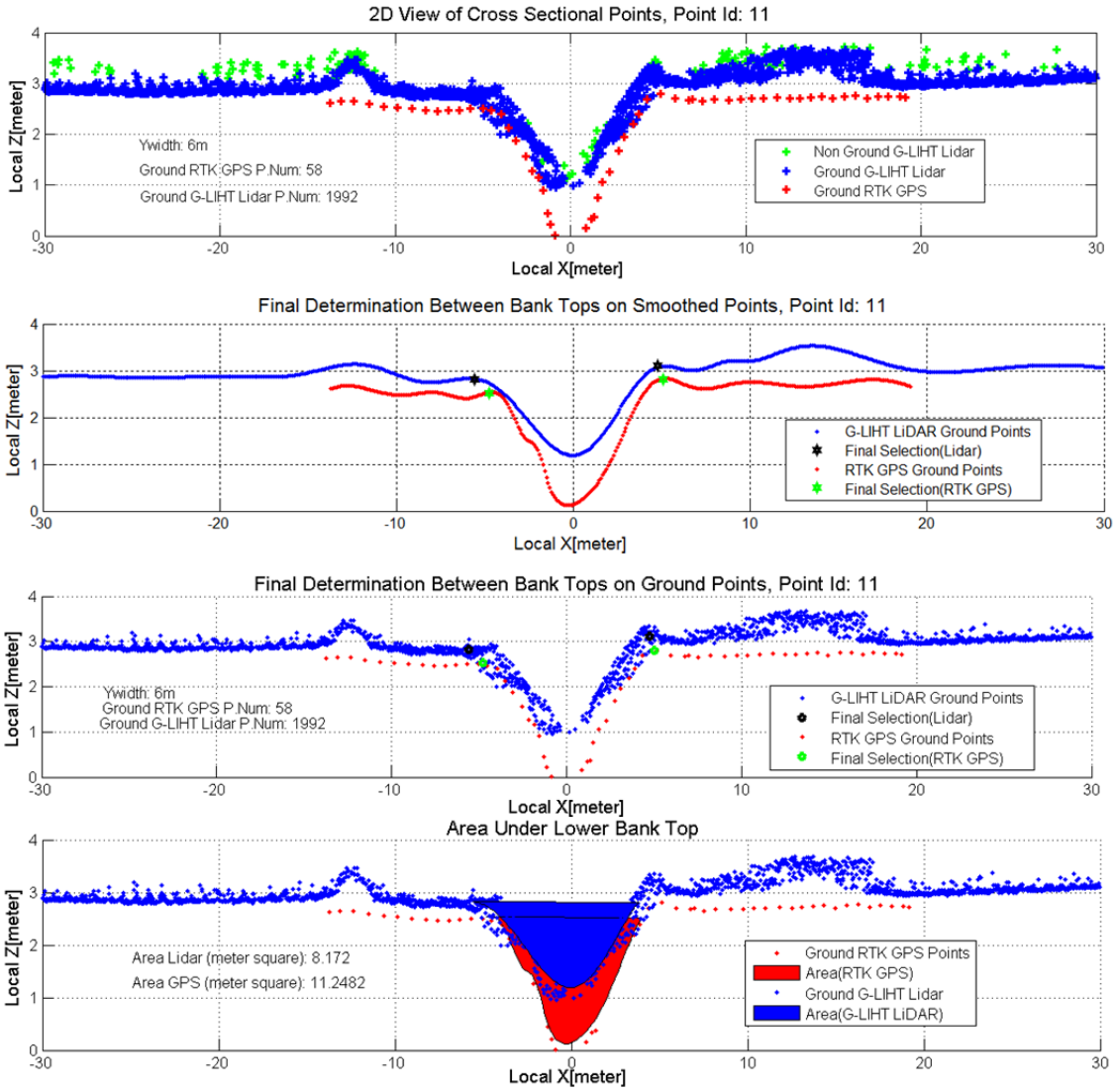

Figure B.33 Site 4 Cross Section 4 G-LiHT LiDAR Top of The Banks in Local Coordinates

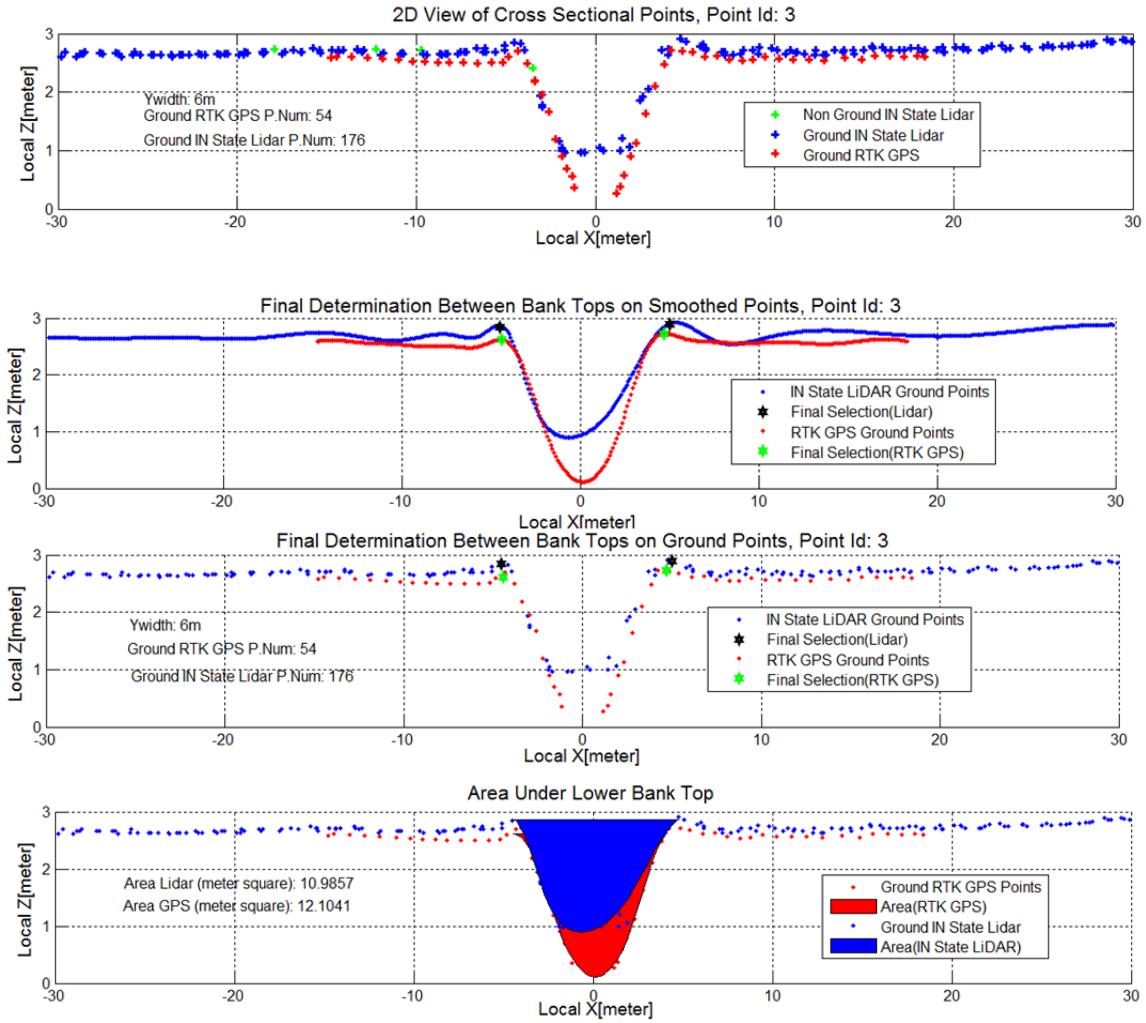

Figure B.34 Site 4 Cross Section 5 IN State LiDAR Top of the Banks in Local Coordinates

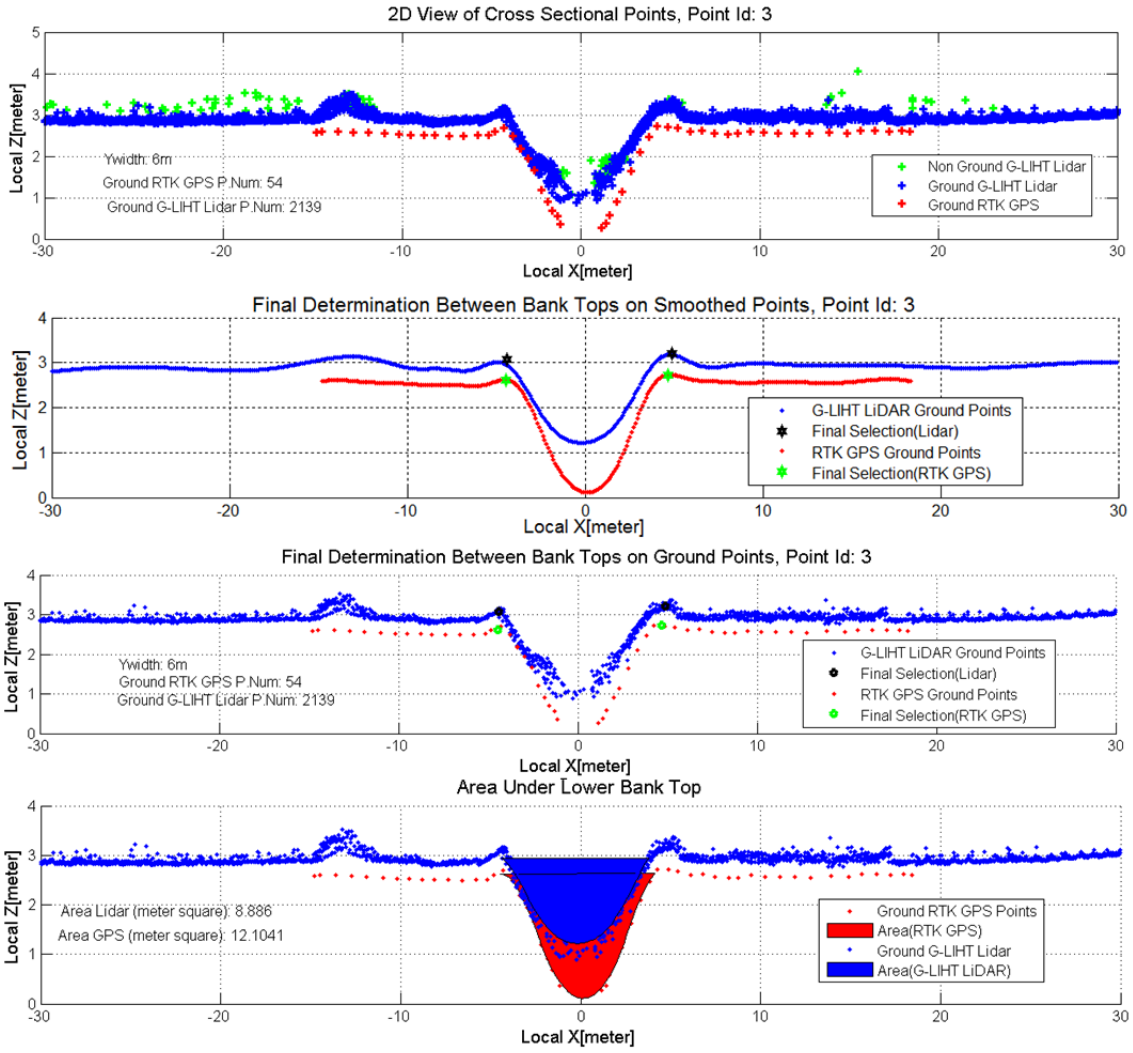

Figure B.35 Site 4 Cross-Section 5 G-LiHT LiDAR Top of the Banks in Local Coordinates

C. Appendix -Global and Local Coordinates, Horizontal and Vertical Difference Tables for Sites

Site 1 Tables

Table C.1 Site 1 Positive Site Bank Top Global Coordinates

Positive Side Top of the Bank Coordinates (NAD83 UTM Zone 16)						
Site 1	IN State LiDAR			RTK GPS		
	X(m)	Y(m)	Z(m)	X(m)	Y(m)	Z(m)
CR1*	549266.18	4437989.35	284.86	549267.27	4437987.89	284.70
CR2*	549291.92	4437999.35	284.96	549291.86	4437999.58	284.88
CR3	549329.12	4438030.76	284.55	549329.31	4438030.79	284.53
CR4	549323.09	4438054.71	284.86	549323.02	4438054.70	284.75
CR5	549320.86	4438082.90	285.04	549321.09	4438082.88	284.95

Table C.2 Site 1 Negative Site Bank Top Global Coordinates

Negative Side Top of the Bank Coordinates (NAD83 UTM Zone 16)						
Site 1	IN State LIDAR			RTK GPS		
	X(m)	Y(m)	Z(m)	X(m)	Y(m)	Z(m)
CR1*	549277.78	4437973.80	284.70	549277.09	4437974.73	284.60
CR2*	549296.79	4437979.29	284.63	549297.08	4437978.10	284.65
CR3	549309.94	4438027.56	284.68	549309.85	4438027.54	284.57
CR4	549307.77	4438051.87	284.66	549306.90	4438051.71	284.48
CR5	549304.46	4438084.55	284.56	549305.04	4438084.49	284.39

Table C.3 Site 1 Bank Top Local Coordinates

	Positive Top				Negative Top			
Site 1	IN STATE LIDAR		RTK GPS		IN STATE LIDAR		RTK GPS	
	Local X (m)	Local Z (m)	Local X (m)	Local Z (m)	Local X (m)	Local Z (m)	Local X (m)	Local Z (m)
CR1*	10.64	3.89	8.81	3.72	-8.76	3.72	-7.60	3.62
CR2*	7.79	4.19	8.03	4.12	-12.85	3.86	-14.07	3.89
CR3	11.42	3.84	11.62	3.82	-8.02	3.97	-8.12	3.86
CR4	7.74	4.04	7.67	3.93	-7.85	3.84	-8.73	3.66
CR5	8.09	4.26	8.32	4.17	-8.39	3.78	-7.81	3.61

Table C.4 Site 1 Vertical Difference

Vertical Difference Between Bank Tops (with Local Z)					
Site 1	IN State LiDAR - RTK GPS		Positive Side –Negative Side		
	Positive(P) Sides (m)	Negative (N) Sides (m)	IN State LiDAR (1) (m)	RTK GPS (2) (m)	(1)- (2) (m)
CR1*	0.16	0.10	0.17	0.10	0.06
CR2*	0.07	-0.02	0.33	0.24	0.09
CR3	0.02	0.11	-0.13	-0.04	-0.09
CR4	0.10	0.18	0.20	0.27	-0.08
CR5	0.09	0.17	0.48	0.56	-0.08

Table C.5 Site 1 Horizontal Difference

Horizontal Difference Between Bank Tops (with Local X)					
Site 1	IN State LiDAR - RTK GPS		Positive Side –Negative Side		
	Positive(P) Sides (m)	Negative (N) Sides (m)	IN State LiDAR(1) (m)	RTK GPS (2) (m)	(1)- (2) (m)
CR1*	1.83	-1.16	19.40	16.41	2.99
CR2*	-0.24	1.23	20.64	22.10	-1.46
CR3	-0.20	0.09	19.44	19.73	-0.29
CR4	0.07	0.88	15.59	16.40	-0.81
CR5	-0.23	-0.58	16.48	16.13	0.35

Site 2 Tables

Table C.6 Site 2 Positive Site Bank Top Global Coordinates

Positive Side Top of the Bank Coordinates (NAD83 UTM Zone 16)						
Site 2 (330)	IN State LiDAR			RTK GPS		
	X(m)	Y(m)	Z(m)	X(m)	Y(m)	Z(m)
CR1	547043.76	4457843.59	269.72	547043.73	4457843.69	269.42
CR2	547060.51	4457847.40	269.92	547060.64	4457846.70	269.65
CR3	547079.34	4457850.32	269.67	547079.44	4457849.95	269.38
CR4	547088.22	4457851.65	269.77	547088.16	4457852.10	269.36
CR5	547101.01	4457854.41	269.63	547101.23	4457853.39	269.42
CR5D	547101.01	4457854.41	269.63	547100.95	4457854.68	269.27

Table C.7 Site 2 Negative Site Bank Top Global Coordinates

Negative Side Top of the Bank Coordinates (NAD83 UTM Zone 16)						
Site 2	IN State LiDAR			RTK GPS		
	X(m)	Y(m)	Z(m)	X(m)	Y(m)	Z(m)
CR1	547039.70	4457854.33	269.57	547039.67	4457854.41	269.44
CR2	547058.53	4457858.26	269.59	547058.54	4457858.18	269.40
CR3	547076.31	4457861.06	269.63	547076.23	4457861.37	269.44
CR4	547086.80	4457862.29	269.55	547086.81	4457862.20	269.38
CR5	547098.78	4457864.62	269.72	547099.60	4457860.85	269.24
CR5D	547098.78	4457864.62	269.72	547098.86	4457864.24	269.56

Table C.8 Site 2 Bank Top Local Coordinates

	Positive Top				Negative Top			
Site 2	IN State LIDAR		RTK GPS		IN State LIDAR		RTK GPS	
	Local X (m)	Local Z (m)	Local X (m)	Local Z (m)	Local X (m)	Local Z (m)	Local X (m)	Local Z (m)
CR1	5.79	2.22	5.68	1.92	-5.70	2.07	-5.78	1.94
CR2	5.11	2.30	5.83	2.03	-5.93	1.97	-5.85	1.78
CR3	4.18	1.82	4.57	1.54	-6.98	1.79	-7.29	1.60
CR4	4.85	2.06	4.39	1.65	-5.89	1.84	-5.80	1.67
CR5	3.74	2.09	4.78	1.87	-6.71	2.17	-2.85	1.69
CR5D	3.74	2.09	3.46	1.72	-6.71	2.17	-6.32	2.01

Table C.9 Site 2 Vertical Difference

Vertical Difference Between Bank Tops (Local Z)					
Site 2	IN State LiDAR - RTK GPS		Positive Side –Negative Side		(1)- (2) (m)
	Positive(P) Sides (m)	Negative (N) Sides (m)	IN State LiDAR (1)(m)	RTK GPS (2) (m)	
CR1	0.30	0.13	0.15	-0.02	0.17
CR2	0.27	0.18	0.33	0.25	0.09
CR3	0.28	0.19	0.04	-0.05	0.09
CR4	0.41	0.16	0.22	-0.02	0.25
CR5	0.21	0.48	-0.09	0.18	-0.27
CR5D	0.36	0.16	-0.08	-0.29	0.21

Table C.10 Site 2 Horizontal Difference

Horizontal Difference Between Bank Tops (Local X)					
Site 2	IN State LiDAR - RTK GPS		Positive Side –Negative Side		(1)- (2) (m)
	Positive(P) Sides (m)	Negative (N) Sides (m)	IN State LiDAR(1) (m)	RTK GPS (2) (m)	
CR1	0.11	0.08	11.49	11.46	0.03
CR2	-0.72	-0.08	11.04	11.68	-0.64
CR3	-0.39	0.32	11.16	11.86	-0.71
CR4	0.46	-0.09	10.74	10.19	0.55
CR5	-1.04	-3.86	10.45	7.63	2.82
CR5D	0.28	-0.39	10.45	9.78	0.67

Site 3 Tables

Table C.11 Site 3 Positive Site Bank Top Global Coordinates

Positive Side Top of the Bank Coordinates (NAD83 UTM Zone 16)						
Site 3	IN State LiDAR			RTK GPS		
(200)	X(m)	Y(m)	Z(m)	X(m)	Y(m)	Z(m)
CR1	538805.35	4455179.69	263.32	538805.23	4455180.16	263.14
CR2	538787.91	4455173.62	263.35	538788.14	4455173.17	263.08
CR3	538776.72	4455171.18	263.37	538776.70	4455171.40	263.22
CR4	538762.19	4455170.24	263.46	538762.18	4455170.38	263.28
CR5	538750.77	4455167.95	263.46	538750.77	4455168.02	263.29

Table 6.C.12 Site 3 Negative Site Bank Top Global Coordinates

Negative Side Top of the Bank Coordinates (NAD83 UTM Zone 16)						
Site 3	IN State LiDAR			RTK GPS		
	X(m)	Y(m)	Z(m)	X(m)	Y(m)	Z(m)
CR1	538808.79	4455166.37	263.22	538808.74	4455166.58	263.09
CR2	538793.65	4455162.76	263.04	538793.63	4455162.79	262.88
CR3	538777.40	4455159.48	262.98	538777.41	4455159.21	262.84
CR4	538762.98	4455156.85	262.95	538763.02	4455156.32	262.80
CR5	538750.35	4455154.64	262.95	538750.34	4455154.34	262.78

Table C.13 Site 3 Bank Top Local Coordinates

	Positive Top				Negative Top			
Site 3	IN State LIDAR		RTK GPS		IN State LIDAR		RTK GPS	
	Local X (m)	Local Z (m)	Local X (m)	Local Z (m)	Local X (m)	Local Z (m)	Local X (m)	Local Z (m)
CR1	6.64	2.39	7.12	2.21	-7.13	2.29	-6.91	2.16
CR2	6.14	2.50	5.63	2.22	-6.14	2.19	-6.11	2.03
CR3	7.14	2.62	7.36	2.47	-4.59	2.23	-4.85	2.09
CR4	8.18	2.69	8.32	2.51	-5.24	2.18	-5.77	2.03
CR5	6.50	2.75	6.58	2.58	-6.81	2.24	-7.11	2.07

Table C.14 Site 3 Vertical Difference

Vertical Difference Between Bank Tops (Local Z)					
Site 3	IN State LiDAR - RTK GPS		Positive Side –Negative Side		(1)- (2) (m)
	Positive(P) Sides (m)	Negative (N) Sides (m)	IN State LiDAR (1)(m)	RTK GPS (2) (m)	
CR1	0.18	0.13	0.10	0.05	0.05
CR2	0.27	0.16	0.31	0.19	0.12
CR3	0.15	0.14	0.39	0.38	0.01
CR4	0.18	0.15	0.51	0.48	0.03
CR5	0.17	0.17	0.51	0.51	0.00

Table C.15 Site 3 Horizontal Difference

Horizontal Difference Between Bank Tops (Local X)					
Site 3	IN State LiDAR - RTK GPS		Positive Side –Negative Side		(1)- (2) (m)
	Positive(P) Sides (m)	Negative (N) Sides (m)	IN State LiDAR(1) (m)	RTK GPS (2) (m)	
CR1	-0.48	-0.22	13.76	14.03	-0.26
CR2	0.51	-0.04	12.28	11.74	0.55
CR3	-0.22	0.26	11.73	12.21	-0.48
CR4	-0.14	0.53	13.42	14.09	-0.67
CR5	-0.08	0.30	13.32	13.69	-0.37

Site 4 Tables

Indiana State LiDAR

Table C.16 Site 4 Positive Site Bank Top Global Coordinates

Positive Side Top of the Bank Coordinates (NAD83 UTM Zone 16)						
Site 4	IN State LiDAR			RTK GPS		
	X(m)	Y(m)	Z(m)	X(m)	Y(m)	Z(m)
CR1*	588899.18	4489366.56	253.81	588899.89	4489366.57	253.67
CR2	588901.32	4489331.46	254.23	588901.30	4489331.50	254.07
CR3	588871.82	4489321.41	254.42	588871.90	4489321.06	254.34
CR4	588841.97	4489307.26	253.92	588842.15	4489307.08	253.84
CR5	588822.79	4489276.19	254.00	588822.49	4489276.37	253.84

Table C.17 Site 4 Negative Site Bank Top Global Coordinates

Negative Side Top of the Bank Coordinates (NAD83 UTM Zone 16)						
Site 4	IN State LIDAR			RTK GPS		
	X(m)	Y(m)	Z(m)	X(m)	Y(m)	Z(m)
CR1*	588908.94	4489366.59	254.08	588909.52	4489366.60	254.07
CR2	588893.58	4489340.74	254.21	588893.85	4489340.42	253.95
CR3	588869.45	4489332.13	253.76	588869.39	4489332.43	253.67
CR4	588834.73	4489314.25	253.57	588835.07	4489313.92	253.55
CR5	588814.59	4489281.14	253.96	588814.69	4489281.09	253.73

Table C.18 Site 4 Bank Top Local Coordinates

	Positive Top				Negative Top			
Site 4	IN STATE LIDAR		RTK GPS		IN STATE LIDAR		RTK GPS	
	Local X (m)	Local Z (m)	Local X (m)	Local Z (m)	Local X (m)	Local Z (m)	Local X (m)	Local Z (m)
CR1*	5.08	2.71	4.37	2.57	-4.69	2.97	-5.26	2.96
CR2	5.72	3.00	5.68	2.84	-6.37	2.98	-5.95	2.72
CR3	6.45	3.39	6.81	3.31	-4.52	2.73	-4.84	2.64
CR4	4.81	2.88	5.06	2.81	-5.25	2.54	-4.78	2.52
CR5	5.03	2.89	4.68	2.73	-4.55	2.85	-4.44	2.62

Table C.19 Site 4 Vertical Difference

Vertical Difference Between Bank Tops (Local Z)					
Site 4	IN State LiDAR - RTK GPS		Positive Side –Negative Side		(1)- (2) (m)
	Positive(P) Sides (m)	Negative (N) Sides (m)	IN State LiDAR (1)(m)	RTK GPS (2) (m)	
CR1*	0.14	0.01	-0.27	-0.40	0.13
CR2	0.16	0.25	0.02	0.12	-0.10
CR3	0.08	0.10	0.66	0.67	-0.02
CR4	0.08	0.03	0.34	0.29	0.05
CR5	0.16	0.23	0.04	0.11	-0.07

Table C.20 Site 4 Horizontal Difference

Horizontal Difference Between Bank Tops (Local X)					
Site 4	IN State LiDAR - RTK GPS		Positive Side –Negative Side		(1)- (2) (m)
	Positive(P) Sides (m)	Negative (N) Sides (m)	IN State LiDAR(1) (m)	RTK GPS (2) (m)	
CR1*	0.71	0.58	9.76	9.63	0.13
CR2	0.04	-0.42	12.08	11.62	0.46
CR3	-0.36	0.31	10.97	11.65	-0.67
CR4	-0.25	-0.47	10.06	9.84	0.22
CR5	0.35	-0.11	9.58	9.11	0.46

G-LiHT LiDAR

Table C.21 Site 4 Positive Site Bank Top Global Coordinates

Positive Side Top of the Bank Coordinates (NAD83 UTM Zone 16)						
Site 4	G-LiHT LiDAR			RTK GPS		
	X(m)	Y(m)	Z(m)	X(m)	Y(m)	Z(m)
CR1*	588899.52	4489366.57	254.01	588899.89	4489366.57	253.67
CR2	588901.36	4489331.42	254.46	588901.30	4489331.50	254.07
CR3	588871.86	4489321.25	254.84	588871.90	4489321.06	254.34
CR4	588841.94	4489307.28	254.13	588842.15	4489307.08	253.84
CR5	588822.66	4489276.27	254.32	588822.49	4489276.37	253.84

Table C.22 Site 4 Negative Site Bank Top Global Coordinates

Negative Side Top of the Bank Coordinates (NAD83 UTM Zone 16)						
Site 4	G-LiHT LiDAR			RTK GPS		
	X(m)	Y(m)	Z(m)	X(m)	Y(m)	Z(m)
CR1*	588908.91	4489366.59	254.19	588909.52	4489366.60	254.07
CR2	588893.88	4489340.39	254.37	588893.85	4489340.42	253.95
CR3	588869.46	4489332.09	253.92	588869.39	4489332.43	253.67
CR4	588834.49	4489314.48	253.84	588835.07	4489313.92	253.55
CR5	588814.72	4489281.07	254.19	588814.69	4489281.09	253.73

Table C.23 Site 4 Bank Top Local Coordinates

	Positive Top				Negative Top			
Site 4	G-LiHT LIDAR		RTK GPS		G-LiHT LIDAR		RTK GPS	
	Local X (m)	Local Z (m)	Local X (m)	Local Z (m)	Local X (m)	Local Z (m)	Local X (m)	Local Z (m)
CR1*	4.73	2.91	4.37	2.57	-4.66	3.08	-5.26	2.96
CR2	5.78	3.23	5.68	2.84	-5.91	3.14	-5.95	2.72
CR3	6.62	3.82	6.81	3.31	-4.49	2.89	-4.84	2.64
CR4	4.78	3.10	5.06	2.81	-5.59	2.81	-4.78	2.52
CR5	4.88	3.21	4.68	2.73	-4.40	3.08	-4.44	2.62

Table C.24 Site 4 Vertical Difference

Vertical Difference Between Bank Tops (Local Z)					
Site 4	G-LiHT LiDAR - RTK GPS		Positive Side –Negative Side		(1)- (2) (m)
	Positive(P) Sides (m)	Negative (N) Sides (m)	G-LiHT LiDAR (1)(m)	RTK GPS (2) (m)	
CR1*	0.34	0.12	-0.18	-0.40	0.22
CR2	0.39	0.42	0.09	0.12	-0.03
CR3	0.51	0.25	0.93	0.67	0.26
CR4	0.29	0.29	0.29	0.29	0.00
CR5	0.48	0.46	0.13	0.11	0.02

Table C.25 Site 4 Horizontal Difference

Horizontal Difference Between Bank Tops (Local X)					
Site 4	G-LiHT LiDAR - RTK GPS		Positive Side –Negative Side		(1)- (2) (m)
	Positive(P) Sides (m)	Negative (N) Sides (m)	G-LiHT LiDAR(1) (m)	RTK GPS (2) (m)	
CR1*	0.37	0.61	9.39	9.63	-0.24
CR2	0.10	0.04	11.69	11.62	0.06
CR3	-0.19	0.35	11.10	11.65	-0.54
CR4	-0.28	-0.81	10.37	9.84	0.53
CR5	0.20	0.03	9.28	9.11	0.17

D. Appendix -Survey Site Section Results of Method With Digitization

Site 2 Ditch Section

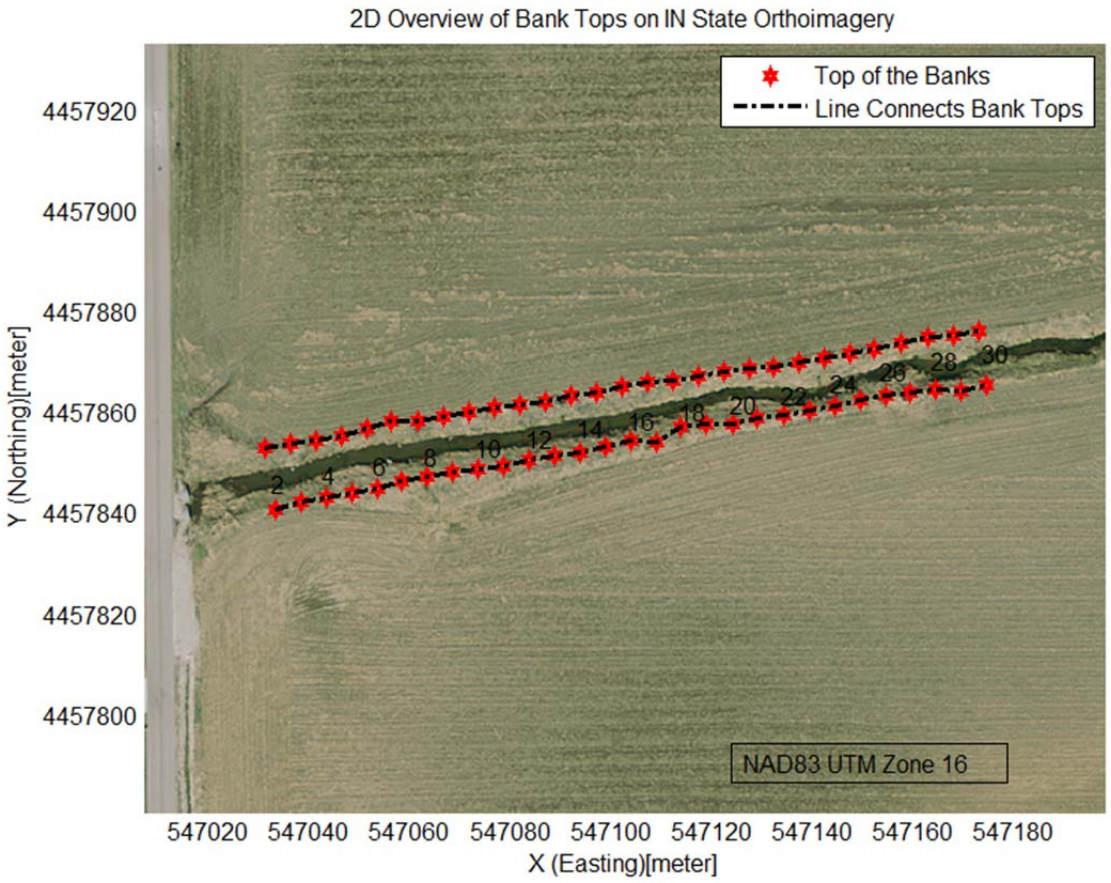

Figure D.1 Bank Tops over Indiana State Imagery in Site 2

Table D.1 Bank Top Coordinates for Site 2

Top of the Bank Coordinates (NAD83 UTM Zone 16)						
Site 2	North Side of the Stream			South Side of the Stream		
	X(m)	Y(m)	Z(m)	X(m)	Y(m)	Z(m)
CR1	547031.33	4457853.19	269.65	547033.52	4457840.93	269.74
CR2	547036.40	4457853.96	269.56	547038.45	4457842.47	269.74
CR3	547041.50	4457854.54	269.61	547043.47	4457843.49	269.73
CR4	547046.54	4457855.46	269.63	547048.52	4457844.34	269.71
CR5	547051.48	4457856.92	269.53	547053.60	4457845.07	269.82
CR6	547056.41	4457858.47	269.53	547058.54	4457846.54	269.88
CR7	547061.59	4457858.63	269.66	547063.57	4457847.52	269.93

CR8	547066.65	4457859.42	269.72	547068.62	4457848.37	269.87
CR9	547071.70	4457860.26	269.70	547073.70	4457849.03	269.76
CR10	547076.73	4457861.24	269.63	547078.78	4457849.72	269.73
CR11	547081.84	4457861.79	269.64	547083.81	4457850.73	269.76
CR12	547086.93	4457862.43	269.53	547088.84	4457851.69	269.76
CR13	547091.93	4457863.55	269.52	547093.92	4457852.38	269.77
CR14	547097.09	4457864.23	269.71	547098.90	4457853.37	269.73
CR15	547102.13	4457865.40	269.66	547103.84	4457854.76	269.69
CR16	547107.19	4457866.19	269.62	547109.09	4457854.39	269.61
CR17	547112.29	4457866.70	269.64	547113.79	4457857.39	269.60
CR18	547117.33	4457867.63	269.65	547118.87	4457858.07	269.67
CR19	547122.40	4457868.41	269.62	547124.07	4457858.05	269.79
CR20	547127.49	4457868.96	269.68	547129.09	4457859.08	269.84
CR21	547132.27	4457869.15	269.84	547134.38	4457859.81	269.80
CR22	547137.17	4457870.24	269.83	547139.52	4457860.61	269.83
CR23	547142.24	4457871.07	269.76	547144.58	4457861.47	269.85
CR24	547147.29	4457871.99	269.74	547149.59	4457862.58	269.71
CR25	547152.34	4457872.91	269.70	547154.59	4457863.68	269.53
CR26	547157.68	4457874.03	269.78	547159.39	4457864.08	269.69
CR27	547162.82	4457875.19	269.80	547164.32	4457864.67	269.78
CR28	547167.96	4457875.42	269.85	547169.51	4457864.60	269.62
CR29	547173.00	4457876.39	269.83	547174.54	4457865.60	269.61

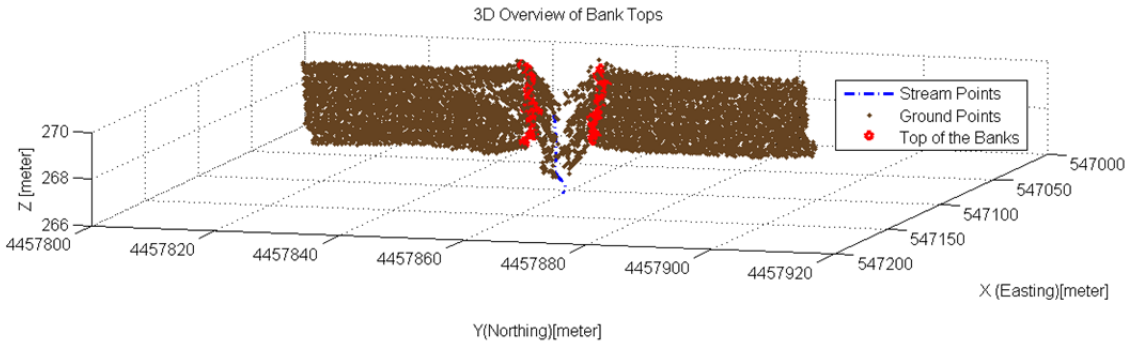

Figure D.2 Top of the banks over 3D view Site 2 (with only ground points)

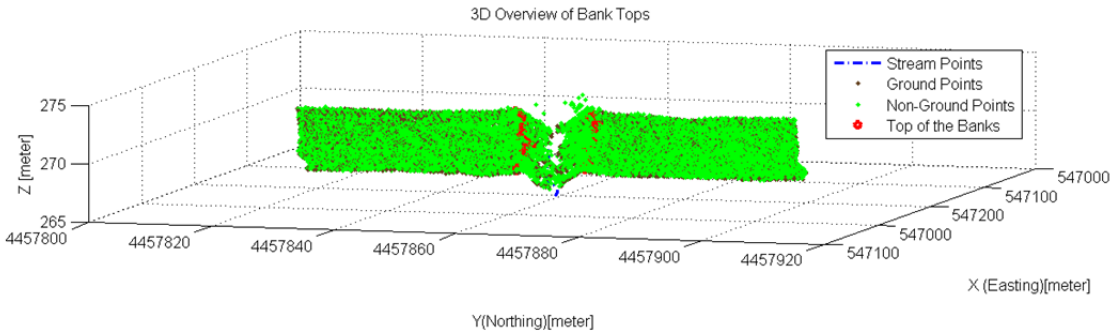

Figure D.3 Top of the banks over 3D view Site 2 (with ground and non-ground points)

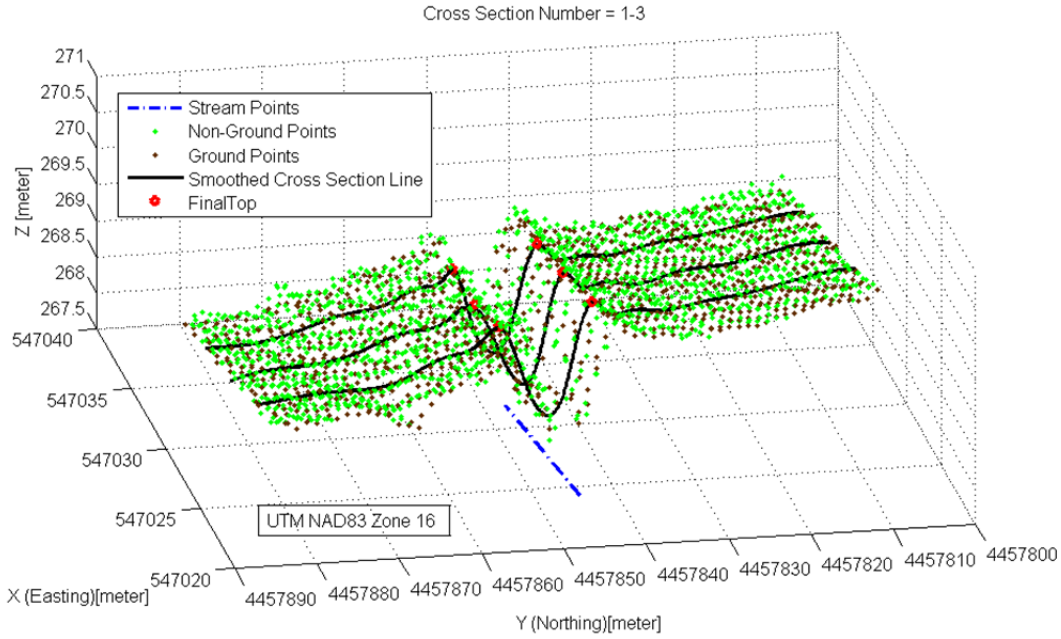

Figure D.4 Cross Sections 1-3 with smoothed lines

Site 3 Ditch Section

Figure D.5 Bank Tops over Indiana State Imagery in Site 3

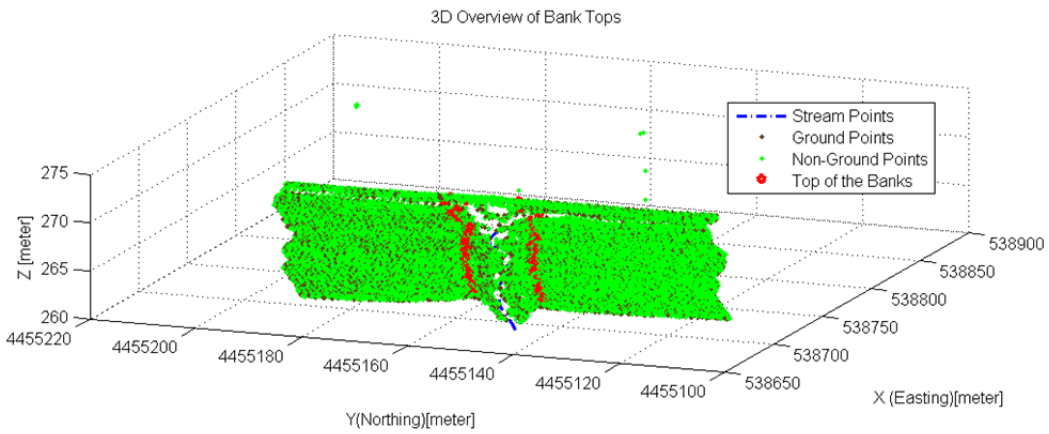

Figure D.6 Top of the banks over 3D view Site 3

Table D.2 Bank Top Coordinates for Site 3

Top of the Bank Coordinates (NAD83 UTM Zone 16)						
Site 3	North Side of the Stream			South Side of the Stream		
	X(m)	Y(m)	Z(m)	X(m)	Y(m)	Z(m)
CR1	538688.38	4455154.60	263.44	538691.61	4455142.34	262.76
CR2	538693.25	4455156.05	263.46	538696.88	4455143.12	262.77
CR3	538698.46	4455156.74	263.50	538702.03	4455144.07	262.76
CR4	538703.57	4455157.99	263.51	538707.00	4455145.46	262.75
CR5	538708.69	4455159.39	263.49	538712.03	4455146.44	262.72
CR6	538713.85	4455160.21	263.46	538717.17	4455147.36	262.80
CR7	538719.02	4455161.24	263.49	538722.12	4455148.76	262.86
CR8	538724.77	4455162.58	263.46	538726.40	4455149.74	262.89
CR9	538729.87	4455163.71	263.43	538731.47	4455151.17	262.92
CR10	538734.68	4455165.17	263.40	538736.83	4455151.92	262.96
CR11	538739.28	4455165.46	263.43	538742.56	4455152.59	263.00
CR12	538744.40	4455166.43	263.47	538747.58	4455153.97	262.99
CR13	538750.56	4455168.00	263.47	538751.59	4455154.77	262.93
CR14	538755.98	4455168.20	263.46	538756.51	4455155.59	262.93
CR15	538760.76	4455169.59	263.49	538761.97	4455156.24	262.97
CR16	538765.44	4455170.49	263.47	538767.37	4455157.43	263.00
CR17	538770.59	4455171.28	263.45	538772.50	4455158.27	263.02
CR18	538775.87	4455171.15	263.34	538777.51	4455159.99	262.98
CR19	538779.19	4455172.27	263.57	538783.91	4455159.90	262.99
CR20	538784.60	4455172.67	263.33	538788.90	4455161.46	263.04
CR21	538790.14	4455173.83	263.50	538793.64	4455162.46	263.01
CR22	538795.16	4455177.20	263.45	538798.20	4455163.51	263.03

CR23	538800.17	4455178.72	263.38	538803.18	4455165.02	263.10
CR24	538805.23	4455179.93	263.33	538808.28	4455166.07	263.17
CR25	538810.02	4455181.45	263.28	538813.65	4455166.64	263.09
CR26	538817.02	4455181.58	263.18	538818.82	4455166.54	262.95
CR27	538823.03	4455182.47	263.02	538824.26	4455167.22	262.97
CR28	538828.85	4455185.88	263.46	538829.63	4455171.58	263.40
CR29	538834.71	4455185.76	263.52	538835.40	4455173.15	263.60
CR30	538839.93	4455183.91	262.97	538841.62	4455173.74	263.05

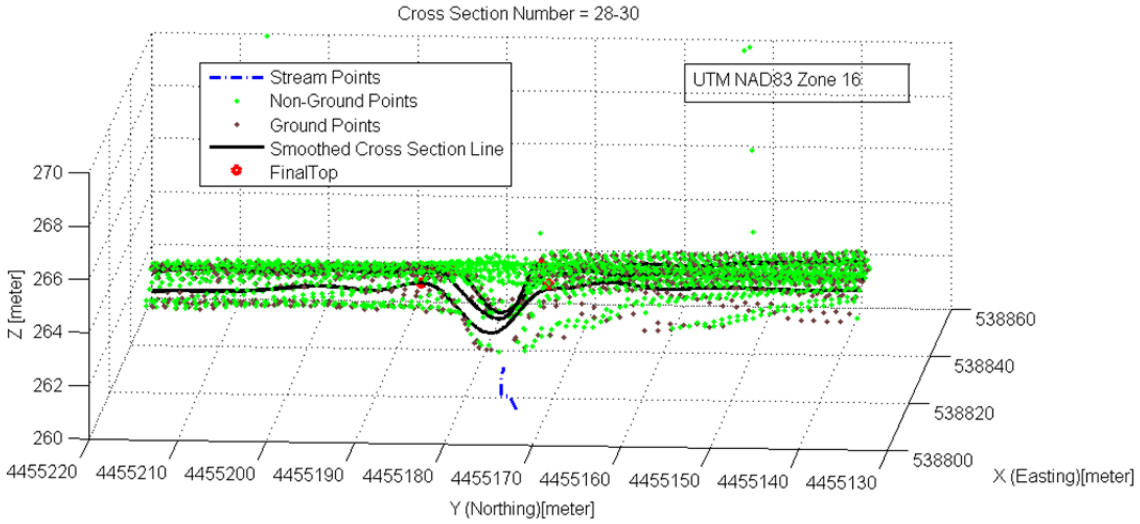

Figure D.7 Ditch Geometry Under bridge (bridge was classified as non-ground)

Site 4 Ditch Section

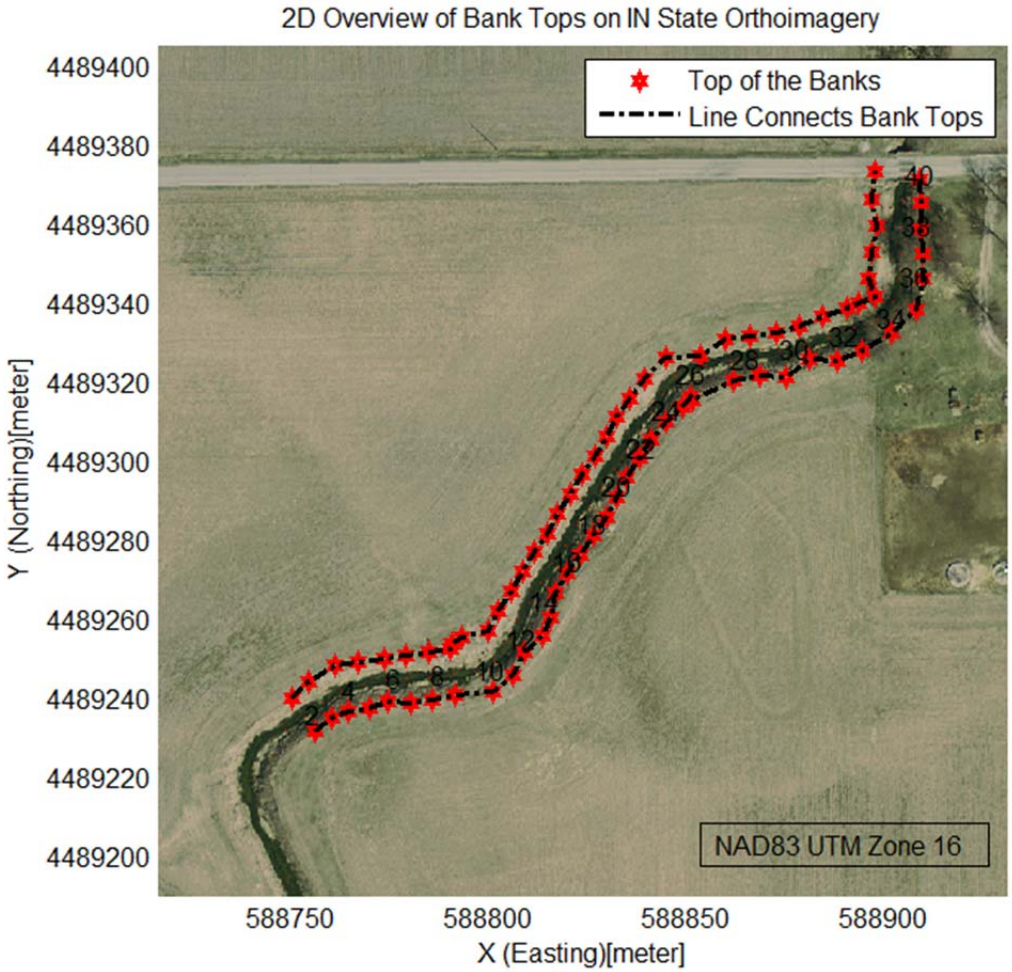

Figure D.8 Bank Tops over Indiana State Imagery in Site 4

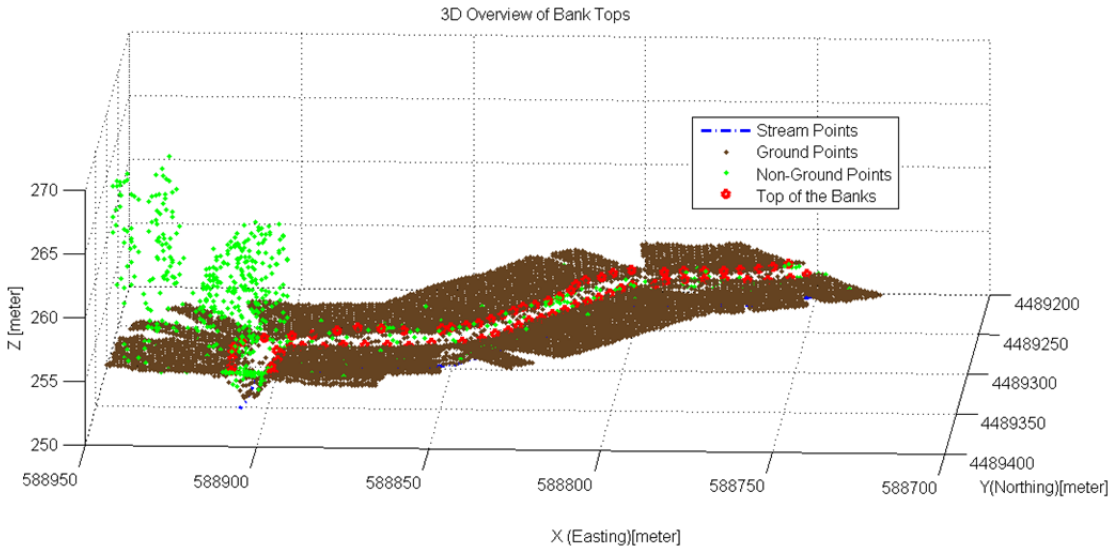

Figure D.9 Top of the banks over 3D view Site 4

Table D.3 Bank Top Coordinates for Site 4

Top of the Bank Coordinates (NAD83 UTM Zone 16)						
Site 4	North-West Side of the Stream			South-East Side of the Stream		
	X(m)	Y(m)	Z(m)	X(m)	Y(m)	Z(m)
CR1	588750.31	4489240.56	253.97	588756.29	4489232.15	254.24
CR2	588754.78	4489244.86	253.90	588760.61	4489235.44	254.21
CR3	588761.12	4489248.75	254.00	588764.56	4489237.18	254.14
CR4	588767.08	4489249.76	254.05	588769.92	4489238.29	254.10
CR5	588773.61	4489250.74	254.15	588774.57	4489239.67	254.14
CR6	588779.31	4489251.23	254.20	588780.32	4489239.47	254.12
CR7	588784.96	4489252.09	254.21	588786.01	4489240.23	254.12
CR8	588790.41	4489253.22	254.18	588791.79	4489241.48	254.08
CR9	588790.75	4489254.30	254.21	588801.29	4489242.23	254.27
CR10	588793.47	4489256.20	254.02	588806.41	4489246.60	254.34
CR11	588799.99	4489257.70	254.03	588809.04	4489252.36	254.33
CR12	588802.68	4489262.79	254.13	588813.64	4489256.22	254.32
CR13	588805.88	4489267.74	254.02	588816.05	4489261.17	254.32
CR14	588808.75	4489272.69	253.96	588817.11	4489267.29	254.21
CR15	588811.85	4489277.49	253.94	588820.18	4489272.11	254.03
CR16	588814.96	4489282.29	253.96	588823.19	4489276.98	253.94

CR17	588817.72	4489287.32	253.93	588826.52	4489281.64	253.96
CR18	588820.76	4489292.16	253.91	588829.85	4489286.29	254.05
CR19	588823.73	4489297.05	253.88	588832.40	4489291.45	254.04
CR20	588827.23	4489301.59	253.95	588835.11	4489296.50	254.04
CR21	588829.90	4489306.67	253.88	588838.20	4489301.32	254.03
CR22	588832.39	4489311.87	253.77	588841.46	4489306.02	253.95
CR23	588835.97	4489316.43	253.79	588844.83	4489310.60	254.04
CR24	588839.48	4489321.20	253.68	588849.05	4489314.45	254.12
CR25	588844.82	4489326.86	253.77	588851.45	4489316.60	254.16
CR26	588853.73	4489327.32	253.72	588851.69	4489316.07	254.03
CR27	588860.19	4489331.25	253.74	588862.30	4489320.80	254.25
CR28	588866.33	4489332.06	253.82	588868.83	4489322.27	254.50
CR29	588872.78	4489332.84	253.89	588875.55	4489321.98	254.52
CR30	588878.80	4489334.87	253.94	588881.17	4489326.42	254.54
CR31	588884.47	4489336.98	253.96	588888.44	4489326.13	254.24
CR32	588890.69	4489339.06	254.13	588894.36	4489328.32	254.27
CR33	588893.88	4489340.33	254.14	588902.04	4489333.07	254.39
CR34	588897.91	4489342.14	254.00	588908.24	4489338.96	254.41
CR35	588896.33	4489346.92	254.07	588910.17	4489346.65	254.51
CR36	588896.98	4489353.22	253.87	588910.05	4489353.20	254.44
CR37	588898.26	4489359.98	253.83	588909.46	4489359.39	254.37
CR38	588897.00	4489366.67	253.76	588909.36	4489365.74	254.13
CR39	588897.83	4489373.68	254.07	588909.05	4489371.93	254.15